

PEER-TO-PEER POWER SHARING IN DC MICROGRIDS  
FOR RURAL ELECTRIFICATION

By

RABIA KHAN

A dissertation submitted in partial fulfillment of  
the requirements for the degree of

DOCTOR OF PHILOSOPHY

WASHINGTON STATE UNIVERSITY  
School of Electrical Engineering and Computer Science

MAY 2024

© Copyright by RABIA KHAN, 2024  
All Rights Reserved

© Copyright by RABIA KHAN, 2024  
All Rights Reserved

To the Faculty of Washington State University:

The members of the Committee appointed to examine the dissertation of RABIA KHAN find it satisfactory and recommend that it be accepted.

Noel N. Schulz, Ph.D., Chair

Anjan Bose, Ph.D.

Anamika Dubey, Ph.D.

Sanjeev Pannala, Ph.D.

## ACKNOWLEDGMENT

My dissertation journey would not have been possible without the continuous support and guidance of my advisor, committee members, family, and friends.

First, I would like to express my gratitude to my advisor, Dr. Noel N. Schulz, for giving me an opportunity to work under her supervision for my Ph.D. I am forever grateful for her constant motivation, inspiration, and support in excelling in my field and life. I am obliged to her for critical inspection at each step of my work and for providing constructive feedback. I acknowledge her immense understanding and support throughout my maternity leaves as well as Ph.D. journey.

I want to sincerely thank the rest of my dissertation committee members, Dr. Anjan Bose, Dr. Anamika Dubey, and Dr. Sanjeev Pannala, for their time, encouragement, and valuable comments. I am indebted for their constructive criticism, informative suggestions, and critical questions, which helped me achieve my desired goal in this dissertation. I would like to extend my true appreciation to my all course teachers at WSU. I would also like to thank WSU ESIC Staff, Jeannine, Smitha, and Darlene for their help and support at every step. I am grateful to the U.S. Department of Energy for their support through US-India CollAborative For Smart DiStribution System With SStorage (UI-ASSIST) project. I want to extend my thanks to Ian Baring-Gould and the team at the National Renewable Energy Laboratory for their assistance in my project work, which has significantly developed my skill set.

I am thankful to the Almighty for His blessings and to my family for their invaluable contributions to my life journey. I appreciate my labmates and friends' line of thought, discussions, and useful feedback. I am grateful to my parents, siblings, and inlaws for their support and motivation throughout my doctoral journey. I would like to thank my parents, Kausar and Zahid, who are among my life's best human beings. Their unconditional love, sacrifices, support, and hard work are the reasons behind my success, and I dedicate this

dissertation to them.

Lastly, I want to extend my gratitude to my husband, Umer, who has been my unwavering support. Words fail to capture the depth of my appreciation for him. He is my greatest cheerleader, best friend, and an exceptional partner and parent. Completing this dissertation would have been impossible without his positivity, love, encouragement, and support. I am also thankful to my children, Anabia and Anaya, whose remarkable understanding and patience have enabled me to persevere through these past few years and complete my Ph.D.

PEER-TO-PEER POWER SHARING IN DC MICROGRIDS  
FOR RURAL ELECTRIFICATION

Abstract

by Rabia Khan, Ph.D.  
Washington State University  
May 2024

Chair: Noel N. Schulz

Remote rural regions without electricity access suffer from energy poverty and reduced opportunities for the population. Microgrid architectures with optimal planning, design, and operation strategies are essential to meet rural inhabitants' energy demands. DC microgrids based on photovoltaic panels and batteries are used for remote rural electrification. Centralized islanded systems have shortcomings, i.e., high distribution losses, less efficiency, and are comparatively more expensive than distributed microgrids. The distributed systems comprise independent household prosumers that may work independently or integrated.

The first concept presented in this thesis is a detailed distribution loss analysis of both centralized and distributed microgrid architectures with dynamic load and generation profiles. The distribution loss modeling is extended to low-voltage, low-power islanded DC microgrids. A detailed network loss analysis of four different microgrid architectures is performed using modified Newton-Raphson power flow for DC systems. These architectures include, 1) Centralized generation centralized storage (CGCS), 2) Centralized generation distributed storage (CGDS), 3) Distributed generation centralized storage (DGCS), and 4) Distributed generation distributed storage (DGDS), which are implemented with both radial

and ring interconnection schemes using time-varying load demand and dynamic PV generation. A comparative distribution loss analysis with various conductor sizes and voltage levels shows that the distributed ring architecture has significant advantages based on low distribution losses, high efficiency, and low voltage drop. It offers an additional feature of scalability and lower capital cost. Secondly, a detailed distribution and conversion loss modeling and analysis is performed for centralized and distributed microgrid architectures using the bus injection method and modified Newton-Raphson power flow method. A comparative power system and power electronic loss analysis for both architectures show that distributed architectures have higher efficiency and lower losses than centralized. Third, the optimal power dispatch and power-sharing among spatially distributed nanogrids are performed to minimize distribution losses and maximize power electronic conversion efficiency in a typical islanded DC microgrid (IDCMG) for rural electrification. A branch flow model is proposed for modeling the power system with DC-DC converters. The optimal power flow is performed by relaxing the original non-convex constraints using second-order conic programming and is implemented on the modified IEEE-14 bus system. This generic framework can be used for optimal energy management in islanded microgrids using the regional solar irradiance information, climate situations, and energy requirements.

The key contributions of this dissertation are: i) A comprehensive distribution loss analysis of centralized and distributed microgrid architectures, ii) Developing a mathematical framework and modeling of distribution and power electronic losses, and iii) Optimal peer-to-peer power sharing in DC microgrids for rural electrification.

# TABLE OF CONTENTS

	Page
ACKNOWLEDGMENT . . . . .	iii
ABSTRACT . . . . .	v
LIST OF TABLES . . . . .	xiii
LIST OF FIGURES . . . . .	xvi
CHAPTER	
1 INTRODUCTION . . . . .	1
1.1 Background and Motivation . . . . .	1
1.2 Problem Statement . . . . .	3
1.3 Research Objectives and Task . . . . .	4
1.4 Contributions . . . . .	5
1.5 Dissertation Organization . . . . .	6
2 MODIFIED NEWTON-RAPHSON POWER FLOW FOR DC MICROGRIDS	7
2.1 Introduction . . . . .	7
2.2 Modified Newton-Raphson Power Flow Model with Time-Varying Generation and Load Demand for DC Systems . . . . .	8
2.3 Islanded Microgrid Model . . . . .	11
2.3.1 Model of nanogrid . . . . .	12
2.3.2 Model of village . . . . .	12
2.3.3 Centralized Microgrid Model . . . . .	13
2.3.4 Distributed Microgrid Model . . . . .	14
2.3.5 Conductor Sizes and Ampacity . . . . .	16



	Page
2.4 Case Study: Performance Analysis of Microgrid Architectures . . . . .	16
2.4.1 Time series generation and dynamic load . . . . .	17
2.4.2 Comparison between radial and ring microgrid architectures . . . .	19
2.4.3 Comparison between centralized and distributed microgrid archi- tectures . . . . .	23
2.5 Summary . . . . .	26
3 DISTRIBUTION LOSS ANALYSIS IN LOW-VOLTAGE LOW-POWER DC MICROGRIDS FOR RURAL ELECTRIFICATION . . . . .	27
3.1 Introduction . . . . .	27
3.2 Village Orientation-based Microgrid Architectures . . . . .	27
3.2.1 Spatial Village Orientations . . . . .	28
3.2.2 CGCS Microgrid Architecture . . . . .	28
3.2.3 DGCS Microgrid Architecture . . . . .	28
3.2.4 CGDS Microgrid Architecture . . . . .	29
3.2.5 DGDS Microgrid Architecture . . . . .	31
3.3 MODIFIED NEWTON-RAPHSON DC power flow Analysis with Dynamic Load Demand . . . . .	31
3.3.1 Conductor Sizes . . . . .	32
3.3.2 Time-varying generation and load demand . . . . .	33
3.4 Results and Discussions . . . . .	33
3.4.1 Comparison between radial and ring microgrid architectures . . . .	33
3.4.2 Comparison between CGCS and DGDS ring microgrid architecture with conductor sizes . . . . .	33

3.4.3	Comparison between DGCS and CGDS radial microgrid architecture with conductor sizes . . . . .	34
3.4.4	CGCS ring microgrid architecture . . . . .	35
3.4.5	DGDS radial microgrid architecture . . . . .	35
3.5	Summary . . . . .	39
4	POWER ELECTRONIC LOSS MODELING IN MODIFIED NEWTON-RAPHSON POWER FLOW FOR DC MICROGRID SYSTEMS . . . . .	40
4.1	Introduction . . . . .	40
4.2	Modeling of Islanded DC microgrid system . . . . .	41
4.2.1	Centralized Microgrid Architecture . . . . .	41
4.2.2	Distributed Microgrid Architecture . . . . .	42
4.2.3	Framework of Microgrids . . . . .	42
4.3	Power Loss Modeling . . . . .	43
4.3.1	Distribution Losses . . . . .	43
4.3.2	Converter Losses . . . . .	44
4.4	Bus Injection Method with Modified Newton-Raphson Power Flow . . . . .	48
4.5	Results And Discussion . . . . .	50
4.5.1	Test System . . . . .	50
4.5.2	Performance Analysis . . . . .	50
4.6	Summary . . . . .	53
5	OPTIMAL POWER DISPATCH IN DC ISLANDED MICROGRIDS AND OPTIMAL POWER FLOW IN DGDS DC MICROGRIDS . . . . .	54
5.1	Introduction . . . . .	54
5.2	Modeling of islanded DC microgrid system . . . . .	56

5.2.1	Nanogrid Model . . . . .	56
5.2.2	Distributed Generation Distributed Storage Architecture . . . . .	57
5.2.3	Distribution Losses . . . . .	58
5.2.4	Converter Losses . . . . .	59
5.3	Optimal Power Flow Problem Formulation of DC islanded microgrid system	61
5.3.1	Branch flow Model . . . . .	61
5.3.2	Converter Efficiency and Distribution Loss Optimization . . . . .	62
5.3.3	Proposed Algorithm . . . . .	64
5.4	Results And Discussion . . . . .	64
5.4.1	Test System . . . . .	65
5.4.2	Case Study . . . . .	65
5.4.3	Static Loads . . . . .	66
5.4.4	Dynamic Loads . . . . .	67
5.4.5	Scheduled Power . . . . .	68
5.4.6	Converter Efficiency . . . . .	68
5.4.7	Number of Operating Converters . . . . .	69
5.4.8	Loss Evaluation . . . . .	70
5.5	Optimal Power Dispatch in Islanded DC Clustered Nanogrids for Rural Electrification . . . . .	79
5.5.1	DC Islanded Microgrid Model . . . . .	80
5.5.2	Proposed Algorithm . . . . .	80
5.5.3	Test System . . . . .	81
5.6	Summary . . . . .	87
6	CONCLUSIONS AND FUTURE WORK . . . . .	88

6.1	Summary of Contributions . . . . .	88
6.1.1	Distribution Loss Analysis of Centralized and Distributed Microgrid Architectures . . . . .	89
6.1.2	Mathematical Framework and Modeling of Distribution and Power Electronic Losses . . . . .	89
6.1.3	Optimal Power Dispatch and Peer-to-Peer Power Sharing Scheme for Rural Electrification . . . . .	90
6.2	Future Research Directions . . . . .	90
6.3	Publications . . . . .	91
	REFERENCES . . . . .	98

## LIST OF TABLES

TABLE	Page
2.1 American Wire Gauge (AWG) Conductor Sizes and Properties ( <i>Ampacity</i> : n.d.). . . . .	16
2.2 Ampacity for distributed ring and radial interconnections . . . . .	17
2.3 Comparison between distributed radial and ring architectures for winters . .	19
2.4 Comparison between centralized radial and ring architectures for summers .	22
2.5 Comparison between centralized radial and ring architectures for winters . .	22
2.6 Comparison between distributed radial and ring architectures for summers .	22
2.7 Comparison between centralized and distributed ring architectures for summers	23
2.8 Comparison between centralized and distributed ring architectures for winters	23
3.1 Comparison between radial and ring interconnections for microgrid architec- tures at 48V . . . . .	34
3.2 Comparison between CGCS and DGDS ring microgrid architecture with con- ductor sizes . . . . .	34
3.3 Comparison between DGCS and CGDS radial microgrid architecture with conductor sizes . . . . .	35
4.1 Topologies of DC–DC Converters (Martander, 2002,). . . . .	44
4.2 Parameters for the Inductance of DC-DC Converter . . . . .	47
4.3 Parameters for the Diode of DC-DC Converter . . . . .	47
4.4 Parameters for the MOSFET of DC-DC Converter . . . . .	48
4.5 Analytical comparison of centralized vs. distributed systems (Mshood Nasir, 2018.) . . . . .	51

5.1	OPF-1 for modified 14 bus DC Microgrid System. . . . .	67
5.2	OPF-2 for modified 14 bus DC Microgrid System. . . . .	68
5.4	OPF-2 with Unbalanced SOCs. . . . .	69
5.5	OPF-1 for DC Clustered Microgrid System. . . . .	82
5.6	OPF-2 for DC Clustered Microgrid System. . . . .	82

## LIST OF FIGURES

FIGURE	Page
1.1	Number of people without electricity access by region. (Küfeoğlu, 2022) . . . . . 2
1.2	Annual reduction in the number of people by region (Küfeoğlu, 2022). . . . . 2
2.1	Power system for modified Newton-Raphson for DC systems . . . . . 8
2.2	Model of nanogrid . . . . . 12
2.3	Radial interconnection of the microgrid (Mashood Nasir, Hassan Abbas Khan, Hussain, et al., 2017) . . . . . 13
2.4	Ring interconnection of the microgrid (Mashood Nasir, Hassan Abbas Khan, Hussain, et al., 2017) . . . . . 14
2.5	Centralized microgrid model (Jonnes, 2004). . . . . 15
2.6	Distributed Microgrid Model (Mashood Nasir, Hassan Abbas Khan, Hussain, et al., 2017). . . . . 15
2.7	PV generation and Load multiplier curves for summers . . . . . 18
2.8	Percentage Voltage Drop at different voltages and conductor sizes for centralized radial and ring architectures for summer season . . . . . 20
2.9	Percentage Voltage Drop at different voltages and conductor sizes for distributed radial and ring architectures for summer season . . . . . 21
2.10	Percentage efficiency at different voltages and conductor sizes for ring interconnection of summer season . . . . . 24
2.11	Percentage efficiency at different voltages and conductor sizes for radial interconnection of summer season . . . . . 25
3.1	Centralized Generation Centralized Storage Microgrid Architecture (Mashood Nasir, Hassan Abbas Khan, Hussain, et al., 2017). . . . . 29
3.2	Distributed Generation Centralized Storage Microgrid Architecture . . . . . 30

3.3	Centralized Generation Distributed Storage Microgrid Architecture . . . . .	30
3.4	Distributed Generation Distributed Storage Microgrid Architecture (Mashood Nasir, Hassan Abbas Khan, Hussain, et al., 2017). . . . .	31
3.5	Percentage voltage drop of CGCS . . . . .	36
3.6	Percentage voltage drop of DGDS . . . . .	36
3.7	Percentage efficiency of DGDS in radial connection . . . . .	37
3.8	Percentage efficiency of DGDS in ring connection . . . . .	38
4.1	Schematic Diagram of GS Block . . . . .	41
4.2	Schematic of individual household in centralized and distributed microgrids .	42
4.3	Ring orientation of households in microgrid . . . . .	43
4.4	DC-DC converter . . . . .	45
4.5	Loading vs. efficiency curve of a DC-DC converter . . . . .	47
4.6	Power losses of centralized vs. distributed architectures . . . . .	51
4.7	Percentage efficiency of centralized vs. distributed architectures . . . . .	52
4.8	Percentage voltage drop of centralized vs. distributed architectures . . . . .	52
5.1	Nanogrid model with components. . . . .	57
5.2	Distributed Generation Distributed Storage Architecture. . . . .	58
5.3	Framework for loss estimation. . . . .	59
5.4	Loading vs. efficiency curve of a DC-DC converter. . . . .	60
5.5	Proposed Algorithm for Optimal Power Dispatch. . . . .	65
5.6	Modified 14 Bus Test System Architecture as DC Microgrid for rural areas. .	66
5.7	PV Generation and Load Multipliers. . . . .	70
5.8	Power scheduled in OPF-1 for modified 14 bus DC Microgrid System. . . . .	71
5.9	Power scheduled in OPF-2 for modified 14 bus DC Microgrid System. . . . .	72
5.10	Converter Efficiency in OPF-1 for 14 bus system. . . . .	73
5.11	Converter Efficiency in OPF-2 for 14 bus system. . . . .	74



5.12 Comparison of operating converters in 14 bus system. . . . .	75
5.13 Comparison of distribution losses of 14 bus system. . . . .	76
5.14 Comparison of conversion losses of 14 bus system. . . . .	77
5.15 Comparison of total losses of 14 bus system. . . . .	78
5.16 Clusters of nanogrids in DGDS Architecture. . . . .	80
5.17 Proposed Algorithm For Power Dispatch Strategy . . . . .	84
5.18 Power dispatch at users in OPF-2 . . . . .	85
5.19 Power dispatch at users in OPF-1 . . . . .	85
5.20 Total System losses in OPF-1 and OPF-2 . . . . .	86

## Dedication

This dissertation is dedicated to  
my Mother, Kausar Zarin Khan, and Father, Zahid Iqbal Khan

# CHAPTER ONE

## INTRODUCTION

### 1.1 Background and Motivation

According to the International Energy Agency (IEA), 745 million people (12% of the global population) are still suffering from energy poverty (Küfeoğlu, 2022), as shown in Fig. 1.1 and Fig. 1.2. The United Nations (UN) has introduced sustainable development goals (SDG), where SDG-7 aims to provide clean, affordable, reliable, and sustainable energy to everyone by 2030 (Nations, 2015). Approximately 85% of people without power are rural inhabitants who depend on kerosene, candles, and wood to fulfill their basic requirements of domestic lighting and heating (Hamza et al., 2017). The usage of these resources harms public health and the environment. Alternatively, these communities must be electrified to improve their socio-economic status and enhance human development factors, e.g., education, health, agriculture, and employment opportunities (R. Khan and Schulz, 2020; Parimalram Achintya Madduri et al., 2016).

Extending the grid to remote rural regions is prohibitive because of i) high infrastructure costs, ii) significant transmission line losses, iii) electricity theft, and iv) unreliable service with frequent load shedding (Moksnes et al., 2020; Moner-Girona et al., 2017). Alternatively, there has been an increase in the deployment of stand-alone systems over the past decade due to their ease of installation (J. Khan and Arsalan, 2016). However, individual solar home systems lack scalability and require complex financial resources. They are expensive and suboptimal compared to integrated microgrid systems, which have a better leveled cost of electricity (LCOE) and benefit from usage diversity (Mshood Nasir, 2018; PwC, 2016). Therefore, this research focuses on DC microgrids for their utility and higher electrification potential.

Most rural areas in Southeast Asia and Africa receive abundant sunlight, with solar

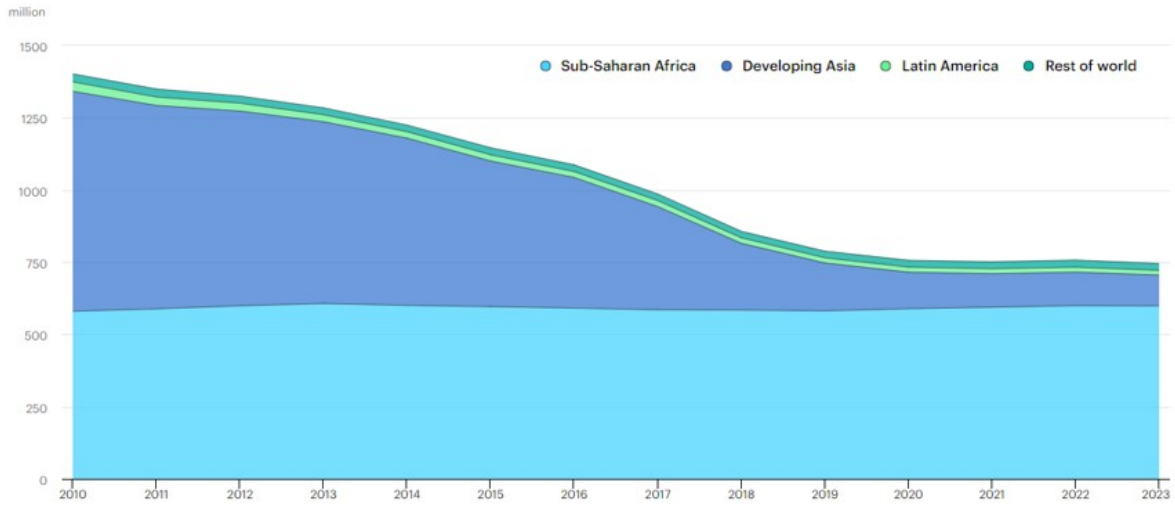


**Figure 1.1** Number of people without electricity access by region. (Küfeoğlu, 2022)

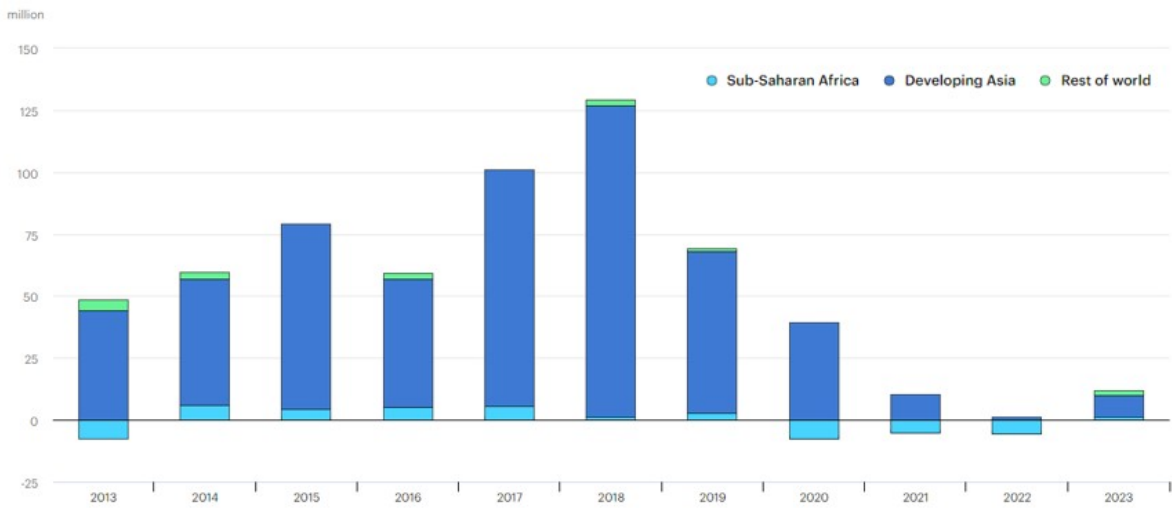


**Figure 1.2** Annual reduction in the number of people by region (Küfeoğlu, 2022).

irradiance of  $5.5kWh/m^2/day$  and above (Mashood Nasir, Jin, et al., 2018), making solar a promising DC source compared to other renewable energy resources. Over the past decade, there has been a significant increase in the practical installation of solar PV-based DC microgrids in these areas (Balls and Fischer, 2019; Palit, 2013; Gelani, Dastgeer, et al., 2021). The reasons include; i) rapid decrease in the prices of solar panels and batteries, ii) extensive market availability of DC Loads, iii) development of power electronics resulting in high-efficiency DC-DC converters (Williams et al., 2015; Ubilla et al., 2014; Bardouille et al., 2012), and iv) reduction of redundant conversion stages (AC-DC and vice versa) (P Achintya Madduri et al., 2013; Zhang et al., 2011; Liu et al., 2021). PV-Battery-based Islanded DC microgrids (IDCMGs) are a viable solution for rural electrification in remote areas, offering additional benefits of high operational efficiency, cost-effectiveness, and availability of DC sources and loads (Mashood Nasir, Jin, et al., 2018).

## 1.2 Problem Statement

Nasir et al. proposed a scalable distributed DC microgrid architecture with power-sharing capability in (Mashood Nasir, Hassan Abbas Khan, Hussain, et al., 2017; Mashood Nasir, Jin, et al., 2018; Mashood Nasir, Hassan Abbas Khan, Niazi, et al., 2019; Iqbal, Mehran, and Mashood Nasir, 2021). The peer-to-peer energy-sharing approach was developed in (Iqbal, Mehran, and Mashood Nasir, 2021). However, the research presented in the literature focused solely on addressing distribution losses.

The Optimal Power Flow (OPF) algorithm is paramount for optimizing power system planning, operation, analysis, and scheduling. Its implementation is challenging due to the non-linear nature of power flow equations, rendering the optimization problem non-convex. Consequently, obtaining a globally optimal solution is very detailed, although the problem can be approximated through relaxation to form a convex problem (Farivar and S. H. Low, 2013). This relaxed problem can be verified by ensuring that the obtained solutions satisfy

the nonlinear inequality constraints. The Second-Order Cone Program (SOCP) and Semi-Definite Program (SDP) represent widely used relaxation techniques. In a previous study, the Branch Flow Method (BFM) was employed (Gan and Steven H Low, 2014; Li et al., 2018), by Low et al. and it was demonstrated that the SOCP relaxation can be exact. Particularly, the optimal solution can be unique within DC networks, independent of system topologies and operational modes. They successfully solved the OPF for DC microgrids.

### 1.3 Research Objectives and Task

The research presented in this work utilizes the DGDS microgrid architecture with neighborhood-level peer-to-peer power-sharing capability to model both distribution and conversion losses. In (Mashood Nasir, Hassan Abbas Khan, Hussain, et al., 2017), the optimal planning of DC microgrids was performed with constant converter losses. Nevertheless, subsequent research by Kolar et al. (Kolar et al., 2012) and Gelani et al. (Gelani, Mashood Nasir, et al., 2017) has demonstrated that the efficiency of a DC-DC converter varies with the output power. As a result, power electronic losses are not static throughout the operation; they depend on the percentage loading and the output power. A notable contribution of our work involves evaluating and optimizing all distribution and conversion losses, encompassing i) constant, ii) linear, and iii) quadratic losses.

Our research improves the BFM introduced in (Li et al., 2018) to incorporate converter and distribution losses. Given that many distributed DC microgrid systems are dominated by power electronics converters, considering only distribution losses while neglecting power electronic conversion losses may lead to inaccurate system-level analysis. Our approach addresses this gap by including the power electronic conversion losses in the OPF problem to optimize the power dispatch of distributed energy resources (DERs). An optimization algorithm is developed to allow optimal peer-to-peer power-sharing by minimizing total distribution losses and maximizing power electronics efficiencies.

## 1.4 Contributions

To summarize, the key overall contribution of this dissertation is developing a mathematical framework based on the improved BFM, which offers detailed modeling of distribution and power electronics conversion losses for IDCMGs aimed at rural electrification.

Our first contribution is a detailed distribution loss analysis of both centralized and distributed microgrid architectures with dynamic load and generation profiles. The distribution loss modeling is extended to low-voltage, low-power islanded DC microgrids. A detailed network loss analysis of four different microgrid architectures is performed using modified Newton-Raphson power flow for DC systems. These architectures include 1) Centralized generation centralized storage (CGCS), 2) Centralized generation distributed storage (CGDS), 3) Distributed generation centralized storage (DGCS), and 4) Distributed generation distributed storage (DGDS), which are implemented with both radial and ring interconnection schemes using time-varying load demand and dynamic PV generation. A comparative distribution loss analysis with various conductor sizes and voltage levels shows that the distributed ring architecture is significantly advantageous based on low distribution losses, high efficiency, and low voltage drop. It offers an additional feature of scalability and low capital cost.

Our second contribution is a detailed distribution and conversion loss modeling and analysis for centralized and distributed microgrid architectures using the bus injection method and modified Newton-Raphson power flow method. A comparative power system and power electronic loss analysis for both architectures show that distributed architectures have higher efficiency and lower losses than centralized.

Our third contribution is the development of a mathematical framework based on the improved BFM, which offers detailed modeling of distribution and power electronics conversion losses for IDCMGs aimed at rural electrification. It involves formulating a multi-objective optimization problem that seeks to maximize conversion efficiencies and minimize distri-

bution losses within the system while optimally dispatching power by distributed energy resources. An optimization algorithm is developed to allow peer-to-peer energy sharing among households while minimizing total system losses.

## 1.5 Dissertation Organization

The dissertation consists of five chapters. Chapter 2 presents a detailed distribution loss analysis of both centralized and distributed microgrid architectures with dynamic load and generation profiles.

Chapter 3 involves extending distribution loss modeling to low-voltage, low-power islanded DC microgrids. A detailed network loss analysis of four different microgrid architectures is performed using modified Newton-Raphson power flow for DC systems.

Chapter 4 covers the mathematical modeling of DC-DC converters in the Newton Raphson Power Flow for DC systems. It discusses the development of a loss model for the DC-DC converter that can describe the losses in all the converter elements. This chapter implements the converter loss model in distributed and centralized architectures to analyze system- and device-level losses in DC microgrids.

Chapter 5 is based on developing a mathematical framework through improved BFM, which offers detailed modeling of distribution and power electronics conversion losses for IDC MGs. It involves formulating a multi-objective optimization problem for optimal peer-to-peer power sharing in DC microgrids.

Chapter 6 concludes the dissertation and outlines the future scope of the research outlined in this thesis.



## CHAPTER TWO

### MODIFIED NEWTON-RAPHSON POWER FLOW FOR DC MICROGRIDS

#### 2.1 Introduction

This chapter introduces the modified Newton-Raphson power flow method for DC microgrids. Power flow analysis is used to determine the steady-state operating characteristics of the power system at a given set of conditions. For decades, various power flow methods have been used for AC power system analysis, e.g., Gauss-Seidel, Newton-Raphson, and Fast Decoupled methods (Saadat et al., 1999; Grainger and Stevenson Jr, 1994). However, the modified NR method for DC power flow analysis is presented in (**eight**; Farooq et al., 2014). It can be used for the performance analysis of any DC system to select optimal voltage levels and conductor sizes. Some critical factors, i.e., line losses, efficiency, and voltage drop, can also be calculated. The operation of a microgrid is dependent on the optimal voltage level, which further affects the control features and protection strategies (Glover, Sarma, and Overbye, 2012; Mashood Nasir, Hassan Abbas Khan, Hussain, et al., 2017). DC microgrid systems are analyzed in (Mashood Nasir, Zaffar, and Hassan Abbas Khan, 2016; Glover, Sarma, and Overbye, 2012; Mashood Nasir, Hassan Abbas Khan, Hussain, et al., 2017) for constant power generation and static loads.

The key contribution in this chapter is the improvement of the Newton-Raphson method for DC microgrids introduced in (Mashood Nasir, Zaffar, and Hassan Abbas Khan, 2016). The existing method is modified for time-varying distribution loss analysis with variable generation and load demand.

The Newton-Raphson method for AC systems is modified for DC based on their differences. The AC transmission lines have resistance, inductance, and capacitance depending on the length of the transmission line, while DC systems lack inductance and capacitance. So the admittance matrix is reduced to the conductance matrix due to zero susceptance in

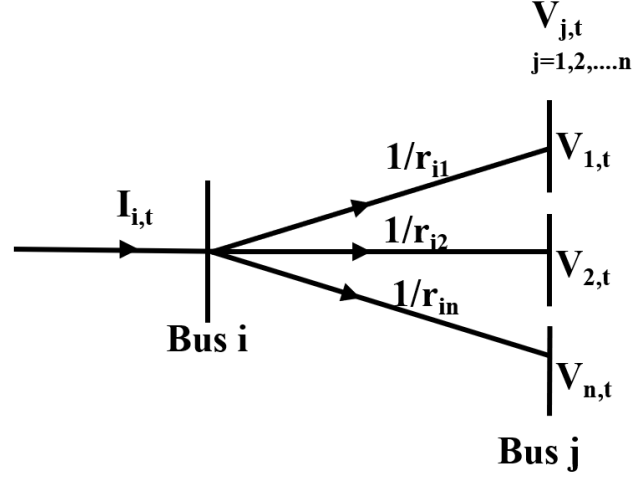


**Figure 2.1** Power system for modified Newton-Raphson for DC systems

DC systems, i.e.,  $Y_{ij}$  is replaced by  $G_{ij}$ . Secondly for DC sources of generation and loads, the reactive power generation and consumption are zero, i.e.,  $Q_i, Q_j=0$ . Third, there is no phase angle between the voltages at sending and receiving buses, i.e.,  $\delta_i, \delta_j=0$ .

## 2.2 Modified Newton-Raphson Power Flow Model with Time-Varying Generation and Load Demand for DC Systems

A typical power system for modified Newton-Raphson power flow is shown in Fig. 2.1. The values of conductance matrix  $G$  between any two buses  $i$  and  $j$  is  $g_{ij}$  calculated using resistance  $r_{ij}$  between the two buses as given by Eq. (2.1). These values formulate the conductance matrix of size  $2n \times 2n$  using Eq. (2.2).

$$G_{ij} = \left\{ \begin{array}{ll} \sum_{\substack{j=1 \\ j \neq i}}^{2n} \frac{1}{r_{ij}} & ; \forall i = j \\ -\frac{1}{r_{ij}} & ; \forall i \neq j \end{array} \right\} \quad (2.1)$$

$$G = \begin{bmatrix} G_{11} & G_{12} & \cdots & G_{1,2n-1} & G_{1,2n} \\ G_{21} & G_{22} & \cdots & G_{2,2n-1} & G_{2,2n} \\ \vdots & \vdots & \ddots & \vdots & \\ G_{2n-1,1} & G_{2n-1,2} & \cdots & G_{2n-1,2n-1} & G_{2n-1,2n} \\ G_{2n,1} & G_{2n,2} & \cdots & G_{2n-1,2n-1} & G_{2n,2n} \end{bmatrix}; G \in \mathbb{R}^{2n \times 2n} \quad (2.2)$$

Based on the load requirements, the power is scheduled at each bus, i.e.,  $P_t^{\text{sch}}$  using Eq. (2.3). The power scheduled at time instant  $t$  for  $2*n$  buses is given using Eq. (2.4). The actual power present at the bus at any instant is  $P_t^{\text{calc}}$ , calculated power. The difference between scheduled and calculated powers is used to evaluate voltages at each bus in multiple iterations until their mismatch is reduced to approximately zero or within some small tolerance.

$$P_t^{\text{sch}} = P_t^{\text{gen}} - P_t^{\text{load}} \quad (2.3)$$

$$P_t^{\text{sch}} = \begin{bmatrix} P_{1,t}^{\text{sch}} & P_{2,t}^{\text{sch}} & P_{3,t}^{\text{sch}} & \cdots & P_{2n,t}^{\text{sch}} \end{bmatrix}; P_t^{\text{sch}} \in \mathbb{R}^{2n \times 24} \quad (2.4)$$

The instantaneous power can be calculated by using the voltage of that bus and the total current flowing into that bus. The instantaneous calculated power at any bus is given by Eq. (2.5).

$$P_{i,t}^{\text{calc}} = V_{i,t} * I_{i,t} \quad (2.5)$$

Considering the power system shown in Fig. 2.1. With a conductance value of  $G_{ij}$  between buses  $i$  and  $j$ , the current at any bus  $i$  can be calculated using Kirchoff's current law (KCL) as given in Eq. (2.6).

$$I_{i,t} = \sum_{j=1}^{2n} G_{ij} * V_{j,t} \quad (2.6)$$

By inserting Eq. (2.6) in Eq. (2.5), we get the final equation for calculating power at each bus.

$$P_{i,t}^{\text{calc}} = \sum_{j=1}^{2n} V_{i,t} * V_{j,t} * G_{ij} \quad (2.7)$$

Therefore, the calculated power matrix is shown in Eq. (2.8);

$$P_t^{\text{calc}} = \begin{bmatrix} P_{1,t}^{\text{calc}} & P_{2,t}^{\text{calc}} & P_{3,t}^{\text{calc}} & \dots & P_{2n,t}^{\text{calc}} \end{bmatrix}; P_t^{\text{calc}} \in \mathbb{R}^{2n \times 1} \quad (2.8)$$

$$\begin{bmatrix} \Delta P_{2,t}^{(k)} \\ \Delta P_{3,t}^{(k)} \\ \vdots \\ \Delta P_{2n,t}^{(k)} \end{bmatrix} = \begin{bmatrix} \frac{\partial P_{2,t}^{(k)}}{\partial V_{2,t}} & \dots & \frac{\partial P_{2,t}^{(k)}}{\partial V_{2n,t}} \\ \frac{\partial P_{3,t}^{(k)}}{\partial V_{2,t}} & \dots & \frac{\partial P_{3,t}^{(k)}}{\partial V_{2n,t}} \\ \vdots & \ddots & \dots \\ \frac{\partial P_{2n,t}^{(k)}}{\partial V_{2,t}} & \dots & \frac{\partial P_{2n,t}^{(k)}}{\partial V_{2n,t}} \end{bmatrix} \begin{bmatrix} \Delta V_{2,t}^{(k)} \\ \Delta V_{3,t}^{(k)} \\ \vdots \\ \Delta V_{2n,t}^{(k)} \end{bmatrix} \quad (2.9)$$

In Eq. (2.9),  $\Delta P_{i,t}^{(k)}$  is a mismatch between scheduled  $P_{i,t}^{\text{sch}}$  and calculated powers  $P_{i,t}^{\text{calc}}$  at bus  $i$ , which are evaluated using Eqs. (2.3) and (2.7) respectively for  $k$  iterations. The term  $\Delta V_{i,t}$  represents the change in the voltage of bus  $i$  at each iteration  $k$  and time instant  $t$ . For multiple iterations,  $\Delta V$  is calculated at each bus until the power mismatch is approximately zero and the system is converged. The voltages at each bus are updated by adding  $\Delta V_{i,t}$  and the voltage  $V_{i,t}$  from the previous iteration until convergence is obtained. The converged value of voltages is used for finding the line losses  $LL_g(t)$  and the respective percentage line losses  $\%LL_g(t)$  using Eq. (2.10) and (2.11). Additionally percentage efficiency  $\%\eta_g(t)$  and percentage voltage drop  $\%VD_g(t)$  can be evaluated using Eq. (2.12) to (2.14) (Mashood

Nasir, Zaffar, and Hassan Abbas Khan, 2016).

$$LL_g(t) = \frac{1}{2} \sum_{i=1}^n \sum_{j=1}^n ((V_{i,t}(V_{i,t} - V_{j,t}) + V_{j,t}(V_{j,t} - V_{i,t})) * G_{ij}) \quad (2.10)$$

$$\%LL_g(t) = \frac{LL_g(t)}{P_G(t)}; \quad P_G(t) = \sum_{i=1}^n (P_{i,t} > 0) \quad (2.11)$$

$$\%\eta_g(t) = 100 - \%LL_g(t) \quad (2.12)$$

The percentage voltage drop is calculated by taking a difference between  $V_{\max}(t)$  and  $V_{\min}(t)$  and dividing by the  $V_{\max}(t)$  as given in Eq. (2.14) where  $V_{\max}(t)$  and  $V_{\min}(t)$  are the maximum and minimum values of voltage at any bus 'i' after  $k^{\text{th}}$  iteration at the time  $t$ .

$$VD_g(t) = V_{\max}(t) - V_{\min}(t) \quad (2.13)$$

$$\%VD_g(t) = \frac{V_{\max}(t) - V_{\min}(t)}{V_{\max}(t)} * 100 \quad (2.14)$$

### 2.3 Islanded Microgrid Model

The microgrid model considered in this study is an independent, self-sustaining, and inter-connection of electrical generation, storage, and loads. The current scope of work is related to PV generation, while other RES can also be included. Two microgrid architectures considered in this study include i) CGCS and ii) DGDS. The former architecture had only one point of generation and storage, while the loads were distributed across each household. The latter model assumes each household is an independent PV generation, storage, and load source. Thus, each house is called a nanogrid that can operate independently and in inter-connected forms. These nanogrids are connected in the same orientation as the houses in the villages of rural emerging areas. In this study, the houses are grouped to form clusters, which are connected to one another.

### 2.3.1 Model of nanogrid

In DGDS, each household in the village is termed a nanogrid with an assumption of independent PV generation, storage, and DC loads. It is a small building block for the whole DGDS microgrid architecture. These nanogrids can operate independently and can be connected in a scalable resource-sharing fashion to form the microgrid. The model of a nanogrid is shown in Fig. 2.2. Each household has two buses. The bus where PV, storage, and load are connected is considered a PV bus, while the bus connecting each nanogrid to another one is a feeder bus. The PV bus is connected to the feeder bus through a distribution line, represented by distribution resistance, while the resistance of the lines interconnecting two nanogrids is feeder resistance.

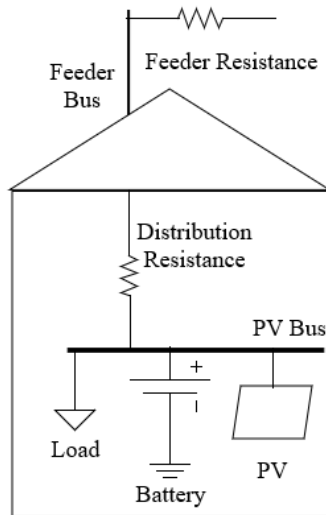


**Figure 2.2** Model of nanogrid

### 2.3.2 Model of village

The village model can have  $n$  different houses, which can be divided into  $x$  clusters based on the orientation of the houses in the selected region of the country. Each cluster is composed of  $n/x$  houses. These clusters can be interconnected in two different orientations, e.g., radial and ring interconnection, shown in Fig. 2.3 and Fig. 2.4, respectively. Radial interconnection

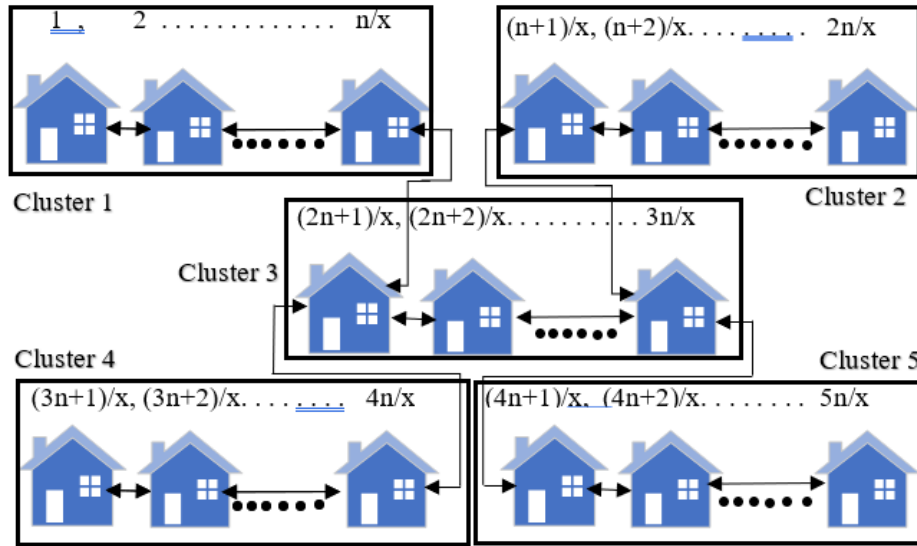


**Figure 2.3** Radial interconnection of the microgrid (Mashood Nasir, Hassan Abbas Khan, Hussain, et al., 2017)

includes fewer conductors, while ring structure uses an extra layer of conductors to connect the houses, making this interconnection expensive but more reliable (Glover, Sarma, and Overbye, 2012; V. Mehta and R. Mehta, 2011).

The village's architecture is assumed to have 40 houses divided into 5 clusters, with eight houses in each cluster. The microgrid configurations based on generation and storage are classified into DGDS and CGCS, which can be further analyzed using the Newton-Raphson method modified for DC power flow analysis.

### 2.3.3 Centralized Microgrid Model

The centralized microgrid model uses the exact orientation of the houses in the village, as discussed in the earlier section. However, each household serves as the load only. There is no PV generation and storage at the houses; however, a centralized PV generation capacity of 6.4 kWp and storage of 28.8 kWh is considered and calculated using the optimal sizing framework developed by Nasir et al. in (Mashood Nasir, Iqbal, and Hassan Abbas Khan, 2017). The centralized microgrid model considered is shown in Fig. 2.5. Each house is assumed to have a peak load capacity of 40 Wp, mainly lighting, fan, and charging phones

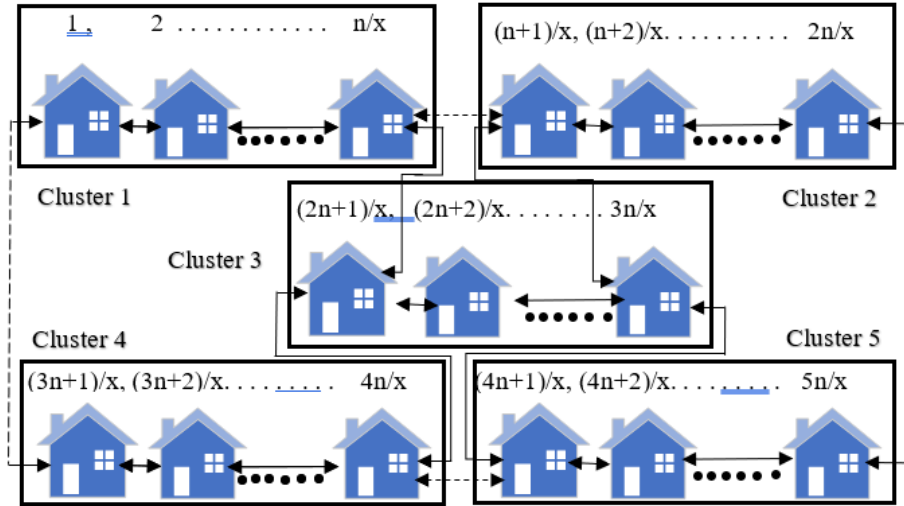


**Figure 2.4** Ring interconnection of the microgrid (Mashood Nasir, Hassan Abbas Khan, Hussain, et al., 2017)

(Mashood Nasir, Iqbal, and Hassan Abbas Khan, 2017). In comparison, the communal load capacity of 200 Wp is placed at the central location for community loads like water pumps, school loads, and medical centers. The supply to the communal load is from only the PV panel, and storage is at one location.

### 2.3.4 Distributed Microgrid Model

In distributed microgrid architecture, each house has self-generation through solar PV panels and local battery storage. The PV and the battery-rated capacities are 1.6 kWp and 0.72 kWh at each house, while the household and communal loads are 40 Wp and 200 Wp, respectively. These values are calculated using the optimal sizing method introduced by Nasir et al. in (Mashood Nasir, Iqbal, and Hassan Abbas Khan, 2017). Based on the load requirements, each house can share the power generated or stored with the neighboring houses and supply it to the communal load. The supply to community load in this scheme does not require the installation of a separate PV with a larger rating. The distributed microgrid model considered is shown in Fig. 2.6.



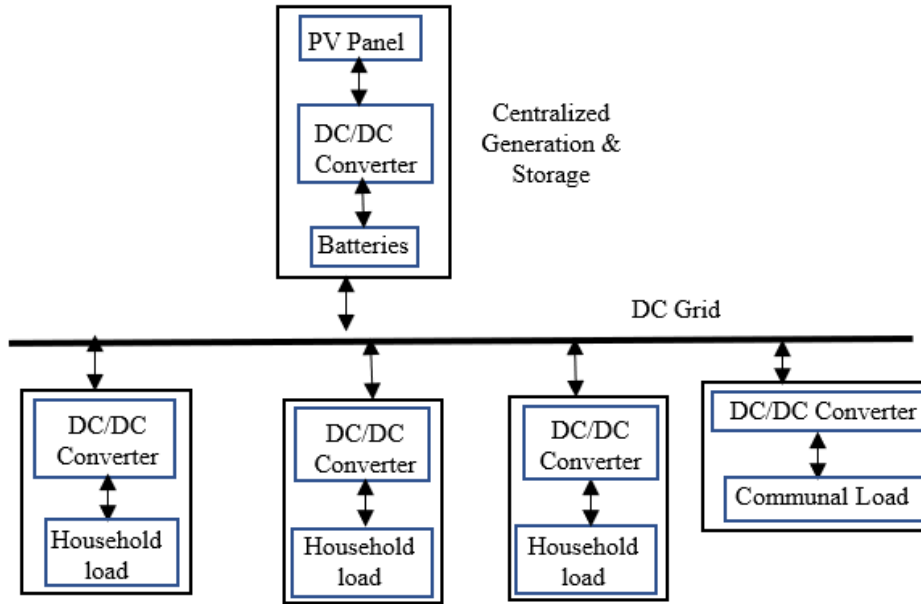


Figure 2.5 Centralized microgrid model (Jonnes, 2004).

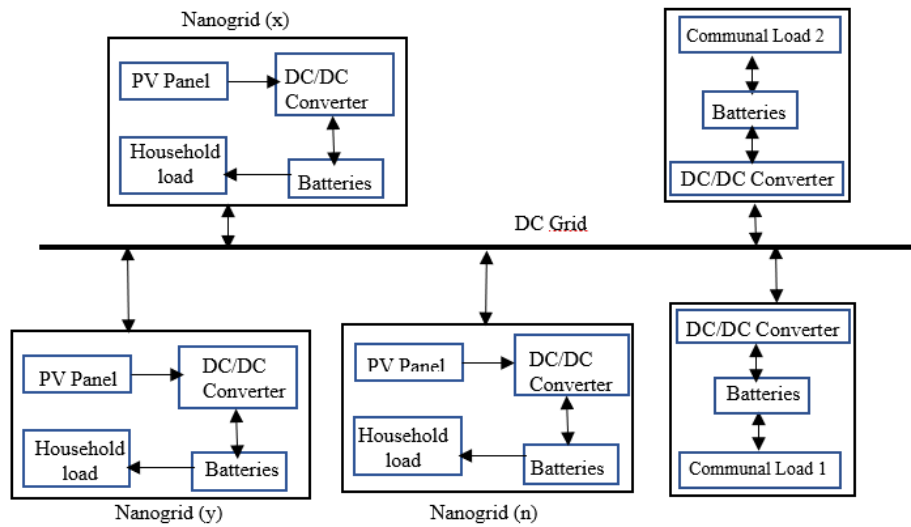


Figure 2.6 Distributed Microgrid Model (Mashood Nasir, Hassan Abbas Khan, Hussain, et al., 2017).

**Table 2.1** American Wire Gauge (AWG) Conductor Sizes and Properties (*Ampacity*: n.d.).

AWG number	Resistances (m/m)	Area (mm <sup>2</sup> )	Ampacity (Amps)
10	3.2	5.26	30
12	5	3.31	20
14	8	2.08	15
16	12.5	1.31	12
18	20	0.823	10

### 2.3.5 Conductor Sizes and Ampacity

The conductors considered are of various sizes, i.e., American Wire Gauge (AWG) number. The cost of each conductor decreases with an increase in the AWG number. Another important factor considered in this study is the ampacity of the conductor, also known as ampere capacity. It is defined by National Electrical Codes (NEC) as the maximum current a conductor can pass continuously under the conditions of use without increasing its temperature rating (*Ampacity*: n.d.). Table 2.1 lists conductors of different AWG numbers, their respective resistances, areas, and ampacities.

## 2.4 Case Study: Performance Analysis of Microgrid Architectures

The microgrid architectures for a typical village comprising of 40 houses are modeled in MATLAB. Different DC voltage levels have been suggested in the literature for the DC microgrid applications (Anand and Fernandes, 2010). In this research, viable DC voltage levels considered for the performance evaluation of the microgrid include 120 V, 240V, 325V, and 380 V. In addition to the voltage level, the conductor sizes are important in planning the microgrid system. Conductors with various possible AWG numbers are considered, i.e., AWG 10, AWG 12, AWG 14, AWG 16, and AWG 18.

b In our research methodology, two different design topologies, 1) Radial and 2) Ring, are studied using the Modified Newton Raphson method for DC systems, and their performance

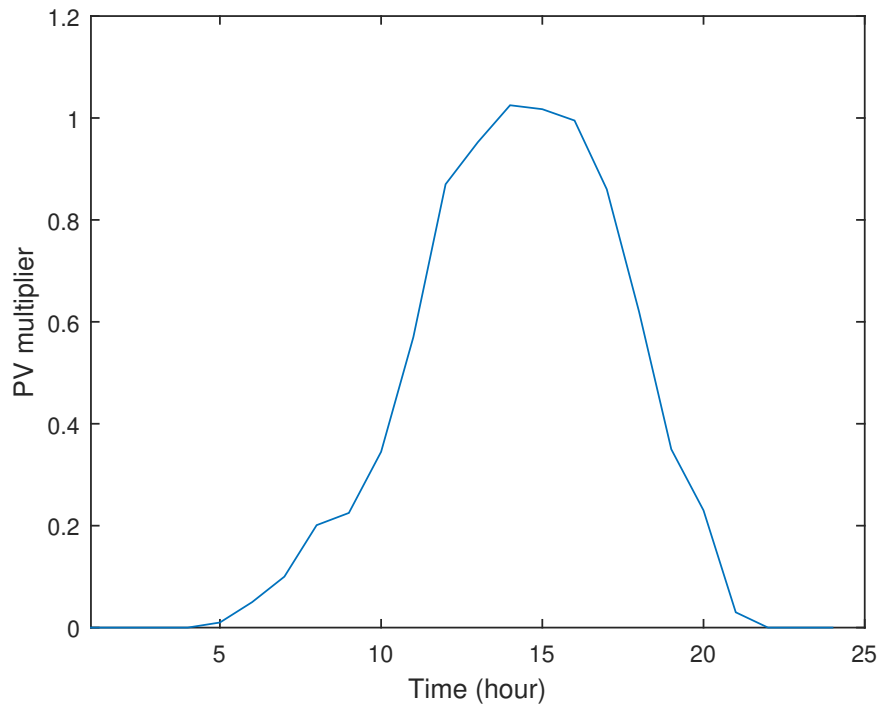
**Table 2.2** Ampacity for distributed ring and radial interconnections

Voltage Level	Ampacity (Radial) (Amps)	Ampacity (Ring) (Amps)
120	2.60	2.41
240	1.19	1.17
325	0.87	0.86
380	0.70	0.69

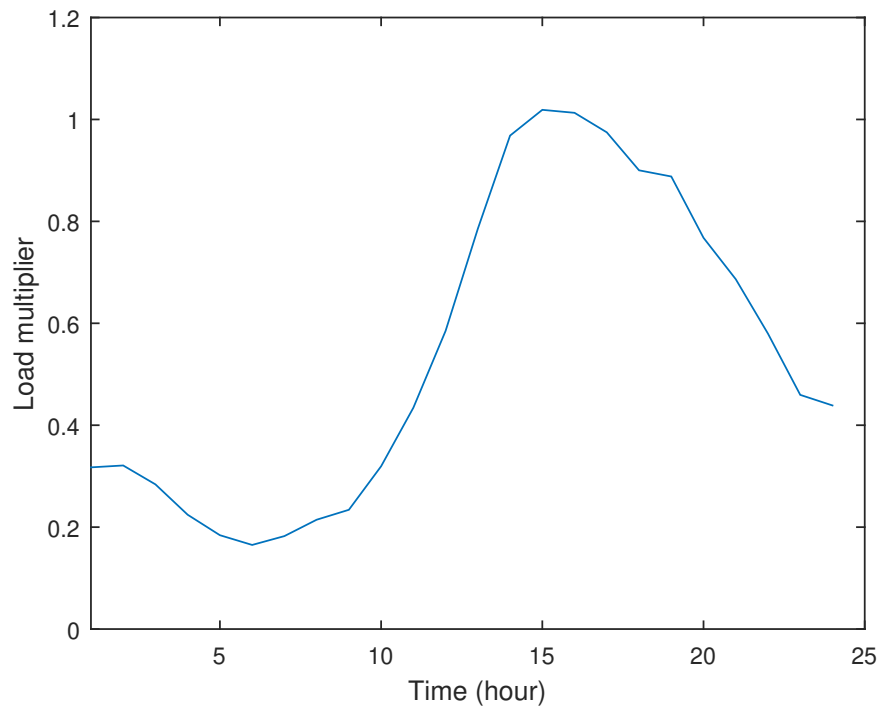
is evaluated by calculating efficiency, voltage drop, and distribution line losses. A time-varying dynamic load demand and the PV generation are assumed, which is discussed in the following sections.

#### 2.4.1 Time series generation and dynamic load

This study analyzes DC microgrid architectures with dynamically time-varying PV generation and load demand. The PV generation and load multiplier curves are obtained from the National Renewable Energy Laboratories (NREL) (*Solar Power Data for Integration Studies*- n.d.) and OpenDSS (*OpenDSS, EPRI Distribution System Simulator* n.d.), respectively for Ethiopia. The load shape is plotted using the default load data available in the OpenDSS resource forum. These curves are considered for 24 hours by interpolating the data with a 15-minute interval. The PV multiplier and load multiplier curves for summers are shown in Fig. 2.7: a and Fig. 2.7:b, respectively, based on the assumption that there is an increase in load demand at each home in the evening while at night and in the early morning the load demand is reduced. These multipliers are used with the assumed rated values of PV generation and load demand. The load demand and PV generation depend entirely on the location and corresponding population. Therefore, these curves can be modified for the chosen location and its residents.



(a) PV generation multiplier curve for summers (*Solar Power Data for Integration Studies*- n.d.)



(b) Load multiplier curve for summers (*OpenDSS, EPRI Distribution System Simulator* n.d.)

**Figure 2.7** PV generation and Load multiplier curves for summers

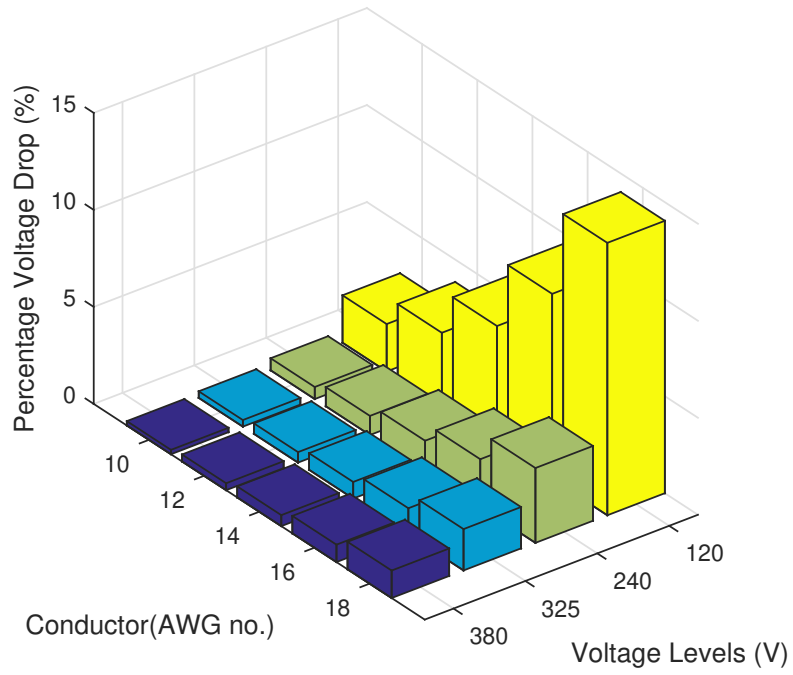
**Table 2.3** Comparison between distributed radial and ring architectures for winters

<b>Voltage (V)</b>	<b>Ring</b>			<b>Radial</b>		
	<b>Efficiency (%)</b>	<b>VD (%)</b>	<b>LL (%)</b>	<b>Efficiency (%)</b>	<b>VD (%)</b>	<b>LL (%)</b>
<b>120</b>	96.56	4.38	3.44	86.32	14.91	13.68
<b>240</b>	99.10	1.12	0.90	96.74	3.69	3.23
<b>325</b>	99.51	0.61	0.49	98.19	2.04	1.81
<b>380</b>	99.67	0.41	0.33	98.80	1.35	1.20

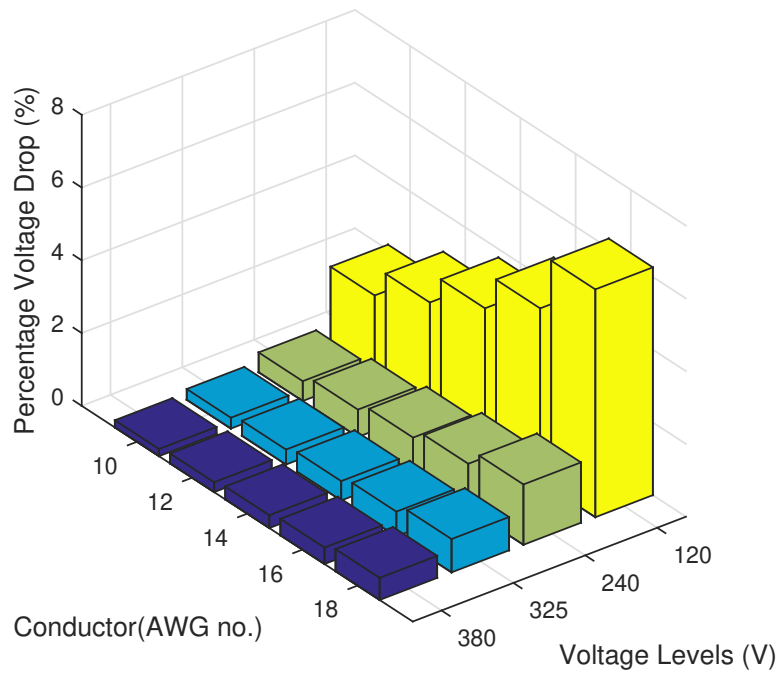
#### 2.4.2 Comparison between radial and ring microgrid architectures

The village modeled in this study can have two different interconnection schemes, 1) Radial and 2) Ring, as shown in Fig. 2.3 and Fig. 2.4, respectively. The microgrid architectures with both interconnecting schemes are compared to the same loading conditions. The ampacity through conductors is calculated and given in Table. 2.2. These values are far less than the rated values in Table. 2.1.

Tables 2.4 and 2.5 show radial and ring architecture results using centralized and distributed generation and storage systems for summers and winters, respectively. It is clear from the results that ring interconnection schemes have higher efficiency, increased reliability, and lower line losses than the radial scheme. Fig. 2.8:a and Fig. 2.8:b compare %voltage drop for a wide range of voltages and conductor sizes for centralized radial and ring interconnections, respectively, for the summer. For distributed microgrid architectures, Fig. 2.9:a and Fig. 2.9:b compare %voltage drop for the winter season. It is evident that the radial scheme has a lower conductor cost but high voltage drops and reliability issues that make it a poor choice for the optimal microgrid design. The ring interconnection scheme has a large number of conductors and an increased cost, but it offers higher reliability. Moreover, the results show mean values of the parameters by using 15-minute time-elapse-based 24-hour load and generation profiles, which helps in planning close to real-time data.

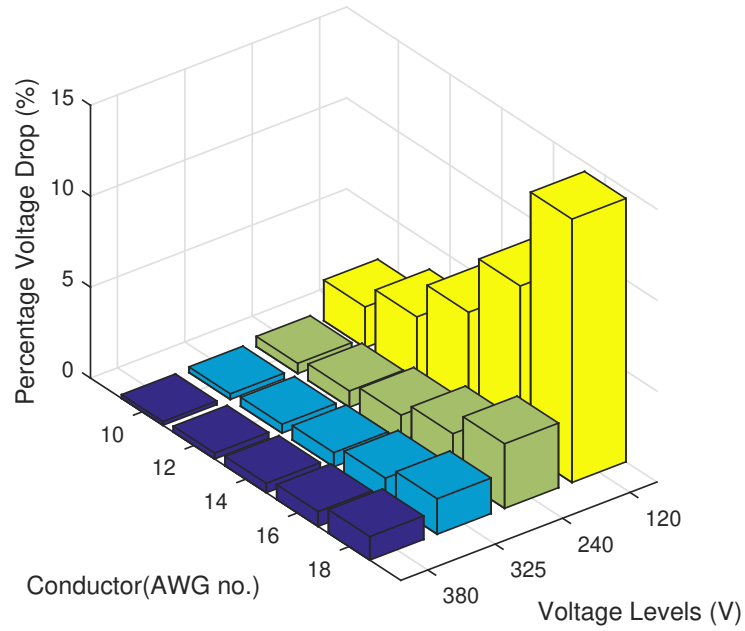


(a) Centralized radial interconnection

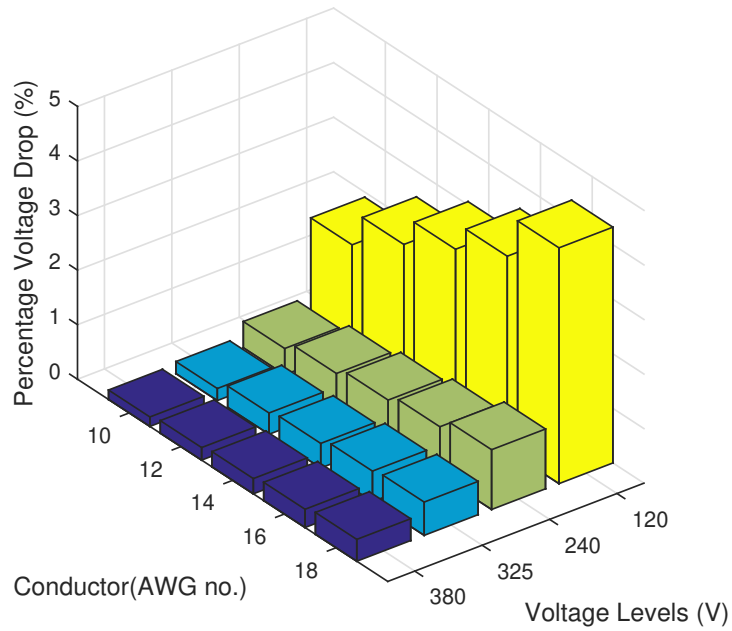


(b) Centralized ring interconnection

**Figure 2.8** Percentage Voltage Drop at different voltages and conductor sizes for centralized radial and ring architectures for summer season



(a) Distributed radial interconnection



(b) Distributed ring interconnection

**Figure 2.9** Percentage Voltage Drop at different voltages and conductor sizes for distributed radial and ring architectures for summer season

**Table 2.4** Comparison between centralized radial and ring architectures for summers

Voltage (V)	Ring			Radial		
	Efficiency (%)	VD (%)	LL (%)	Efficiency (%)	VD (%)	LL (%)
<b>120</b>	95.96	6.26	4.04	91.65	14.04	8.35
<b>240</b>	98.91	1.66	1.09	97.74	3.86	2.26
<b>325</b>	99.40	0.920	0.60	98.75	2.13	1.25
<b>380</b>	99.60	0.61	0.40	99.17	1.42	0.83

**Table 2.5** Comparison between centralized radial and ring architectures for winters

Voltage (V)	Ring			Radial		
	Efficiency (%)	VD (%)	LL (%)	Efficiency (%)	VD (%)	LL (%)
<b>120</b>	94.36	5.87	5.64	82.32	17.49	16.86
<b>240</b>	98.46	1.57	1.54	96.56	3.44	3.88
<b>325</b>	99.14	0.87	0.86	98.08	1.92	2.15
<b>380</b>	99.43	0.58	0.57	98.72	1.28	1.43

**Table 2.6** Comparison between distributed radial and ring architectures for summers

Voltage (V)	Ring			Radial		
	Efficiency (%)	VD (%)	LL (%)	Efficiency (%)	VD (%)	LL (%)
<b>120</b>	98.04	4.32	1.96	92.42	14.48	7.58
<b>240</b>	99.50	1.10	0.51	98.16	3.56	1.84
<b>325</b>	99.72	0.61	0.28	98.99	1.95	1.01
<b>380</b>	99.82	0.40	0.18	99.33	1.29	0.67



**Table 2.7** Comparison between centralized and distributed ring architectures for summers

Voltage (V)	Centralized			Distributed		
	Efficiency (%)	VD (%)	LL (%)	Efficiency (%)	VD (%)	LL (%)
<b>120</b>	95.96	6.27	4.04	98.03	4.32	1.96
<b>240</b>	98.91	1.66	1.09	99.49	1.10	0.51
<b>325</b>	99.40	0.92	0.60	99.72	0.64	0.28
<b>380</b>	99.59	0.60	0.40	99.82	0.40	0.18

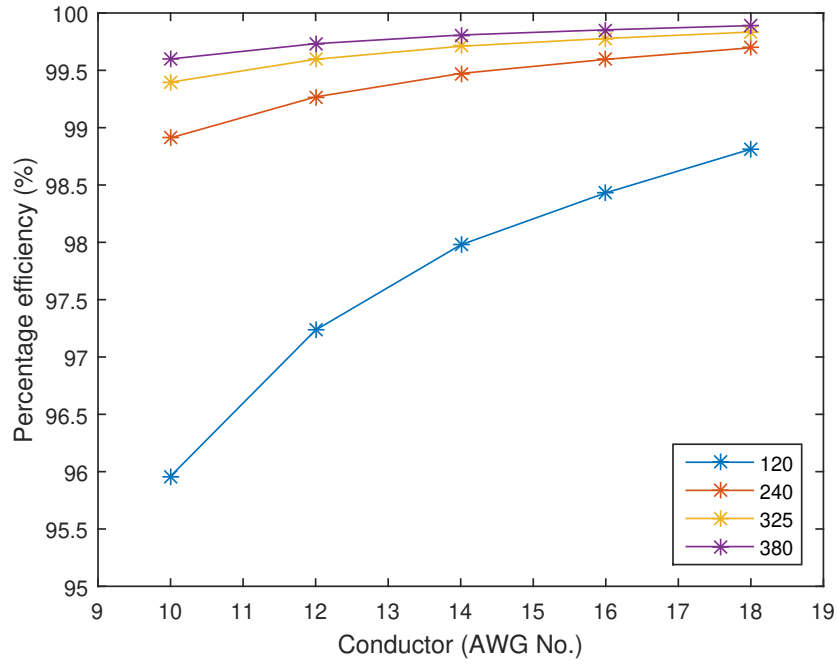
**Table 2.8** Comparison between centralized and distributed ring architectures for winters

Voltage (V)	Centralized			Distributed		
	Efficiency (%)	VD (%)	LL (%)	Efficiency (%)	VD (%)	LL (%)
<b>120</b>	94.36	5.87	5.64	96.56	4.38	3.44
<b>240</b>	98.46	1.57	1.54	99.10	1.12	0.90
<b>325</b>	99.14	0.87	0.86	99.51	0.61	0.49
<b>380</b>	99.43	0.58	0.57	99.67	0.41	0.33

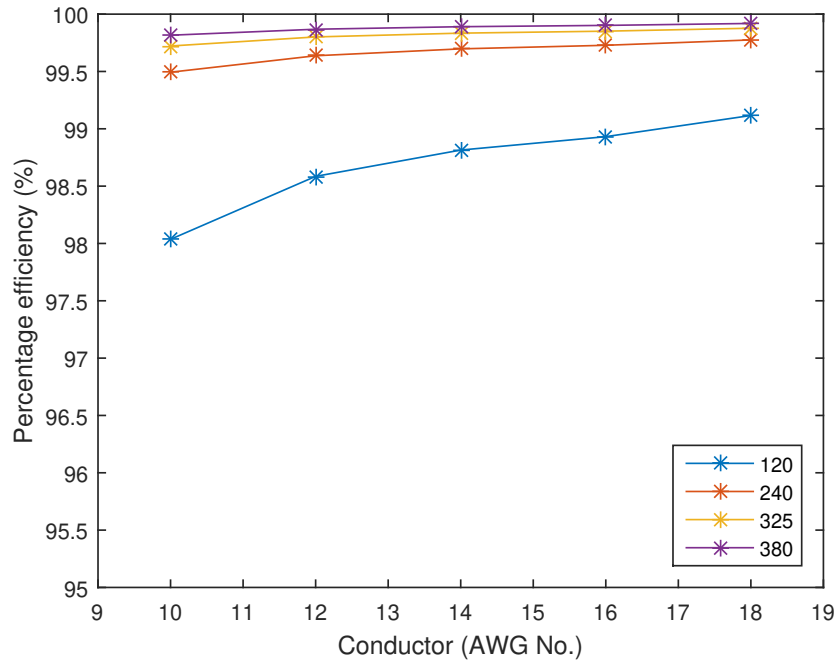
### 2.4.3 Comparison between centralized and distributed microgrid architectures

The centralized and distributed microgrid architectures are compared based on the parameters chosen for this study, i.e., %  $\eta$ , % Voltage Drop(VD), and %Line losses (LL) as given in section 2.2. Tables 2.7 and 2.8 show the analysis for the mentioned parameters at different voltage levels with a conductor of size AWG 18 for winter and summer, respectively.

Figs. 2.10:a and 2.10:b compare average percentage efficiency for centralized and distributed ring connection schemes for the summer season. In radial interconnection, a comparison of average percentage efficiency for centralized and distributed architecture is shown in Fig. 2.11: a and Fig. 2.11:b, respectively, for summers. These results indicate that DGDS is more efficient than CGCS because of usage diversity and mutual resource-sharing capability.

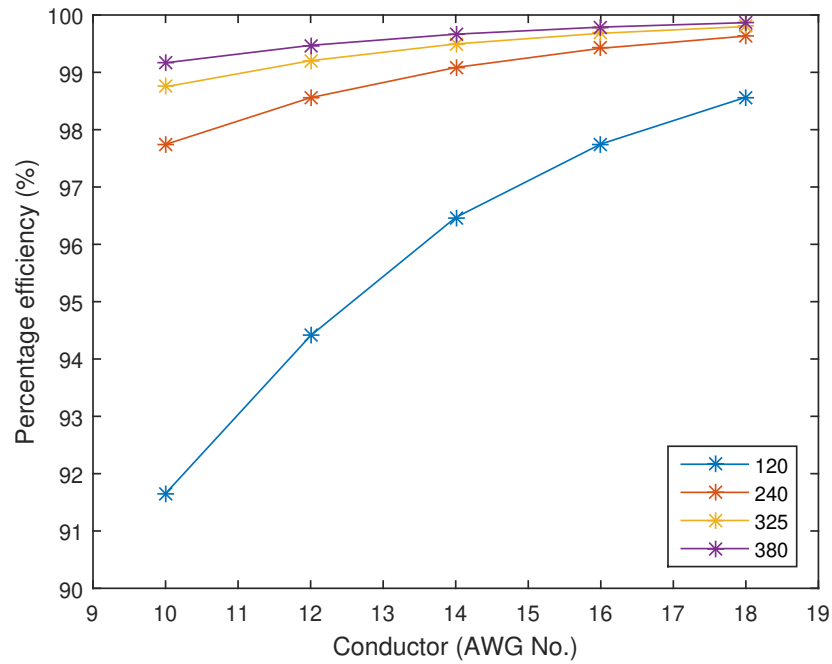


(a) Centralized ring interconnection

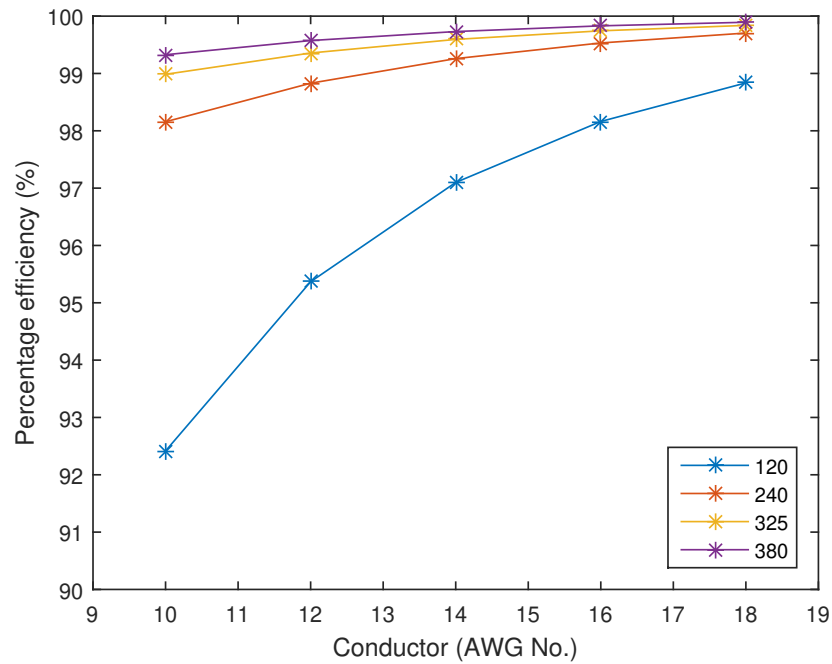


(b) Distributed ring interconnection

**Figure 2.10** Percentage efficiency at different voltages and conductor sizes for ring interconnection of summer season



(a) Centralized radial interconnection



(b) Distributed radial interconnection

**Figure 2.11** Percentage efficiency at different voltages and conductor sizes for radial interconnection of summer season

## 2.5 Summary

This chapter presents a detailed distribution loss analysis of centralized and distributed microgrid architectures with dynamic load and generation profiles. Optimal planning and designing of the microgrid architectures are required to provide electricity access. DC microgrid architectures with static generation and load demand have some limitations for the planning side. Time-based dynamic load demand and generation give an insight into a more practical and real-time approach. In this research study, The distributed architecture consists of individual household consumers that form independent nanogrids, which can operate in both a stand-alone and integrated manner to make the microgrid scalable. The centralized architecture comprises a distributed load with centralized generation and storage. Centralized and distributed systems with ring and radial orientations are considered, and their performance is evaluated using a modified Newton-Raphson method for DC systems. A comparative distribution loss analysis with various conductor sizes and voltage levels shows that the distributed ring architecture is significantly advantageous based on low distribution losses, high efficiency, and low voltage drop. It offers an additional feature of scalability and low capital cost. The microgrid architectures can be tested for any region using real-time solar irradiation data, weather conditions, and the dynamic load demand of that community.

## CHAPTER THREE

### DISTRIBUTION LOSS ANALYSIS IN LOW-VOLTAGE LOW-POWER DC MICROGRIDS FOR RURAL ELECTRIFICATION

#### 3.1 Introduction

This chapter performs a network loss analysis of low-voltage, low-power DC microgrid architectures with multiple village orientations, time-varying load demands, and PV generation. Performance evaluation and analysis on centralized and distributed microgrid architectures are presented in (Mashood Nasir, Zaffar, and Hassan Abbas Khan, 2016) for high voltage DC microgrids. The design and analysis of low voltage DC (LVDC) microgrids are presented in (Hamza et al., 2017). These analyses are performed for constant PV generation and load demand, which is practically impossible in real-time. An analysis of solar-powered DC microgrids with time-varying generation and load demand for low-voltage, low-power microgrids has not been done in the literature, and it is an important consideration for planning and designing microgrids. In Chapter 2, centralized and distributed microgrid architectures were considered for higher power systems with high voltage levels, i.e., (240V, 325V, and 380V). The higher voltage levels are employed to enhance distribution efficiency, but they require sophisticated protection schemes (Salomonsson, Soder, and Sannino, 2009). However, in Chapter 3, further centralized and distributed configurations subclasses are used for low voltage and low power DC microgrid systems.

#### 3.2 Village Orientation-based Microgrid Architectures

The optimal planning and designing of an efficient microgrid architecture requires analyzing the arrangement of houses in the village. The two common house arrangements in most developing countries' villages include 1) Linear orientation and 2) Clustered orientation of houses, while some houses are arranged in the beehives. The linear arrangement of houses

is common in South East Asian countries, while the clustered arrangement in Southern and Northern Africa (Desai, 1994; Linard et al., 2012).

### **3.2.1 Spatial Village Orientations**

The spatial distribution of houses can include the 'n' number of houses, which can be grouped into 'x' clusters based on the arrangement of houses. In this chapter, a common village of 20 houses is considered clustered into five groups. The power flow analysis is performed on the village with, i.e., radial and ring interconnection, shown in chapter 2, section 2.3, in Fig. 2.3 and Fig. 2.4. The selection among these two is a trade-off between the cost of conductors and the reliability of electricity (Glover, Sarma, and Overbye, 2012). The four different microgrid configurations are studied with these interconnecting schemes and are considered in this chapter. The optimal sizing of the batteries and the PV panels for each configuration is calculated using the linear optimization framework developed by Nasir et al. in (Mashood Nasir, Iqbal, and Hassan Abbas Khan, 2017).

### **3.2.2 CGCS Microgrid Architecture**

The CGCS microgrid architecture modeled for the analysis is shown in Fig. 3.1. Each household is the load only, and the PV generation and storage are centrally located. The centralized PV and storage are rated at 240 Wp and 5.76 kWh, respectively. The household load is assumed to be 10 Wp, which is enough to charge a battery, phone, and light. These values are calculated using the optimal sizing framework developed by Nasir et al. in (Mashood Nasir, Iqbal, and Hassan Abbas Khan, 2017)

### **3.2.3 DGCS Microgrid Architecture**

In DGCS architecture, the generation is distributed across each household while the storage is centralized. The DGCS architecture modeled in this study is presented in Fig. 3.2. The PV panel at each house is rated at 12 Wp, while the centralized storage is a large battery

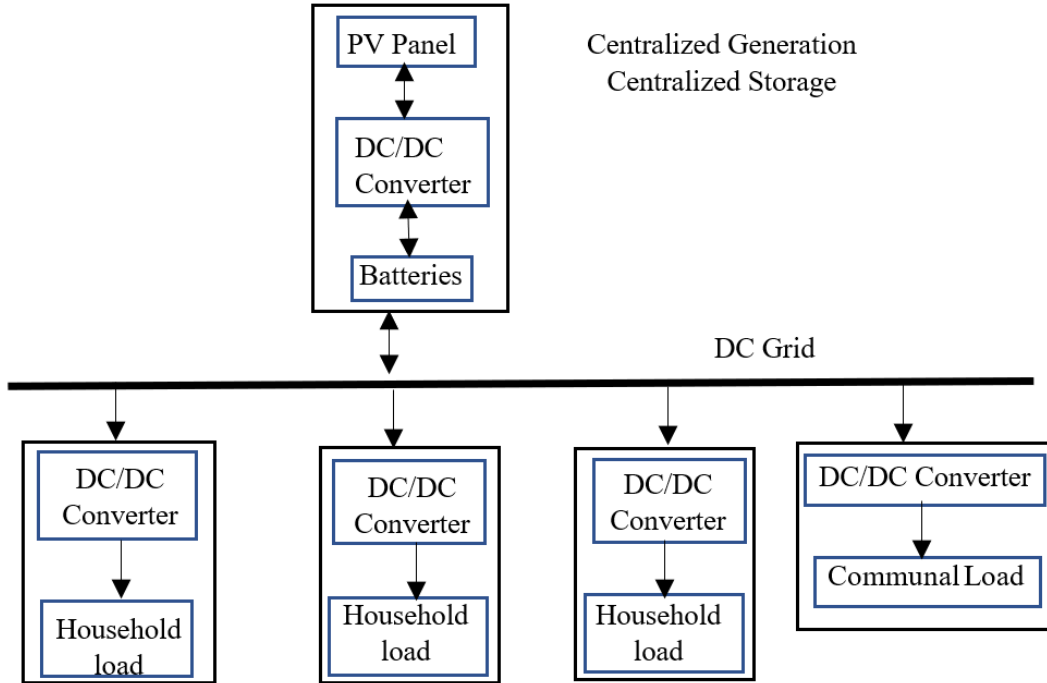


**Figure 3.1** Centralized Generation Centralized Storage Microgrid Architecture (Mashood Nasir, Hassan Abbas Khan, Hussain, et al., 2017).

of 5.760 KWh. These values are calculated using the optimal sizing framework developed by Nasir et al. in (Mashood Nasir, Iqbal, and Hassan Abbas Khan, 2017). The same time-varying loading condition of 10W is assumed at each house in our research for low power demand communities.

### 3.2.4 CGDS Microgrid Architecture

The CGDS microgrid model comprises centralized generation and distributed storage in each household. The CGDS architecture is shown in Fig. 3.3. The centralized generation is rated at 240 Wp, while the distributed storage is 288 Wh at each house. These values are calculated using the optimal sizing framework developed by Nasir et al. in (Mashood Nasir, Iqbal, and Hassan Abbas Khan, 2017). The household loading is assumed to be the same in all microgrid architectures.

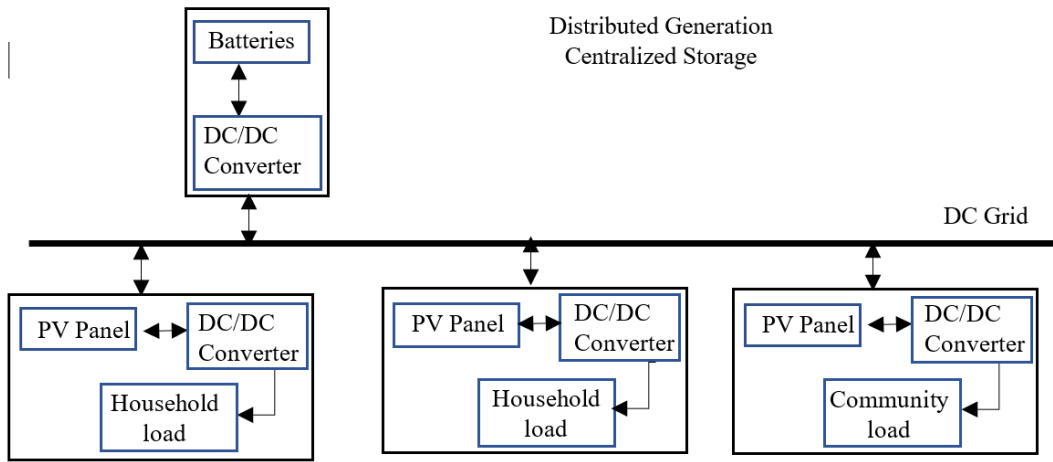


**Figure 3.2** Distributed Generation Centralized Storage Microgrid Architecture

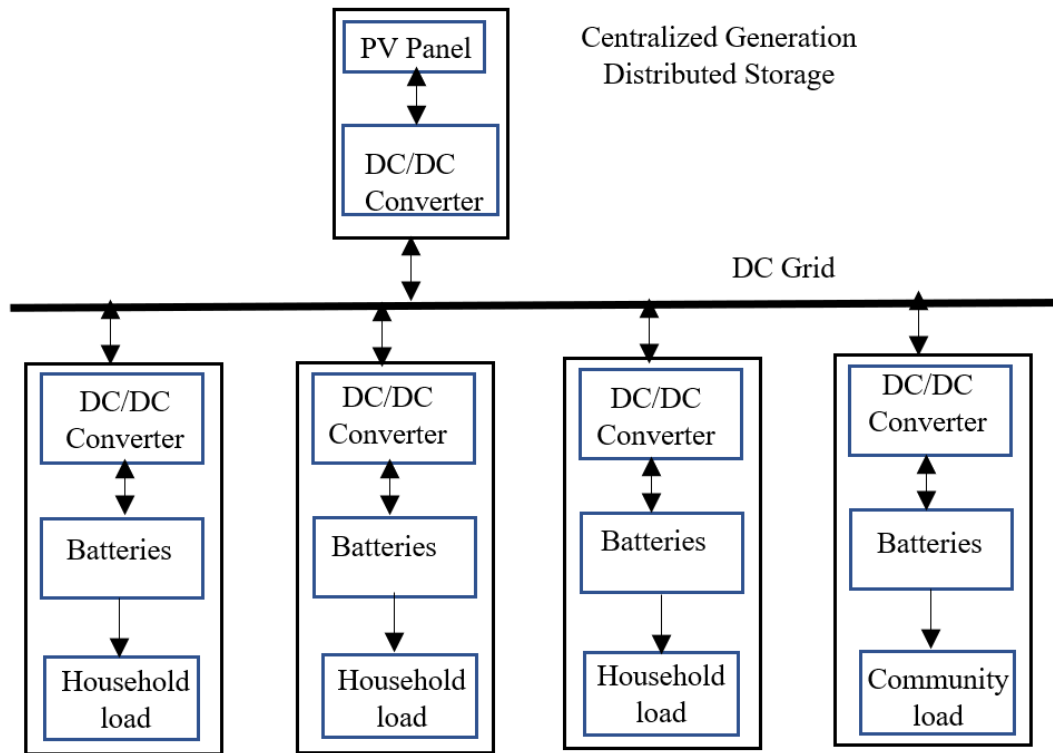


**Figure 3.3** Centralized Generation Distributed Storage Microgrid Architecture



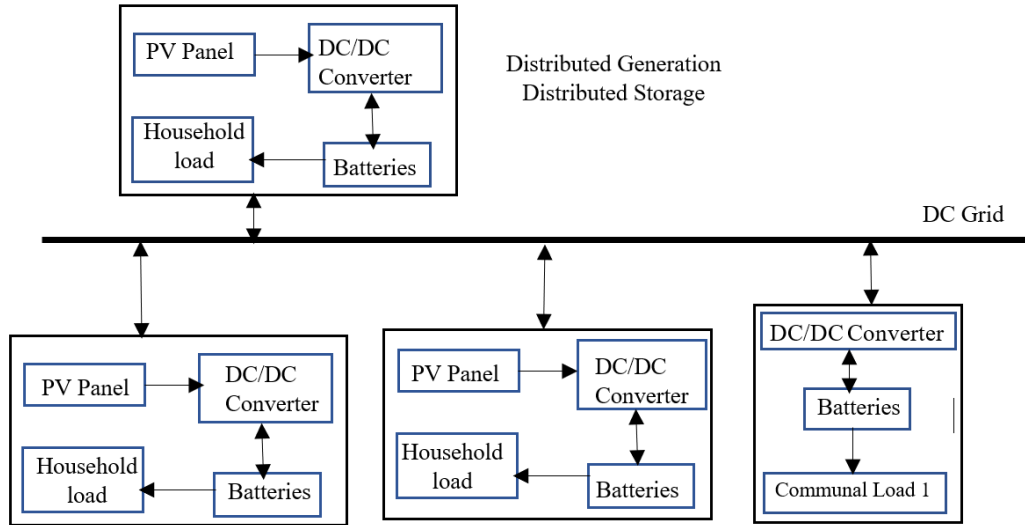


**Figure 3.4** Distributed Generation Distributed Storage Microgrid Architecture (Mashood Nasir, Hassan Abbas Khan, Hussain, et al., 2017).

### 3.2.5 DGDS Microgrid Architecture

The distributed generation microgrid architecture includes each household as a generation, storage, and load set. Thus, each house is a mini-grid that can operate independently and in coordination with the other houses. This topology does not require the installation of a large PV panel or battery with a high rating but small distributed panels and batteries at each house with ratings of 12 Wp and 288 Wh, respectively. These values are calculated using the optimal sizing framework developed by Nasir et al. in (Mashood Nasir, Iqbal, and Hassan Abbas Khan, 2017). The DGDS microgrid model is shown in Fig. 3.4.

## 3.3 MODIFIED NEWTON-RAPHSON DC power flow Analysis with Dynamic Load Demand

The power flow method for DC microgrids is the modified version of Newton-Raphson analysis and is given in Chapter 2. This chapter performs the same power flow analysis for low-voltage DC (LVDC) microgrids with time-varying load demand and generation.

The model of the village considered with different interconnecting schemes is shown in

Chapter 2, section 2.3, in Fig. 2.3 and Fig. 2.4. Each house is connected to the other house through a conductor with its respective resistance. The conductance matrix of the whole village can be formed to indicate all the connections represented by their respective resistances. Based on the length of the conductor laid (depending on the distance among houses), the total resistance can be calculated. The distance between two houses is assumed to be 15m while the distance between two clusters is 45m.

A typical power system is shown in Chapter 2, section 2.2. For any system with two buses,  $i$  and  $j$ , the resistance is  $r_{ij}$ , and the conductance is  $g_{ij}$ , as shown in Fig. 2.1. For a village of  $n$  houses, the  $G$  matrix is  $2n \times 2n$ . The details of the conductance matrix calculation is given in Eq. (2.1) and Eq. (2.2).

The power flow analysis is performed with a 15-minute time-step iteration for 24 hours. The formulation of scheduled power, calculated power, and their difference is shown in Eq. (2.3), Eq. (2.4), and Eq. (2.9). The power flow analysis is performed in multiple iterations until the mismatch is approximately null or within an acceptable tolerance range and the system converges.

The network losses  $LL_g(t)$  and their respective percentage  $\%LL_g(t)$  can be calculated through Eq. (2.10) and (2.11). The percentage efficiency  $\%\eta(t)$  and voltage drop  $\%V_{drop}(t)$  are calculated from Eq. (2.12) to (2.14) (Mashood Nasir, Zaffar, and Hassan Abbas Khan, 2016).

### 3.3.1 Conductor Sizes

The power flow analysis is performed on conductors of different AWG numbers. Each conductor has a different resistance, respective area, and cost based on its AWG number. The list of conductors used with their AWG numbers, resistances, and areas is given in Table 2.1 in Chapter 2.

### **3.3.2 Time-varying generation and load demand**

The analysis performed in this study considers the time-varying generation and load demand for Ethiopia, and the details of the PV data and load data are given in Chapter 2, section 2.4.1.

## **3.4 Results and Discussions**

The four different microgrid architectures are modeled in MATLAB with two interconnecting schemes. The performance evaluation of the designed LVDC microgrid is implemented at 24V and 48V, with conductors of varying AWG numbers, i.e., 10,12,14,16 and 18. Each microgrid architecture's efficacy is calculated using percentage line losses, efficiency, and voltage drop.

### **3.4.1 Comparison between radial and ring microgrid architectures**

A comparison between radial and ring connecting schemes for four different microgrid architectures is given in Table. 3.1 at 48V with AWG 10. It is clear from the results that ring interconnection has fewer losses and higher efficiency than the corresponding radial one. The ring interconnection requires a larger number of conductors, which causes an increase in cost but more reliability. So, a trade-off between cost and efficiency with reliability is important while designing the microgrid architecture.

### **3.4.2 Comparison between CGCS and DGDS ring microgrid architecture with conductor sizes**

The CGCS and CGDS microgrid architectures are compared for different conductor sizes. The results are given for ring interconnection scheme at 48V to evaluate efficiency ( $\% \eta$ ),  $\%$  Voltage drop, and  $\%$  Network losses. Table. 3.2 lists the results. The distributed architecture (DGDS) is more efficient than the centralized one (CGCS), with higher efficiency and low

**Table 3.1** Comparison between radial and ring interconnections for microgrid architectures at 48V

Microgrid	Ring			Radial		
	Efficiency (%)	VD (%)	LL (%)	Efficiency (%)	VD (%)	LL (%)
<b>CGCS</b>	96.09	1.45	3.90	90.89	3.47	9.10
<b>CGDS</b>	99.09	0.77	0.90	96.411	2.26	3.58
<b>DGCS</b>	98.19	1.05	1.80	94.23	2.83	5.76
<b>DGDS</b>	99.71	0.3273	0.2848	97.98	1.47	2.01

**Table 3.2** Comparison between CGCS and DGDS ring microgrid architecture with conductor sizes

AWG No.	CGCS			DGDS		
	Efficiency (%)	VD (%)	LL (%)	Efficiency (%)	VD (%)	LL (%)
<b>10</b>	96.09	1.45	3.90	99.71	0.32	0.28
<b>12</b>	94.03	2.24	5.96	99.55	0.51	0.44
<b>14</b>	91.05	3.39	8.94	99.29	0.81	0.70
<b>16</b>	86.91	5.02	13.08	98.89	1.27	1.10
<b>18</b>	81.49	7.25	18.51	98.29	1.99	1.70

network losses at AWG 10. Conductors with low AWG are expensive, so a trade-off between cost and efficiency has to be made when choosing a conductor for the microgrid system.

### 3.4.3 Comparison between DGCS and CGDS radial microgrid architecture with conductor sizes

The DGCS and CGDS radial microgrid architecture with conductor sizes and radial orientation are considered at 48 V to evaluate efficiency ( $\% \eta$ ), % Voltage drop, and % network losses. Table. 3.3 lists the results, which indicate that with a larger conductor's AWG number, the cost gets reduced but also decreases efficiency.

**Table 3.3** Comparison between DGCS and CGDS radial microgrid architecture with conductor sizes

AWG No.	DGCS			CGDS		
	Efficiency (%)	VD (%)	LL (%)	Efficiency (%)	VD (%)	LL (%)
<b>10</b>	94.23	2.83	5.76	96.41	2.26	3.58
<b>12</b>	92.17	4.06	7.84	95.01	3.28	4.98
<b>14</b>	89.967	5.54	10.03	93.44	4.54	6.55
<b>16</b>	87.22	7.26	12.77	91.40	6.05	8.59
<b>18</b>	83.20	9.47	16.77	88.34	8.05	11.65

#### 3.4.4 CGCS ring microgrid architecture

The percentage voltage drop of CGCS ring microgrid architecture at 24 V and 48 V for different conductor sizes is shown in Fig. 3.5. The voltage drop increases with the increase in AWG number and at low voltage levels.

#### 3.4.5 DGDS radial microgrid architecture

The percentage voltage drop of DGDS radial microgrid architecture at 24 V and 48 V for different conductor sizes is shown in Fig. 3.6. The percentage voltage drop increases with the increase in AWG number and at low voltage levels. The percentage efficiency of DGDS radial and ring interconnection schemes are given in Fig. 3.7 and Fig. 3.8, respectively.

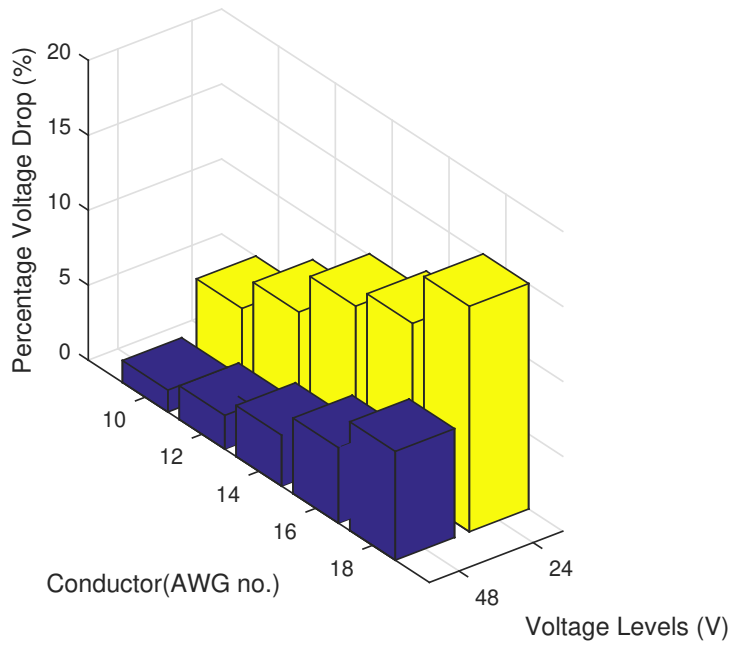


**Figure 3.5** Percentage voltage drop of CGCS

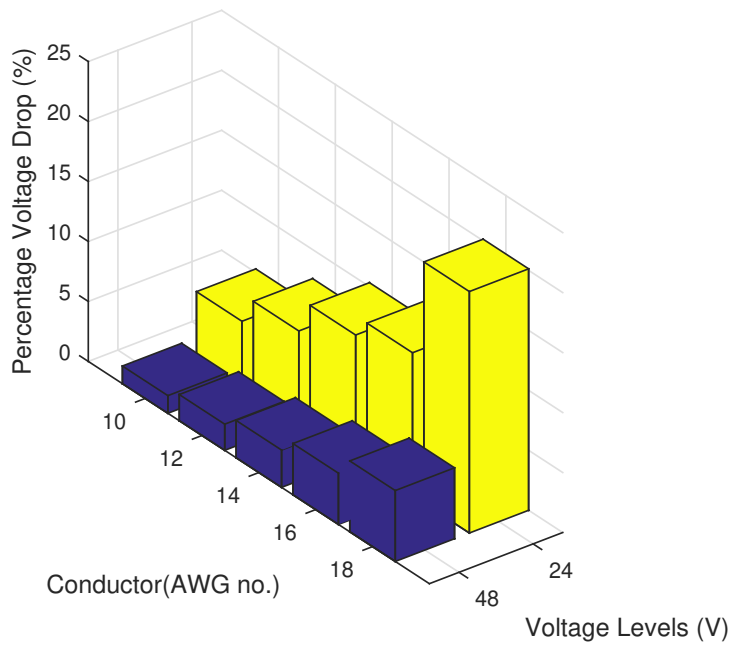


**Figure 3.6** Percentage voltage drop of DGDS

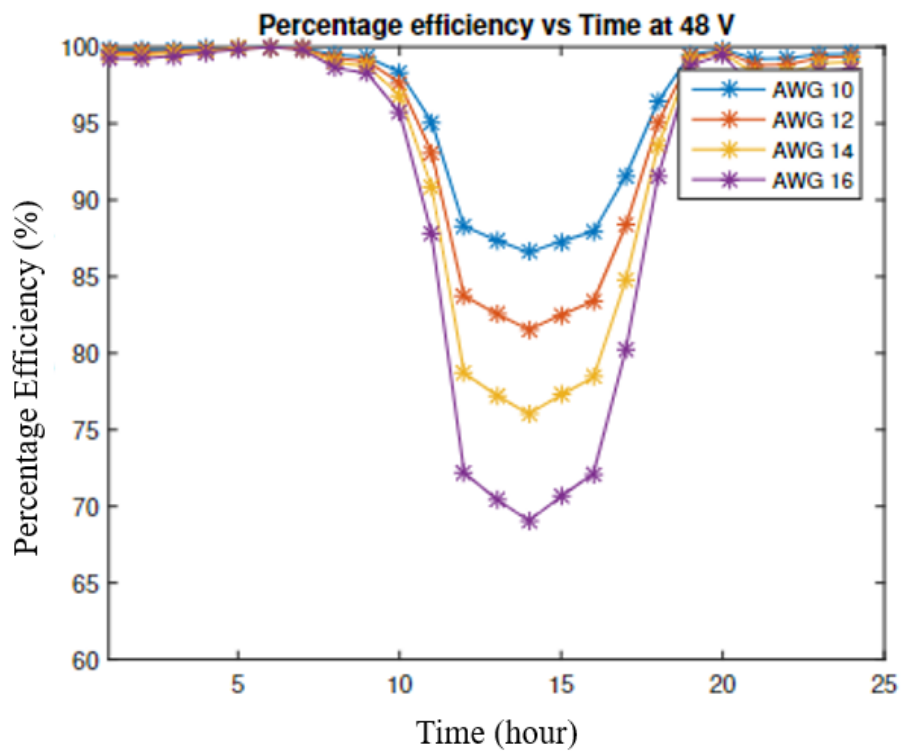


**Figure 3.7** Percentage efficiency of DGDS in radial connection

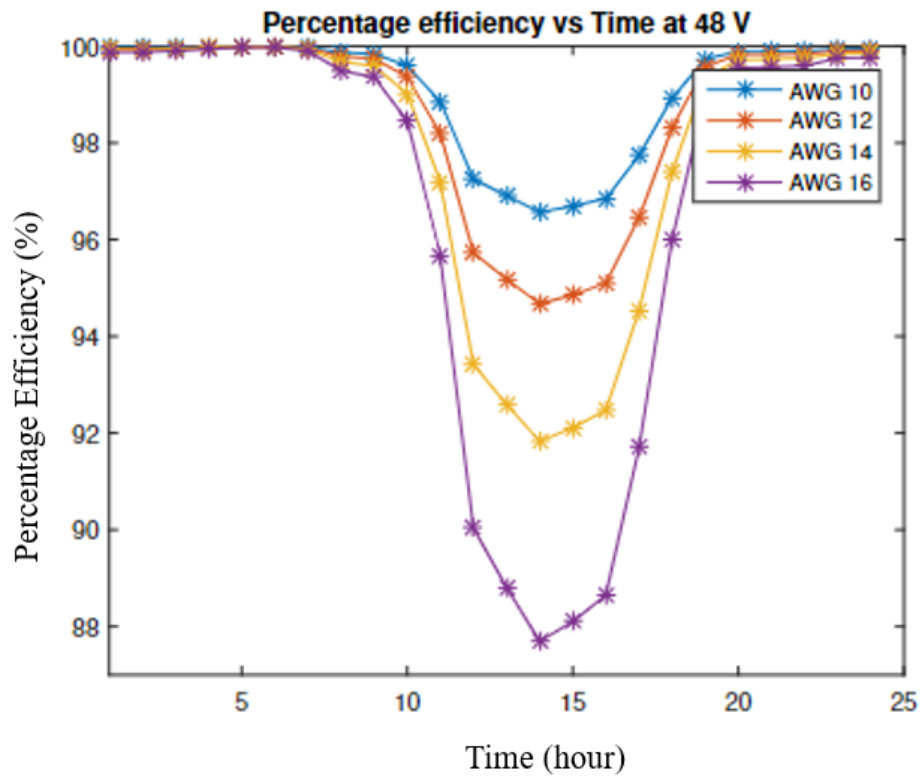


Figure 3.8 Percentage efficiency of DGDS in ring connection



### 3.5 Summary

Rural electrification through low-voltage, low-power PV-based DC microgrids with time-varying generation and dynamic load demand is analyzed using spatial village orientations. The four different microgrid architectures, including 1) CGCS, 2) CGDS, 3) DGCS, and 4) DGDS are implemented with radial and ring interconnection schemes. Comparative performance analysis of these architectures is done using the modified Newton-Raphson power flow method at different low-voltage levels and conductor sizes. The DGDS architecture with ring interconnection is the most efficient and reliable, with the additional advantages of scalability, usage diversity, and mutual resource-sharing capability. However, ring interconnection requires extra conductors, which increases the cost. The efficiency of systems is higher at a low AWG number of conductors, but it is expensive. So, a trade-off between conductor size, voltage level, cost, interconnection scheme, and reliability is to be made while selecting the components for the microgrid architecture. According to the analysis in this chapter, the distributed ring architecture have high efficiency, lower distribution losses, and better resource-sharing than other systems. This analysis will be helpful in the optimal planning and design of new microgrid systems and upgrading existing systems to a more efficient one in non-electrified rural areas of developing countries.

## CHAPTER FOUR

### POWER ELECTRONIC LOSS MODELING IN MODIFIED NEWTON-RAPHSON POWER FLOW FOR DC MICROGRID SYSTEMS

#### 4.1 Introduction

This chapter covers the mathematical modeling of DC-DC converters in the Newton Raphson Power Flow for DC systems. The power loss modeling of the power electronic converters is vital because of its relation with efficiency, reliability, cost, and size. The converter loss model is implemented in the bus injection model, and the power-electronic loss model is applied in both distributed and centralized architectures to analyze system- and device-level losses in DC microgrids.

The main objective of this chapter is to develop a loss model for the DC-DC converter that can describe the losses in all the elements of the converter. The steady-state operation of a power system can be analyzed using different power flow methods, e.g., Gauss-Siedel, Newton-Raphson, and Fast Decoupled (Saadat et al., 1999; Grainger and Stevenson Jr, 1994). However, for DC microgrids, Nasir et al. have proposed a modified Newton-Raphson power flow method (Mashood Nasir, Zaffar, and Hassan Abbas Khan, 2016; Mashood Nasir, Jin, et al., 2018). The method has been used to analyze the performance of DC microgrids at different voltage levels and conductor sizes (Hamza et al., 2017). However, the technique only considered distribution line modeling and system losses. Converter loss modeling is also essential for the optimal planning and operation of the microgrid system. Converter loss modeling plays a significant role in analyzing device-level losses. In the literature, converters and batteries are modeled with constant efficiencies (Mashood Nasir, Zaffar, and Hassan Abbas Khan, 2016; Mashood Nasir, Iqbal, and Hassan Abbas Khan, 2017). Zhao et al. have modeled the DC-DC converters in the power flow model (Zhao, Chen, and Blaabjerg, 2006), but its implementation lacks loss analysis in DC microgrids.

## 4.2 Modeling of Islanded DC microgrid system

The islanded DC microgrid system considered in this study could be distributed or centralized depending on the location of generation and storage. This chapter considers the residential microgrid for rural communities. Each household has only DC loads. The PV generation and battery storage make a generation-storage (GS) block, as shown in Fig. 4.1. The GS block can be located in each household, making it an independent prosumer and the whole microgrid as a distributed architecture. However, if the GS block is located at a central location, it will be considered a centralized microgrid architecture. A schematic diagram of an individual house with GS block in the microgrid architecture is shown in Fig. 4.2.

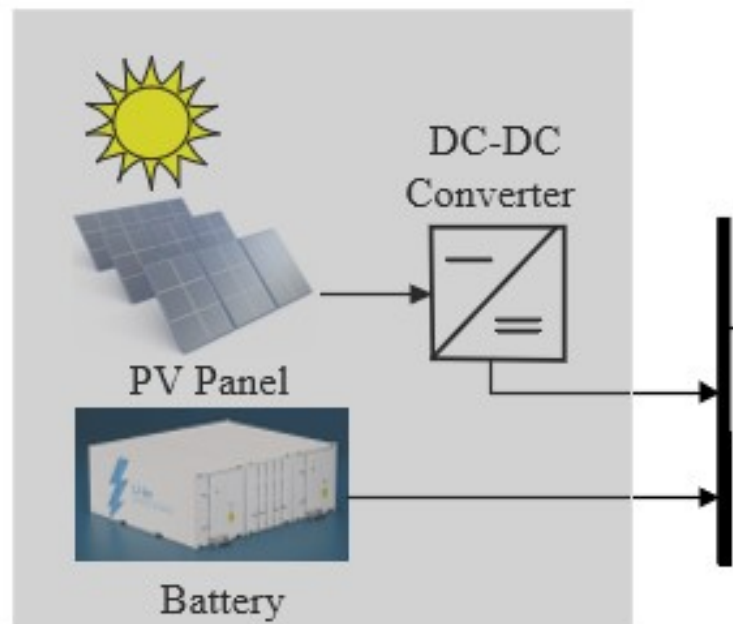
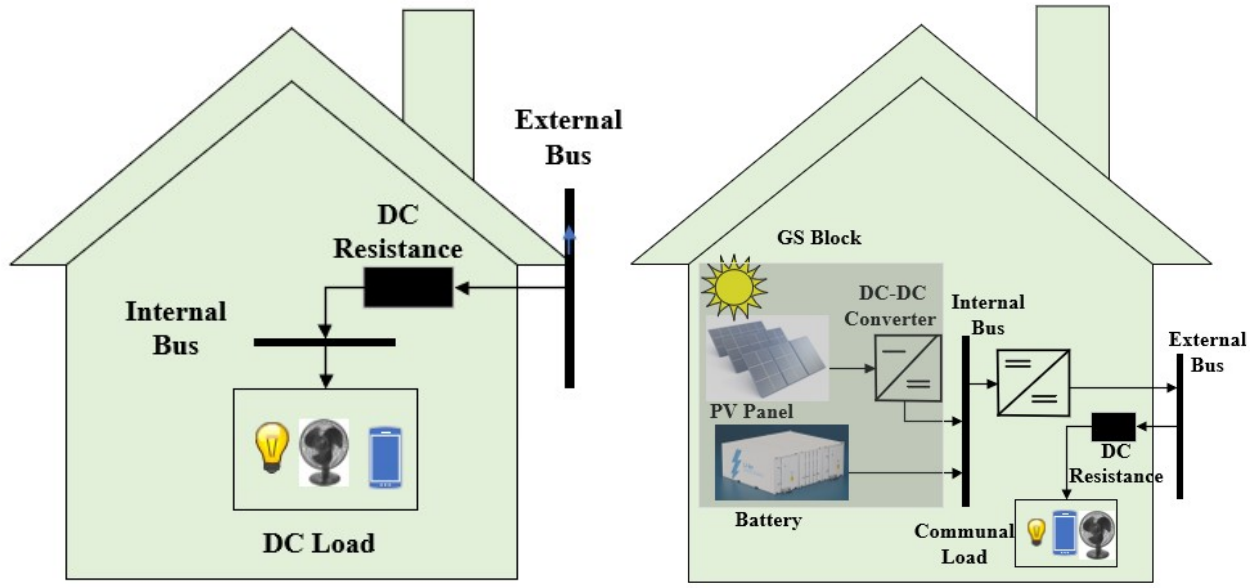


**Figure 4.1** Schematic Diagram of GS Block

### 4.2.1 Centralized Microgrid Architecture

The centralized microgrid architecture consists of multiple households with a DC load. Both generation and storage are located at one central community location. Each household in



(a) Household in centralized architecture      (b) Household in distributed architecture

**Figure 4.2** Schematic of individual household in centralized and distributed micro-grids

the centralized configuration is shown in Fig. 4.2a. The design of the DC-DC converter for the centralized location is given in the next section.

#### 4.2.2 Distributed Microgrid Architecture

The household model in Fig. 4.2b is the basic block of distributed microgrid architecture. Each household is an independent prosumer capable of generating and storing power through PV and batteries, respectively. The prosumers are interconnected, providing an advantage of resource sharing and usage diversity. The distributed microgrid architecture has better efficiency, high reliability, usage diversity, and power-sharing features, as seen in Chapters 2 and 3.

#### 4.2.3 Framework of Microgrids

The residential households are considered to be connected in a ring topology to form the microgrid. Two houses with external buses 'i' and 'j' are interconnected through a conductor

with impedance  $r_{ij}$  or conductance  $g_{ij}$ . The voltage on these buses is  $v_i$  and  $v_j$ , with power injections as  $P_i$  and  $P_{ij}$ , respectively. Our model considers a microgrid with forty houses distributed into five clusters, connected in ring topology as shown in Fig.4.3.

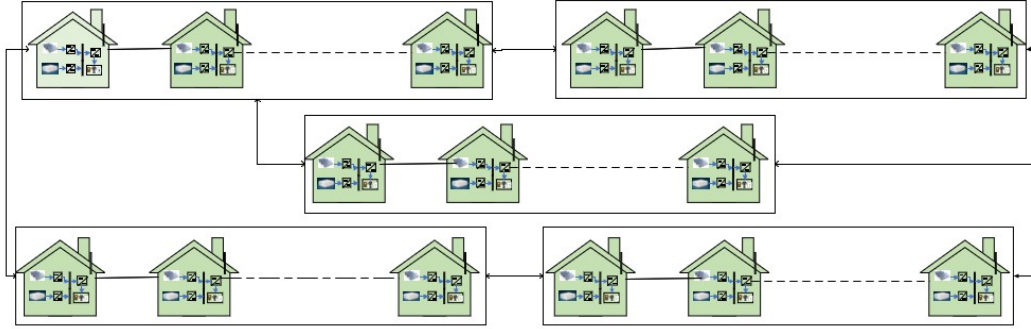


**Figure 4.3** Ring orientation of households in microgrid

### 4.3 Power Loss Modeling

Power system losses include system and device level losses. The system level includes losses across distribution lines. However, the device-level losses include losses across devices. e.g., converters, batteries, etc. In this chapter, the converter losses are calculated by modeling and designing its components. However, the battery is assumed to be operating at a constant efficiency.

#### 4.3.1 Distribution Losses

The power distribution losses are generated by the power flow through the impedance of distribution lines. The losses depend on the conductor sizes, power flow, and voltage level (Mashood Nasir, Hassan Abbas Khan, Hussain, et al., 2017). The distribution losses can be calculated using current magnitude square  $l_{ij}$  and resistance  $r_{ij}$  as given in Eq. 4.1. Here,  $N$  is the number of houses or nodes in the power system.

$$DL = \sum_{j:j \sim i} l_{ij} r_{ij} \quad \forall i \in \mathcal{N} \quad (4.1)$$

### 4.3.2 Converter Losses

In DC microgrid system, the DC–DC converters are used to step up/down the voltage, maximize power point tracking, and regulate the current. DC/DC converters can be of different topologies, primarily divided into two types: non-galvanic isolated and galvanic isolated. The key difference among these topologies is the existence/non-existence of isolating transformers. Multiple DC-DC converter topologies can be used and are listed in Table. 4.1 (Martander, 2002,). However, this work has considered the boost converter topology.

**Table 4.1** Topologies of DC–DC Converters (Martander, 2002,).

Non-Galvanic Isolated Converters	Galvanic Isolated Converters
Boost	Flyback
Cuk	Forward
Sepic	Two transient forward
Zeta	Push pull Luo
Luo	Half bridge
	Full bridge
	Half bridge with voltage doubler

The power processed by each converter causes losses called power electronic losses. The converters are designed to operate at high efficiency with the least converter losses and advancements in power electronics. However, these losses depend on the output power, i.e., the converter’s efficiency is a function of the ratio of output power to the rated capacity (% loading), which is non-linear, as given by equation Eq. 4.2 (Gelani, Mashood Nasir, et al., 2017; Kolar et al., 2012; Mashood Nasir, Iqbal, Hassan A Khan, et al., 2020). The simplified form of Eq. 4.2 is Eq. 4.3.

$$P_{conv} = \sum_{x=0}^K k_x (P_o)^x \quad (4.2)$$

$$P_{conv} = k_0 + k_1 P_o + k_2 P_o^2 \quad (4.3)$$

In equation Eq. 4.3, the  $P_{conv}$  represents the converter's losses,  $P_0$  is output powers, and  $k_x$  is the co-efficient of conversion losses, where x changes from 0 to K. In this work, K is considered equal to 2, so converter losses are i) constant, ii) linear, and iii) quadratic.

To map the converter losses and distribution losses on the same time scale and achieve the combined objective of their minimization, we have assumed that converters are operating in a steady state with constant switching frequency. Therefore, the converters' dynamic characteristics are not considered within the scope of this work.

The main components of a DC-DC converter include an inductor, a power MOSFET, a diode, a filter capacitor, and a load resistance, as shown in Fig. 4.4. The boost converter can operate in continuous or discontinuous conduction mode, depending on the waveform of the inductor current (Wang, Dunford, and Mauch, 1997).

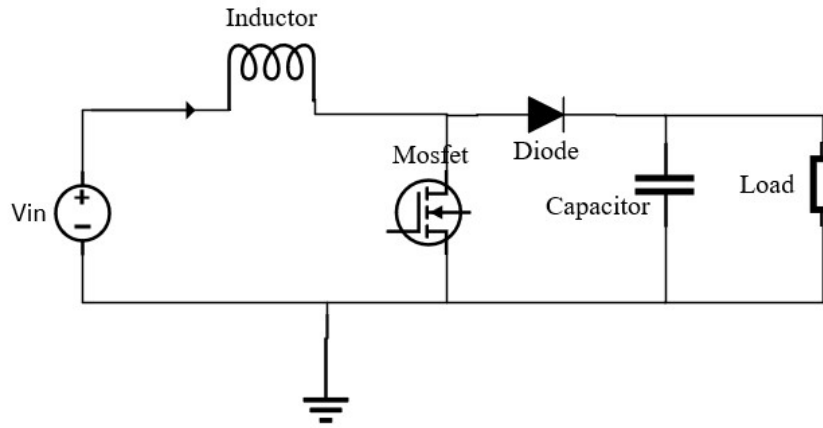


**Figure 4.4** DC-DC converter

$$P_{conv} = P_{inductor} + P_{cond_m} + P_{cond_d} + P_{switch_m} + P_{switch_d} \quad (4.4)$$

$$P_{inductor} = R_{inductor} * I_{input}^2 \quad (4.5)$$

$$P_{cond_m} = \frac{D}{D + D'} (V_{0_m} + R_{0,m} I_{input}) I_{input} \quad (4.6)$$

$$P_{cond_D} = \frac{D'}{D + D'} (V_{0_D} + R_{0,D} I_{input}) I_{input} \quad (4.7)$$

$$P_{switch_m} = \frac{A_{on_{sw}} + A_{off_{sw}}}{T_s} V_{output} * I_{input} \quad (4.8)$$

$$P_{switch_m} = \frac{A_{on_{sw}} + A_{off_{sw}}}{T_s} V_{out} I_{input} \quad (4.9)$$

$$P_{switch_d} = \frac{A_{rccD}}{T_s} V_{output} * I_{input} \quad (4.10)$$

In Eqs. (4.6) to (4.10),  $D$  and  $D'$  are the conducting times for MOSFET and diode, respectively.  $R_{inductor}$  is the resistance of the inductance. The  $V_{0_m}$  and  $V_{0_D}$  are the constant voltage drop across MOSFET and diode, respectively.  $V_{0_m}$  is conducting resistance in IGBT,  $V_{0_D}$  is the voltage drop across the diode, while  $R_{0_m}$  and  $R_{0_D}$  are conducting resistances of MOSFET and diode respectively. The  $A_{on_{sw}}$  &  $A_{off_{switch}}$  are turn on and off switching constants for MOSFET. For the diode,  $A_{rccD}$  is a switching constant with the switching time of  $T_s$ .

$$D = \sqrt{\frac{2L I_{input}}{T_s} \frac{D_z}{D_x D_y}} \quad (4.11)$$

$$D' = \frac{2L I_{input}}{D_x D T_s} - D \quad (4.12)$$

$$D_x = V_{input} - I_{input} (R_{inductor} + R_{0_m}) - V_{0,SW} \quad (4.13)$$

$$D_y = V_{output} + V_{0_D} - V_{0_m} + I_{input} (R_{0_D} - R_{0_m}) \quad (4.14)$$

$$D_z = V_{output} - V_{input} + I_{input} (R_{inductor} + R_{0_D}) + V_{0_D} \quad (4.15)$$



The value of these components is calculated from the power rating of the converter, the input current of the converter, and the power processed by the diode and the MOSFET. The values of components for centralized and distributed architecture are given in Table.4.2, Table.4.3, and Table.4.4. The component selection is verified by plotting the efficiency curve and comparing it with a DC-DC converter curve, as shown in Fig. 4.5.

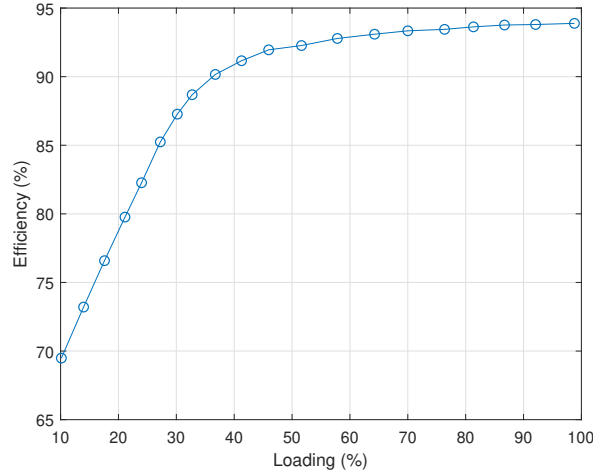


**Figure 4.5** Loading vs. efficiency curve of a DC-DC converter

**Table 4.2** Parameters for the Inductance of DC-DC Converter

Parameters	Centralized	Distributed
Switching Frequency	2000 Hz	2000 Hz
$R_{inductance}$	0.006 ohm	0.018 ohm
$L_{inductance}$	0.0002 H	0.013 H

**Table 4.3** Parameters for the Diode of DC-DC Converter

Parameters	Centralized	Distributed
$V_{0D}$	0.86 V	1.4 V
$R_{0D}$	0.0215 ohm	0.129 ohm
$A_{rccD}$	$28.7 * 10^{-9}$	$11.4 * 10^{-9}$

**Table 4.4** Parameters for the MOSFET of DC-DC Converter

Parameters	Centralized	Distributed
$V_{0m}$	1.25 V	1.4 V
$R_{0m}$	0.022 ohm	0.05 ohm
$A_{on_{sw}}$	$64 * 10^{-9}$	$16 * 10^{-9}$
$A_{off_{sw}}$	$37 * 10^{-9}$	$114 * 10^{-9}$

#### 4.4 Bus Injection Method with Modified Newton-Raphson Power Flow

The power flow model of the islanded DC microgrid system is based on the bus injection method with modified Newton-Raphson power flow implemented, as presented in (Farooq et al., 2014). The residential, rural area is assumed to be of  $n$  houses arranged in clusters to form a microgrid. Each household has two buses, resulting in  $2n$  buses for the whole distribution system. In a distributed architecture, when converters are involved, there is an additional bus in each household, resulting in  $3n$  buses in the microgrid and impedance matrix of size  $G \in \mathbb{R}^{3n \times 3n}$ . The centralized system has only one conductor, so the total nodes are  $2n+1$ , and the size of the conductance matrix is  $2n+1 * 2n+1$ ;  $G \in \mathbb{R}^{2n+1 \times 2n+1}$

$$G_{ij} = \left\{ \begin{array}{ll} \sum_{\substack{j=1 \\ j \neq i}}^{2n} \frac{1}{r_{ij}} & ; \forall i = j \\ -\frac{1}{r_{ij}} & ; \forall i \neq j \end{array} \right\} \quad (4.16)$$

The power is scheduled at the external buses  $P_i^{sch}$  using Eq. (4.17). The power is calculated using the voltage and current at each instant given by Eq. (4.18). The voltages are calculated by solving the power flow model in multiple iterations. The calculated power at each bus uses voltage and injected current. The DC-DC converter is added between buses  $l$  and  $n$ . Corresponding to each converter, three equations are added as Eq.4.19, Eq.4.20, and Eq.4.21. The Jacobian matrix for the modified power flow model is shown in Eq.4.23, an extended version of the Jacobian discussed in Chapter 2, section 2.2 (Zhao, Chen, and Blaabjerg, 2006). Eq.4.24 shows the equations that need to be solved in multiple iterations until the

column on the left side (mismatch) is close to zero, indicating the convergence of the power flow.

$$P_i^{\text{sch}} = P_i^{\text{gen}} - P_i^{\text{load}} \quad (4.17)$$

$$P_i^{\text{calc}} = \sum_{j=1}^{3n/2n+1} V_i * V_j * G_{ij} \quad (4.18)$$

$$P_l = \sum_{m \neq n} V_l V_m G_{lm} + V_l I_l \quad (4.19)$$

$$P_n = \sum_{m \neq l} V_n V_m G_{nm} + V_n I_n \quad (4.20)$$

$$E = V_n I_n + V_l I_l - P_{\text{loss}} = 0 \quad (4.21)$$

$$V_i = V^{\text{spec}} \quad (4.22)$$

$$[J] = \begin{bmatrix} J_{11} & \cdots & J_{1N} & 0 & 0 \\ \vdots & \cdots & \vdots & \vdots & \vdots \\ J_{j1} & J_{jl} + I_l & J_{jN} & 0 & V_l \\ \vdots & & \vdots & \vdots & \vdots \\ J_{N1} & \cdots & J_{NN} & 0 & 0 \\ \partial P_i / \partial V_1 & 0 & \partial P_i / \partial V_N & V_n & 0 \\ 0 & \partial E / \partial V_l & 0 & \partial E / \partial I_n & \partial E / \partial I_l \end{bmatrix} \quad (4.23)$$

$$\begin{bmatrix} \Delta P_1 \\ \vdots \\ \Delta P_N \\ \Delta P_i \\ \Delta E \end{bmatrix} = [J] \begin{bmatrix} V_1 \\ \vdots \\ V_N \\ I_i \\ I_j \end{bmatrix} \quad (4.24)$$

In Eq.4.24,  $\Delta P_i$  and  $\Delta E_l$  are mismatch between scheduled  $P_i^{\text{sch}}$  and calculated powers  $P_i^{\text{calc}}$ , and power loss difference respectively. The solution to these values gives the voltage and currents after being solved iteratively.

## 4.5 Results And Discussion

The centralized and distributed microgrids are compared using technical parameters for the ring-interconnected microgrid system.

### 4.5.1 Test System

Fig. 4.3 shows the test microgrid system for evaluating the different microgrid configurations. The distributed system has prosumers in each household, while the centralized one has one central location with battery and storage, and households have DC loads.

The optimal sizing of the microgrid system's batteries and the PV panels is calculated using the linear optimization framework developed by Nasir et al. in (Mashood Nasir, Iqbal, and Hassan Abbas Khan, 2017). Each prosumer has a PV of 50W peak battery of 100 Wh, and DC load of 40W. The DC load is the same for centralized system houses, but the central PV is 2000Wpk, and the battery is 1000Wh. The communal load is 100W at the cluster's central location in the middle.

### 4.5.2 Performance Analysis

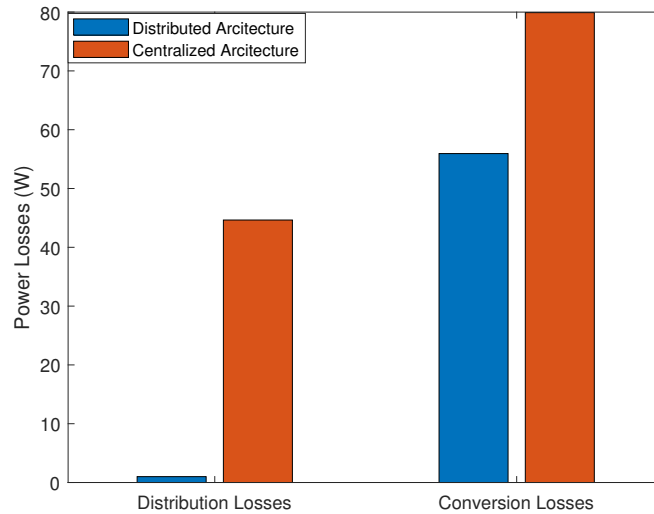
The performance evaluation of the centralized and distributed microgrids is determined using technical parameters, e.g., distribution losses, conversion losses, efficiency, and voltage drop. The technical parameters are given in Chapter 2. The Eq. (2.10) to Eq. (2.14) are used for determining the performance of the microgrid system.

Fig.4.6 compares power losses of centralized and distributed architectures. The distributed architecture has lower distribution and conversion losses. The centralized system

**Table 4.5** Analytical comparison of centralized vs. distributed systems (Mshood Nasir, 2018.)

Parameters	Centralized	Distributed
Installation Cost	Low	High
Levelized Cost of Energy	High	Low
Power Availability	Low	High
Power-Sharing	No	Yes

has one point of generation and storage, so the distribution losses are significantly higher. Fig.4.7, and Fig.4.8 compare both systems' efficiencies and voltage drops, respectively. The distributed system is more efficient than the centralized one with less %voltage drop Table.4.5 shows an analytical comparison of both microgrid architectures. The distributed microgrid architecture has more advantages than the centralized one.



**Figure 4.6** Power losses of centralized vs. distributed architectures

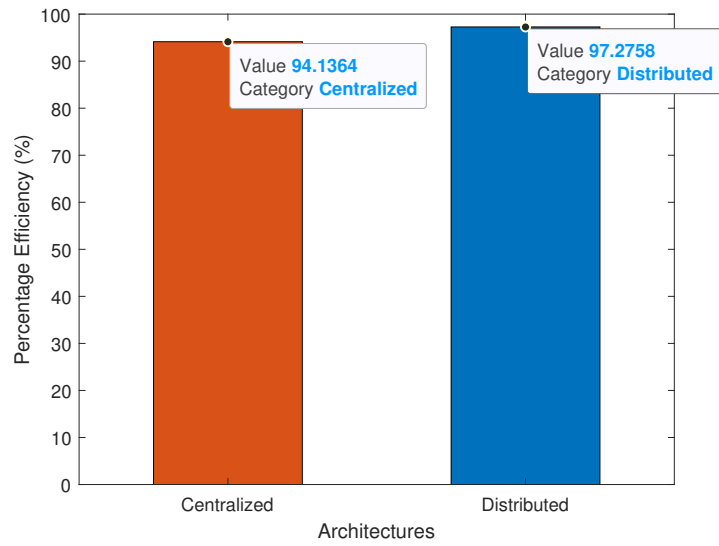


**Figure 4.7** Percentage efficiency of centralized vs. distributed architectures

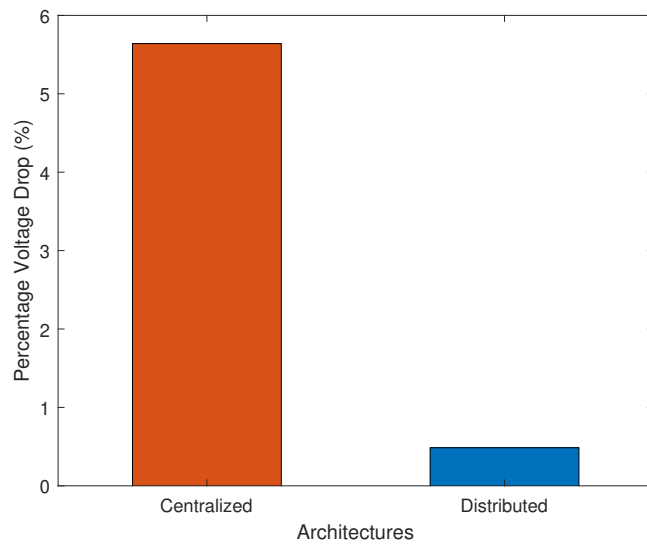


**Figure 4.8** Percentage voltage drop of centralized vs. distributed architectures

## 4.6 Summary

This chapter presents and implements a detailed mathematical model of DC-DC converter losses in DC islanded microgrids for centralized and distributed architectures. When converter losses are incorporated along with distribution losses, the total system losses are determined, which are close to the practical systems. The study helps determine the steady-state operation of the system and its performance, as well as a comparative analysis of different architectures. It is determined that the distributed architecture has more power available at a large time span, has better efficiency, and offer fewer losses than the centralized one. In the next chapter, the operation of the converters will be optimized by load shifting, power-sharing, and reducing losses.

## CHAPTER FIVE

### OPTIMAL POWER DISPATCH IN DC ISLANDED MICROGRIDS AND OPTIMAL POWER FLOW IN DGDS DC MICROGRIDS

#### 5.1 Introduction

In this chapter, optimal power dispatch and optimal peer-to-peer power sharing in DC islanded microgrids is discussed, along with the minimization of total losses. Nasir et al. proposed a scalable distributed DC microgrid architecture with power-sharing capability in (Mashood Nasir, Hassan Abbas Khan, Hussain, et al., 2017; Mashood Nasir, Jin, et al., 2018; Mashood Nasir, Hassan Abbas Khan, Niazi, et al., 2019; Iqbal, Mehran, and Mashood Nasir, 2021). The peer-to-peer energy-sharing approach is developed in (Iqbal, Mehran, and Mashood Nasir, 2021). However, the research presented in the literature focused solely on addressing distribution losses.

In contrast, our research utilizes the DGDS microgrid architecture with neighborhood-level power-sharing capability to model both distribution and conversion losses. In (Mashood Nasir, Hassan Abbas Khan, Hussain, et al., 2017), the optimal planning of DC microgrids was performed with constant converter losses. Nevertheless, subsequent research by Kolar et al. (Kolar et al., 2012) and Gelani et al. (Gelani, Mashood Nasir, et al., 2017) has demonstrated that the efficiency of a DC-DC converter varies with the output power. As a result, power electronic losses are not static throughout the operation; they depend on the percentage loading and the output power. Thus, a notable contribution of our work involves evaluating and optimizing all distribution and conversion losses, encompassing i) constant, ii) linear, and iii) quadratic losses.

The optimal power flow (OPF) algorithm is paramount for optimizing power system planning, operation, analysis, and scheduling. Its implementation is challenging due to the non-linear nature of power flow equations, rendering the optimization problem non-convex.



Consequently, obtaining a globally optimal solution is complex, although the problem can be approximated through relaxation to form a convex problem (Farivar and S. H. Low, 2013). This relaxed problem can be verified by ensuring that the obtained solutions satisfy the nonlinear inequality constraints. The Second-Order Cone Program (SOCP) and Semi-Definite Program (SDP) represent widely used relaxation techniques. In a previous study, the Branch Flow Method (BFM) was employed (Gan and Steven H Low, 2014; Li et al., 2018), and Low et al. demonstrated that the SOCP relaxation can be exact. The optimal solution can be unique within DC networks, independent of system topologies and operational modes. They successfully solved the OPF for DC microgrids. Our research enhances the BFM introduced in (Li et al., 2018) to incorporate converter and distribution losses.

Given that many distributed DC microgrid systems are dominated by power electronics converters, considering only distribution losses while neglecting power electronic conversion losses may lead to inaccurate system-level analysis. Our approach addresses this gap by solving the OPF problem to optimize the power dispatch of distributed energy resources (DERs), thereby minimizing total distribution losses and maximizing power electronics efficiencies. The key contributions are summarized below:

i) Development of a mathematical framework based on the improved BFM, which offers detailed modeling of distribution and power electronics conversion losses for IDCMGs aimed at rural electrification.

ii) Formulation of a multi-objective optimization problem that seeks to simultaneously maximize conversion efficiencies and minimize distribution losses within the system. Converter losses (constant, linear, and quadratic) are incorporated into the constraints to enhance the accuracy of the designed OPF problem.

iii) Determination of solution feasibility and verification of solution accuracy through obtained results.

iv) Adaptation of the proposed OPF problem to suit any DC system for creating a BFM and optimization of objective functions for various interconnection schemes, such as ring and

radial, essential for planning and designing IDCMGs for rural areas.

## 5.2 Modeling of islanded DC microgrid system

The IDCMG considered for rural electrification of a remote rural community is illustrated in Fig. 5.1 (building block) and Fig. 5.2 (architecture). The distributed architecture comprises multiple PV-Battery-based houses interconnected with each other. The objective is to establish an optimal power dispatch mechanism to enhance excess power-sharing among different houses. For operational efficiency considerations, system losses are categorized as a) power electronics converter losses and b) distribution losses. Additionally, certain other losses are assumed to be constant in this study, e.g., heat losses in solar panels and storage charging or discharging losses (Maghami et al., 2016).

### 5.2.1 Nanogrid Model

In DGDS microgrid architecture of a village, several households are present. Each house is assumed to feature an independent rooftop solar panel, battery, and DC loads; this configuration is called a nanogrid. The nanogrids are designed to be self-sufficient and can operate both as prosumers and consumers. They can function independently or integrated to form a microgrid (Mashood Nasir, Hassan Abbas Khan, Hussain, et al., 2017). This integration offers the advantage of resource-sharing and scalability. The nanogrid model with its components is shown in Fig. 5.1. The power generated by each house is denoted as  $P_G$ . It serves one of three purposes: i) meeting internal load demands, ii) being stored in the internal battery, or iii) being shared with other nanogrids. The path of power channeling relies on resource availability and load demand. The power stored in the battery is represented as  $P_B$  with a corresponding state of charge (SOC). Due to the high market availability of the DC loads, each household is assumed to have DC loads with demand  $P_L$ . A DC-DC converter is essential for performing maximum power point tracking (MPPT) and transferring power

among nanogrids. Multiple DC-DC converters are integrated within a system based on their functions, e.g., MPPT, step-up and step-down voltage, and power transfer. However, we assumed a single port converter to model the converter losses explicitly. The power processed by the converter is  $P_{conv}$ . Each nanogrid has a DC external bus for inter-nanogrid interactions. The square of voltage magnitude and power injection at buses are represented by  $v$  and  $P$ , respectively.

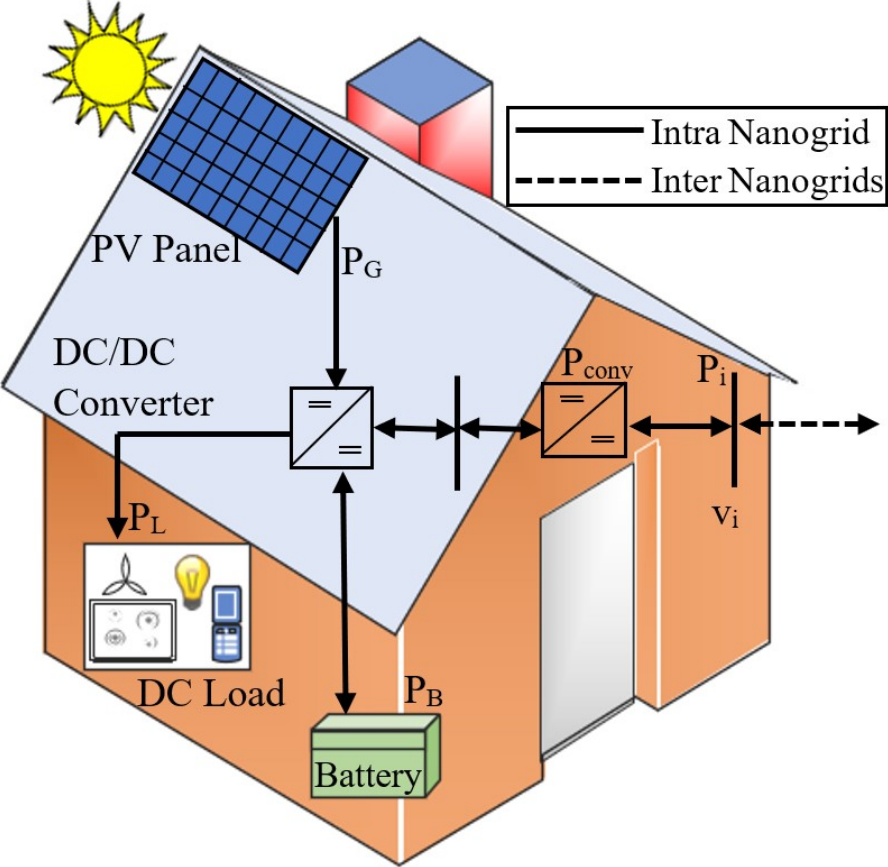
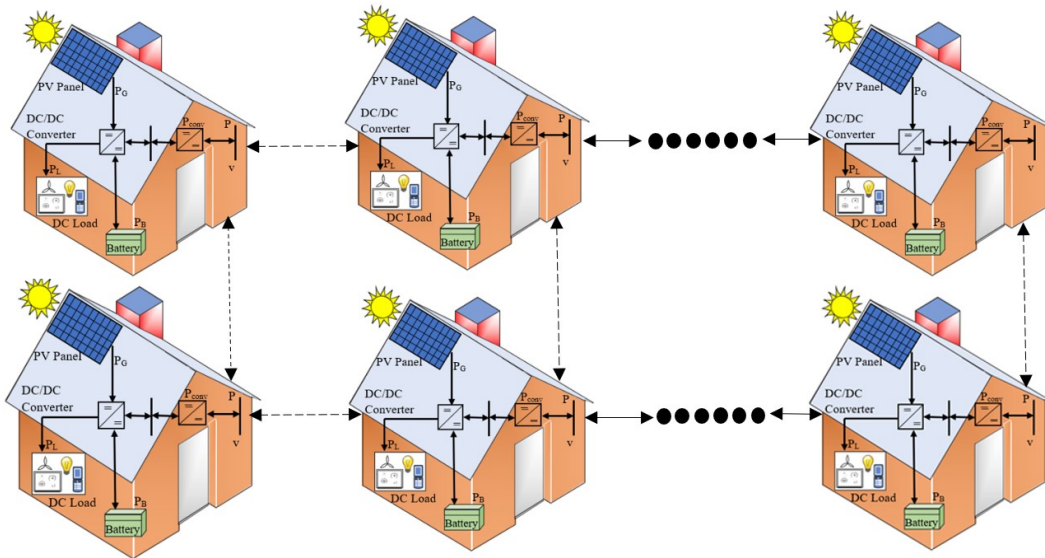


Figure 5.1 Nanogrid model with components.

### 5.2.2 Distributed Generation Distributed Storage Architecture

The nanogrid model illustrated in Fig. 5.1 is a fundamental block for the DGDS microgrid architecture, where multiple nanogrids are interconnected, as depicted in Fig. 5.2. The dotted lines among nanogrids indicate inter-connections, while the solid lines represent intra-

connections. The interconnections offer an additional benefit of peer-to-peer power-sharing through individual resources. A detailed schematic of the distributed architecture, focusing on two nanogrids, is presented in Fig. 5.3. The external bus of each nanogrid is referred to as a node. A node, denoted as “i” is connected to the node, denoted as “j” through a resistance  $r_{ij}$  with a corresponding current flow  $I_{ij}$  and power flow  $P_{ij}$  from node i to node j. The square magnitude of voltage and real power injection at nodes i and j are represented as  $v_i$ ,  $v_j$ ,  $P_i$ , and  $P_j$ .



**Figure 5.2** Distributed Generation Distributed Storage Architecture.

### 5.2.3 Distribution Losses

Distribution losses depend on various factors, with voltage level, distance, and power distribution being the most significant (Mashood Nasir, Hassan Abbas Khan, Hussain, et al., 2017). The framework discussed in the following section employs the branch flow model for DC power systems that accounts for distribution loss calculation. For a DC system with  $N$  nodes, distribution losses are calculated using the square magnitude of current flow  $l_{ij}$

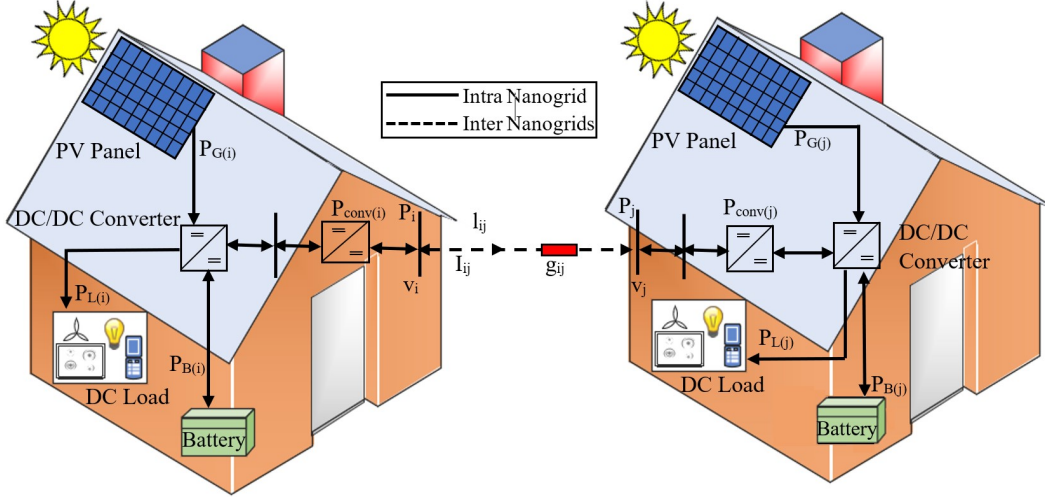


**Figure 5.3** Framework for loss estimation.

through distribution line resistance  $r_{ij}$ , as expressed in Eq. 5.1.

$$DL = \sum_{j:j \sim i} l_{ij} r_{ij} \quad \forall i \in \mathcal{N} \quad (5.1)$$

#### 5.2.4 Converter Losses

The primary function of the DC-DC converter is to perform MPPT or step-up/down transfer. The power processed by each converter results in losses called power electronic losses. With advancements in power electronics, converters are designed to operate efficiently while minimizing these losses. Nonetheless, these losses are contingent upon the output power, whereby the converter's efficiency is a non-linear function of the ratio of output power to the rated capacity (Gelani, Mashood Nasir, et al., 2017; Kolar et al., 2012; Mashood Nasir, Iqbal, Hassan A Khan, et al., 2020) (expressed as % loading), as defined by Eq. 5.2, as illustrated in Chapter 4, section 4.3.2 in Fig. 4.5.

$$\eta_c = \sum_{x=0}^K k_x \left( \frac{P_o}{P_R} \right)^x \quad (5.2)$$

In Eq. 5.2,  $\eta_c$  denotes the converter's efficiency,  $P_o$  and  $P_R$  represent output and rated powers,

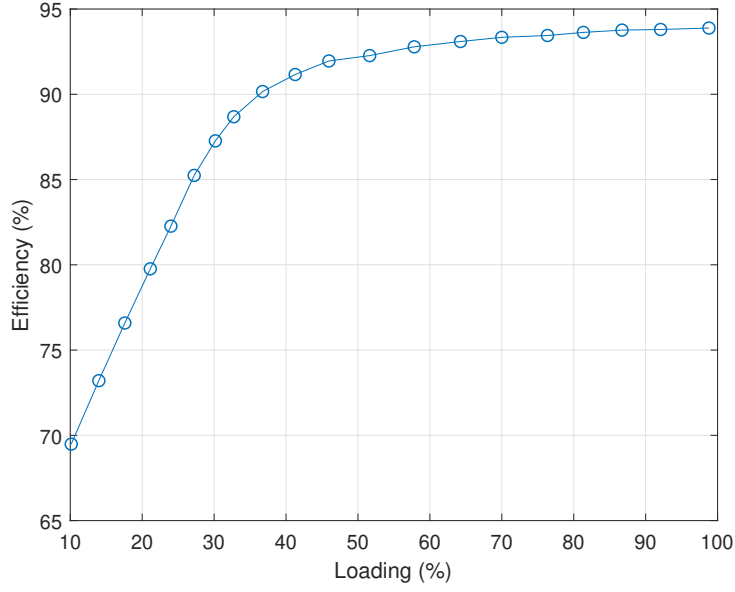


**Figure 5.4** Loading vs. efficiency curve of a DC-DC converter.

respectively, and  $k_x$  stands for the co-efficient of conversion efficiency. The value of  $x$  varies from 0 to  $K$ . In our work, we have only considered the low-order terms, assuming  $K=2$ , so converter losses are modeled as; i) constant, ii) linear, and iii) quadratic. Higher-order terms are disregarded, leading to the simplified form of Eq. 5.2 as shown in Eq. 5.3.

$$\eta_c = k_0 + k_1 \left( \frac{P_o}{P_R} \right) + k_2 \left( \frac{P_o}{P_R} \right)^2 \quad (5.3)$$

$$P_{conv_i} = \frac{1 - \sum_{x=0}^K k_x \left( \frac{P_o}{P_R} \right)^x}{\sum_{x=0}^K k_x \left( \frac{P_o}{P_R} \right)^x} * P_o \quad (5.4)$$

The total conversion losses ( $P_{conv_i}$ ) are given by Eq. 5.4.

### 5.3 Optimal Power Flow Problem Formulation of DC islanded microgrid system

The formulation of BFM and the multi-objective optimization problem for the considered IDCMG system are presented in this section. Next, we elaborate on formulating the multi-objective optimization problem, aiming to minimize distribution losses and maximize conversion efficiencies within the system through optimal power dispatch. Moving forward, we introduce the Second-Order Cone Program (SOCP) relaxation, which involves transforming the non-convex quadratic equality constraints into inequality constraints. The proposed mathematical model is designed to solve the optimization problem on both the system level (distribution lines) and the device level (converters).

#### 5.3.1 Branch flow Model

The IDCMG system depicted in Fig. 5.2 can be represented as a graph denoted as  $\mathcal{G}(\mathcal{N}, \mathcal{E})$ . This graph consists of  $\mathcal{N}$  nodes, where  $\mathcal{N} := \{1, 2, \dots, n\}$  and  $\mathcal{E}$  edges, representing the connections between nodes. The terms 'nodes' and 'edges' are interchangeably used here to correspond to 'buses' and 'branches' within the power system. It can be radial or mesh, assuming  $G$  is connected. Nodes  $i$  and  $j$  are linked through an edge  $(i, j)$  and these nodes are indexed as  $1, 2, \dots, n$ , represented as  $(i, j) \in \mathcal{E}$ , with the condition that  $i \sim j$  and  $i < j$ , denoted as  $i \rightarrow j$ .

In the DC power system, each branch  $(i, j) \in \mathcal{E}$  is characterized by an impedance  $z_{ij} = r_{ij} + \iota x_{ij}$ , which is purely resistive with no reactance, i.e.,  $x_{ij} = 0$ . Consequently  $z_{ij} = r_{ij}$ . Therefore, the admittance  $y_{ij} = g_{ij}$ , where  $g_{ij} = 1/r_{ij}$ . The apparent power  $S_{ij} = P_{ij} + \iota Q_{ij}$  comprises solely real power flow (no reactive component), thus  $S_{ij} = P_{ij}$ . The current magnitude  $I_{ij}$  flows through the line. For each bus  $(i) \in \mathcal{N}$ , let  $V_i$  and  $P_i$  denote the magnitude of the voltage and net real power injection, respectively, as illustrated in Fig. 5.1. In the context of a DC microgrid, all variables, i.e.,  $V_i$ ,  $P_i$ ,  $I_{ij}$ ,  $g_{ij}$ , and  $P_{ij}$  are real numbers.

The power flows in the power system are governed by three primary physical laws (Gan

and Steven H Low, 2014; Li et al., 2018). These principles establish the branch-flow model for the DC islanded microgrid system.

$$\text{Ohm's Law; } \quad I_{ij} = g_{ij}(V_i - V_j) \quad \forall (i, j) \in \mathcal{E} \quad (5.5)$$

$$\text{Current Balance; } \quad I_i = \sum_{j:j \sim i} I_{ij} \quad \forall i \in \mathcal{N} \quad (5.6)$$

$$\text{Power Equation; } \quad P_i = V_i I_i \quad \forall i \in \mathcal{N} \quad (5.7)$$

### 5.3.2 Converter Efficiency and Distribution Loss Optimization

This section aims to reduce the distribution losses and maximize the converter's operational efficiencies within the system, achieving optimal power dispatch at each participating nanogrid and fostering optimal power sharing among nanogrids. An optimization problem, Eq. 5.8 was previously introduced in the literature (Li et al., 2018) for distribution loss minimization.

$$\text{OPF-1; Minimize: } \quad \sum_{j:j \sim i} l_{ij} r_{ij} \quad \forall i \in \mathcal{N} \quad (5.8)$$

Our study extends the optimization problem by incorporating conversion efficiencies into distribution losses. The formulated multi-objective optimization problem (denoted as OPF-2) is presented as follows:

$$\text{OPF-2; Minimize: } \quad \sum_{j:j \sim i} l_{ij} r_{ij} - \sum_{i \in \mathcal{N}} \eta_i \quad \forall i \in \mathcal{N} \quad (5.9)$$

Subject to:

$$P_{G_i}(t) - P_{L_i}(t) - P_{B_i}(t) - P_{conv_i}(t) = \sum_{j:i \rightarrow j} P_{ij}(t) \quad \forall i \in \mathcal{N} \quad (5.10)$$

$$P_i(t) = \sum_{j:i \rightarrow j} P_{ij}(t) \quad \forall i \in \mathcal{N} \quad (5.11)$$

$$P_{ij}(t) + P_{ji}(t) = r_{ij} * l_{ij}(t) \quad i \rightarrow j \quad (5.12)$$



$$v_i(t) - v_j(t) = r_{ij} * (P_{ij}(t) - P_{ji}(t)) \quad i \rightarrow j \quad (5.13)$$

$$v_i(t) * l_{ij}(t) = (P_{ij}(t))^2 \quad i \sim j \quad (5.14)$$

$$l_{ij}(t) \leq (I_{ij,rated})^2 \quad \forall (i, j) \in \mathcal{E} \quad (5.15)$$

$$P_{B_i}(t) - P_{L_i}(t) \leq C_B(t) * [SOC_i(t) - \underline{SOC}_i] \quad \forall i \in \mathcal{N} \quad (5.16)$$

$$P_{L_i}(t) - P_{B_i}(t) \leq C_B(t) * [\overline{SOC}_i - SOC_i(t)] \quad \forall i \in \mathcal{N} \quad (5.17)$$

$$SOC_i(t+1) = SOC_i(t) + 1/C_B(t) * [P_{B_i}(t)] \quad \forall i \in \mathcal{N} \quad (5.18)$$

Voltage limits at each node:

$$\underline{v}_i \leq v_i \leq \overline{v}_i \quad \forall i \in \mathcal{N} \quad (5.19)$$

Power generation limits at each node:

$$\underline{P_{G_i}} \leq P_{G_i} \leq \overline{P_{G_i}} \quad \forall i \in \mathcal{N} \quad (5.20)$$

State of charge limits at each battery:

$$\underline{SOC}_i \leq SOC_i \leq \overline{SOC}_i \quad \forall i \in \mathcal{N} \quad (5.21)$$

where,  $P_{G_i}$  signifies the generated power,  $P_{B_i}$  represents the battery power,  $P_{L_i}$  denotes the load power,  $P_{convloss_i}$  encompass the total converter losses, and  $P_i$  stands for the active power flow injected at each node  $i$ . The terms  $\underline{P_{G_i}}$  and  $\underline{v}_i$  indicate the lower bounds of generated power and squared voltage magnitudes, respectively, while the  $\overline{P_{G_i}}$  and  $\overline{v}_i$  represent the corresponding upper bounds. The terms  $\underline{SOC}_i$  and  $\overline{SOC}_i$  denote lower and upper SOC bounds.

The branch flow equations in Eq. 5.12 to Eq. 5.14 involve  $v_i$  representing the voltage

magnitude squared, and  $l_{ij}$ , signifying the squared current magnitudes,  $v_i = |V_i|^2$  and  $l_{ij} = |I_{ij}|^2$ . Eq. 5.12 corresponds to the power balance equation, while Eq. 5.14 captures the relationship between current flow, power flow, and voltage. Eq. 5.12 and Eq. 5.13 are linear, but equation Eq. 5.14 introduces non-linearity due to its dependence on  $P$ ,  $l$ , and  $v$ .

The Eq. 5.16 to Eq. 5.18 represent the battery's operation considering its state of charge as well as the power management between the battery and load. The optimal values for power dispatch at each bus, obtained by solving SOCP, are not necessarily the original problem's actual value. The feasible domain resulting from relaxing the constraints is larger than the actual problem. Accordingly, the optimal values are checked using the relaxed constraints while satisfying the nonlinear equality constraints. The feasibility and exactness of the conic relaxation are verified.

### 5.3.3 Proposed Algorithm

The pseudo-code for the algorithm proposed for the power flow among nanogrids is represented in Figure 5.5. The power dispatch is determined considering  $P_{Gi}$ ,  $P_{Bi}$ ,  $P_{Li}$ , and  $SOC_i$ . The algorithm developed for optimal power dispatch strategy is independent of the state of charge unbalance.

## 5.4 Results And Discussion

The algorithm's effectiveness is validated for static and dynamic load scenarios by comparing the results of the OPF solved using the Newton-Raphson Power Flow method modified for DC systems. The nonlinear OPF problems, namely OPF-1 and OPF-2, have also been solved. The relaxed SOCP problem is formulated and solved in MATLAB using the "fmincon" function from its optimization toolbox, ensuring the results' global optimality. The centralized optimization is performed for the multi-objective system, where state and control data from each participating house are received, and optimized data values are returned.

---

**Algorithm 1: Optimal Power Dispatch Strategy**

---

**Data:** Data Collection from all nodes:  $P_{Gi}, P_{Bi}, P_{Li}, SOC_i$   
 $\forall i = 1, 2, 3, i, j, \dots N$   
**Result:** Optimal Power Dispatch at each node  
initialization;  
**if**  $P_{Gi} > P_{Li} \ \& \ P_{Gj} < P_{Lj}$  **then**  
    **if**  $P_{Bi} > P_{Li} \ \& \ SOC_{i(min)} < SOC_i$  **then**  
        **if**  $P_{Bj} < P_{Lj} \ \& \ SOC_{j(min)} < SOC_j$  **then**  
            |  $P_{ij} > 0$   
        **end**  
    **end**  
**else**  
    **if**  $P_{Gi} < P_{Li} \ \& \ P_{Gj} < P_{Lj}$  **then**  
        **if**  $P_{Bi} > P_{Li} \ \& \ SOC_{i(min)} < SOC_i$  **then**  
            **if**  $P_{Bj} < P_{Lj} \ \& \ SOC_{j(min)} < SOC_j$  **then**  
                |  $P_{ij} > 0$   
            **end**  
        **end**  
    **end**  
**end**

---

**Figure 5.5** Proposed Algorithm for Optimal Power Dispatch.

#### 5.4.1 Test System

Due to the lack of a benchmark test system for DC islanded microgrids, AC test systems are adapted with certain assumptions detailed below. The test system data is obtained from MATPOWER, a MATLAB toolbox. These test systems are modified to simulate DC microgrid conditions, involving adjustments to line reactance, setting reactive power flows to zero, and reducing line resistance values by 10% (Gan and Steven H Low, 2014; Li et al., 2018). Figure 5.2 illustrates the system diagram for the DGDS microgrid architecture with "n" number of houses. The upper and lower bounds for voltage magnitudes are 1.05 per unit (p.u) and 0.95 p.u, respectively.

#### 5.4.2 Case Study

The case study for implementing our proposed optimization algorithm revolves around multiple independent nanogrids and a communal load. The fourteenth home is assumed as the

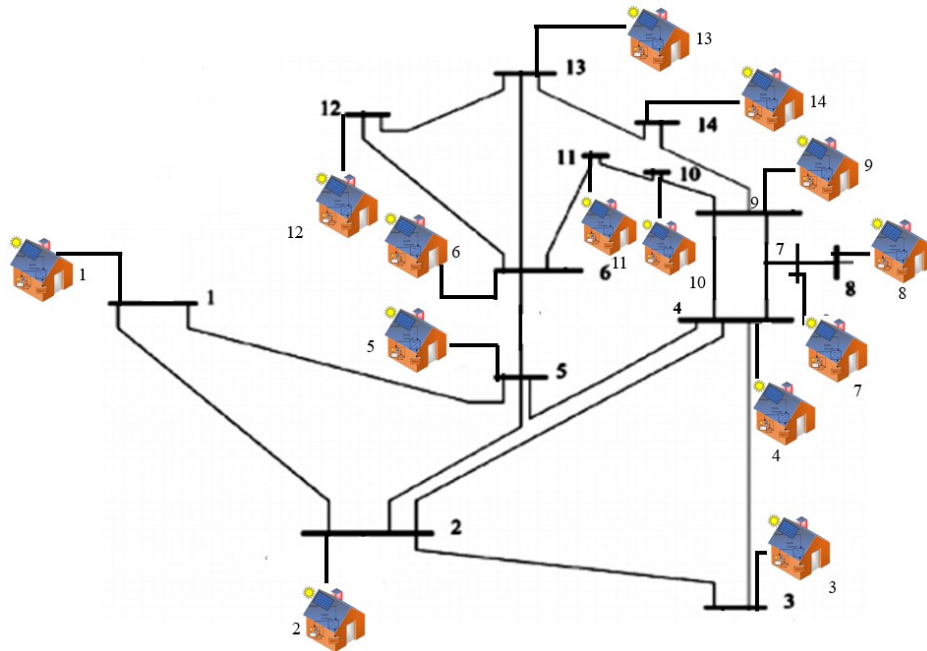


**Figure 5.6** Modified 14 Bus Test System Architecture as DC Microgrid for rural areas.

communal load in the modified fourteen-house microgrid system. Fig. 5.2 showcases the orientation of houses utilized for implementing our proposed optimization algorithm. The architecture of the considered DC system, modified according to the IEEE 14-bus system, is displayed in Fig. 5.6.

### 5.4.3 Static Loads

The optimization problem is solved by analyzing the steady-state performance of the system. Results for i) distribution loss optimization (OPF-1) and ii) optimization for both distribution loss and conversion efficiency (OPF-2) in the modified fourteen-node system are demonstrated in Table. 5.1 and Table. 5.2, respectively. The fourteenth household, assumed to be a community load without PV and battery, has its load demand met through power sharing from neighboring nanogrids. In Table. 5.1, households 6,9,10, and 13 contribute power to the 14th house. However, in Table. 5.2 for OPF-2, only households 1, 3, and 5 contribute to power-sharing with household 14. This suggests that OPF-2 concentrates higher

power scheduling at fewer houses than OPF-1, resulting in fewer operating converters at any given time. The SOC at most non-power scheduling houses is higher for OPF-2, indicating that batteries are generally at a higher state of charge, consuming the available power instead of losses. Moreover, converters in OPF-2 operate more efficiently at each scheduling bus than those in OPF-1. The results for static loads, with unbalanced SOC are shown in tables 5.4 and ??.

**Table 5.1** OPF-1 for modified 14 bus DC Microgrid System.

Bus No.	Pi (p.u.)	PBi (p.u.)	SOCi (%)	Nodal Voltage (p.u.)	Converter Efficiency (%)
1	0.000	0.350	82.914	1.050	Non-Op
2	0.000	-1.200	70.000	1.050	Non-Op
3	0.000	0.500	84.165	1.050	Non-Op
4	0.000	-1.000	71.663	1.050	Non-Op
5	0.000	0.500	84.165	1.050	Non-Op
6	0.002	-1.002	71.647	1.050	77.691
7	0.000	0.300	82.497	1.050	Non-Op
8	0.000	-1.200	70.000	1.050	Non-Op
9	0.238	0.246	82.047	1.050	79.932
10	0.015	0.384	83.203	1.050	77.809
11	0.000	-1.200	70.000	1.050	Non-Op
12	0.002	0.496	84.137	1.050	77.692
13	0.183	-0.095	79.205	1.050	79.406
14	-0.429			1.019	81.752

#### 5.4.4 Dynamic Loads

Using time-based varying load and PV data is more practical and realistic. The optimization utilizes time-based data acquired from National Renewable Energy Laboratories (NREL) (*Solar Power Data for Integration Studies*- n.d.). Fig. 5.7 demonstrates the data for PV and load multipliers, assuming an increase in demand during late afternoon hours, while load requirement decreases during night-time and early morning. Load and PV profiles depend highly on the selected site and its residents and can be adjusted accordingly.

**Table 5.2** OPF-2 for modified 14 bus DC Microgrid System.

Bus No.	Pi (p.u.)	PBi (p.u.)	SOCi (%)	Nodal Voltage (p.u.)	Converter Efficiency (%)
1	0.252	-0.392	70.000	1.050	80.063
2	0.000	-1.200	83.557	1.047	Non-Op
3	0.069	0.500	71.667	1.047	78.319
4	0.000	-1.000	82.836	1.043	Non-Op
5	0.150	0.500	71.667	1.044	79.089
6	0.000	0.400	82.500	0.995	Non-Op
7	0.000	0.300	70.000	1.009	Non-Op
8	0.000	-1.200	84.167	1.009	Non-Op
9	0.000	0.437	83.333	0.991	Non-Op
10	0.000	0.400	70.000	0.992	Non-Op
11	0.000	-1.200	84.158	0.993	Non-Op
12	0.000	0.325	80.833	0.992	Non-Op
13	0.000	0.100	89.6625	0.986	Non-Op
14	-0.429			0.956	81.752

#### 5.4.5 Scheduled Power

The optimization problem proposed in this chapter aims to minimize distribution losses, maximize the converter's efficiencies, and optimize power scheduling and peer-to-peer power sharing among nanogrids. The power scheduling results for the modified 14-bus system are shown in Fig. 5.8 and Fig. 5.9. During time instants  $t=1$  to  $t=5$  and  $t=21$  to  $t=24$ , no PV generation occurs, and batteries meet the load demand. For OPF-1, two buses contribute to meeting the load demand at the 14th bus, whereas for OPF-2, only one bus is involved, albeit with a higher power value. Throughout the remaining time, OPF-2 schedules more power for fewer buses compared to OPF-1, which schedules power for more buses but at a lower magnitude. Notably, the power scheduled for the community load remains the same due to the assumption that the community load lacks generation and storage in this study.

#### 5.4.6 Converter Efficiency

The primary objective of our research in this chapter is to enhance conversion efficiency such that only a single household contributes (if feasible) when power is needed instead of

**Table 5.4** OPF-2 with Unbalanced SOCs.

Bus No.	Pi (p.u.)	PBi (p.u.)	SOCi (%)	Nodal Voltage (p.u.)	Converter Efficiency (%)
1	0.379	-0.055	79.546	1.050	77.673
2	0.000	-1.200	50.000	1.046	Non-Op
3	0.065	0.430	63.584	1.046	Non-Op
4	0.000	-1.000	61.667	1.040	Non-Op
5	0.000	0.500	64.167	1.041	Non-Op
6	0.000	-1.000	71.667	0.995	77.700
7	0.000	0.300	62.500	1.008	Non-Op
8	0.000	-1.200	50.000	1.008	Non-Op
9	0.000	0.500	84.167	0.992	Non-Op
10	0.025	0.373	73.111	0.993	77.830
11	0.000	-1.200	50.000	0.994	Non-Op
12	0.000	0.499	84.158	0.992	Non-Op
13	0.000	0.100	70.833	0.986	Non-Op
14	-0.429			0.976	82.750

involving multiple houses. This approach leads to the operation of fewer converters, each operating at a higher efficiency. These outcomes are evident from Fig. 5.10 and Fig. 5.11. During time instants  $t=1$  to  $t=5$  and  $t=21$  to  $t=24$ , with zero PV generation and battery fulfilling the load, OPF-1 involves multiple households in contributing to the communal load at the 14th bus. However, in OPF-2, only one household participates, leading to higher efficiency in its DC-DC converter. Consequently, converters of multiple households in OPF-1 operate with lower efficiency compared to the single household's converter operating at higher efficiency in OPF-2.

#### 5.4.7 Number of Operating Converters

The optimization problem addressed in OPF-2 ensures power scheduling at houses to minimize the necessary number of DC/DC converters for power-sharing. The reduced converter count, coupled with higher efficiency, results in lower costs, improved operational efficiency, and reduced system losses. The comparison of results for OPF-1 and OPF-2 in the modified 14-bus DC system is depicted in Fig. 5.12.

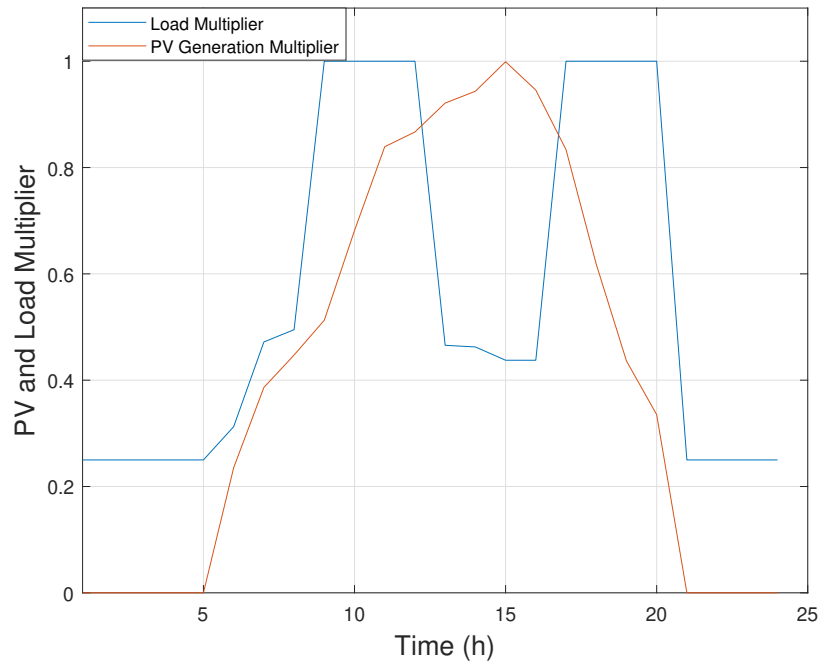


**Figure 5.7** PV Generation and Load Multipliers.

#### 5.4.8 Loss Evaluation

The objective of OPF-1 is to minimize distribution losses, while OPF-2 aims to minimize distribution losses and maximize conversion efficiencies. The total losses encompass distribution and conversion losses, which are calculated and compared for both OPF-1 and OPF-2.

#### Distribution Losses

The distribution loss results for the modified 14-bus DC system are shown in Fig. 5.13. These losses are minimal when PV generation is absent and the load is less. During daytime hours with high PV generation and load consumption, the generated power primarily charges batteries and fulfills the load demand. Distribution losses are higher for OPF-1 than for OPF-2.



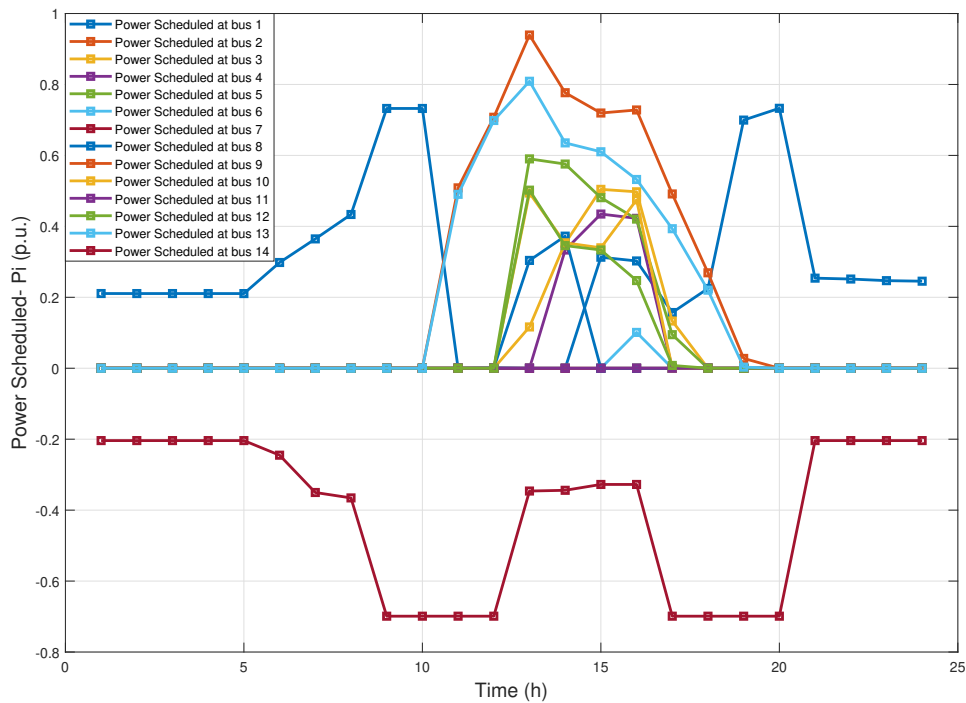


**Figure 5.8** Power scheduled in OPF-1 for modified 14 bus DC Microgrid System.

### Conversion Losses

The results for conversion losses shown in Fig. 5.14 are less when we don't have PV generation and the load is less. When both PV generation and load consumption are high during the daytime, the generation is used mostly to charge batteries besides meeting the load demand. The conversion losses are higher for OPF-1 than OPF-2.

### Total Losses

Fig. 5.15 showcases the results for total losses in the modified 14-bus DC system. Losses are lower during nighttime and early morning but higher during daytime. Overall, OPF-1 results in higher total losses compared to OPF-2 throughout the 24 hours, indicating that OPF-2 enhances efficiency and reduces total system losses.

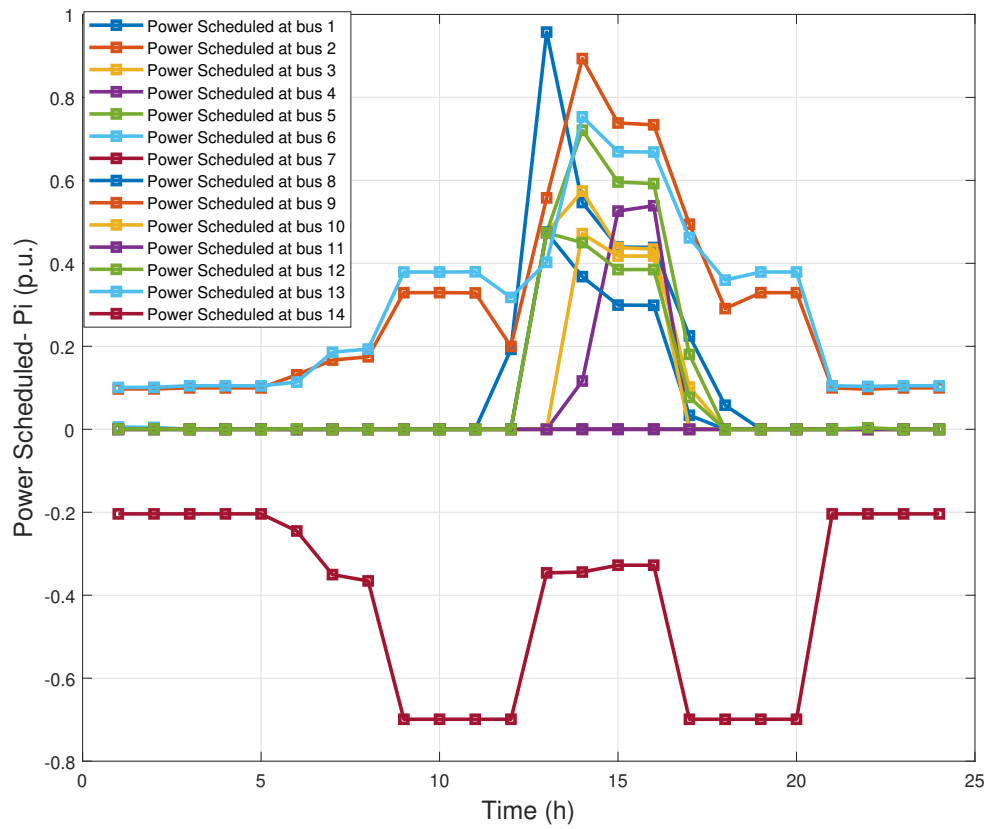
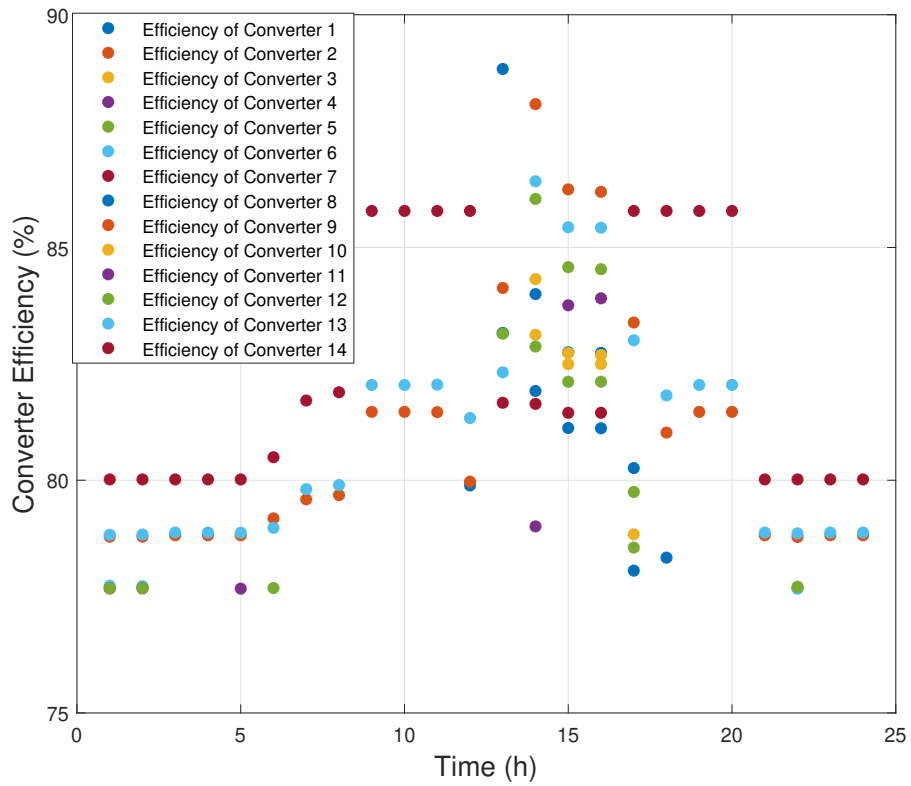


Figure 5.9 Power scheduled in OPF-2 for modified 14 bus DC Microgrid System.



**Figure 5.10** Converter Efficiency in OPF-1 for 14 bus system.

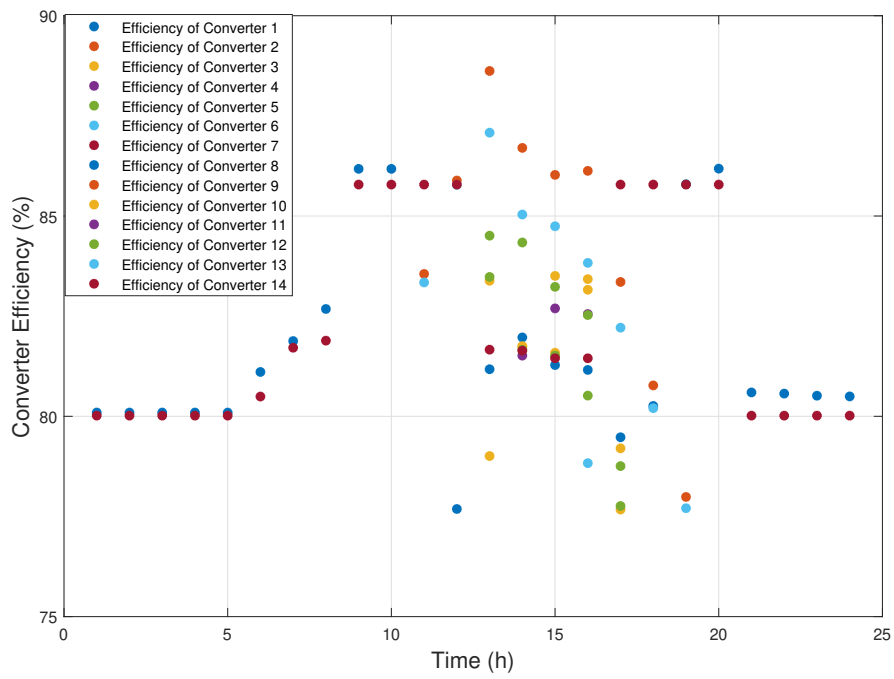
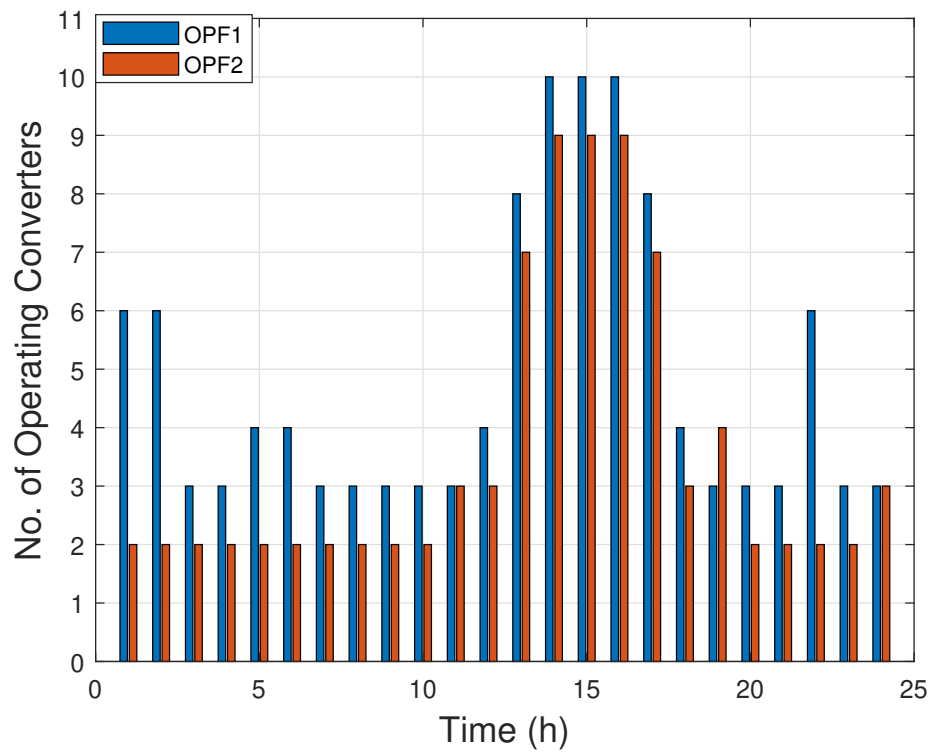
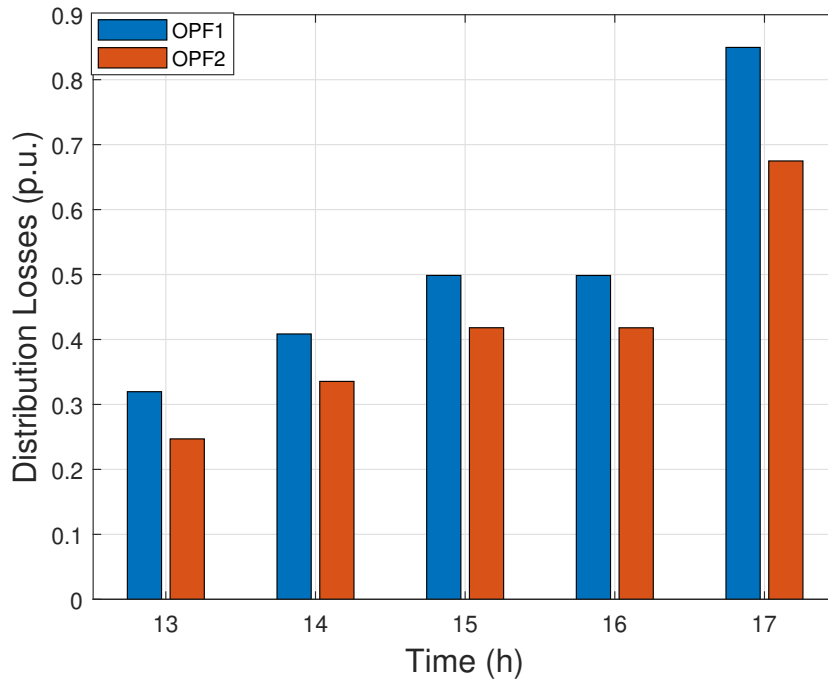
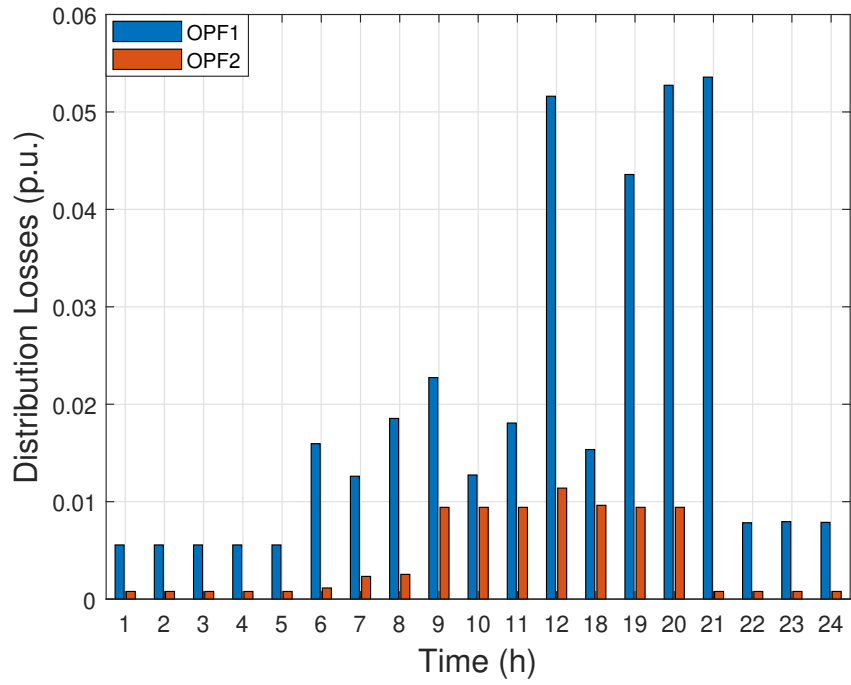


Figure 5.11 Converter Efficiency in OPF-2 for 14 bus system.



**Figure 5.12** Comparison of operating converters in 14 bus system.



**Figure 5.13** Comparison of distribution losses of 14 bus system.

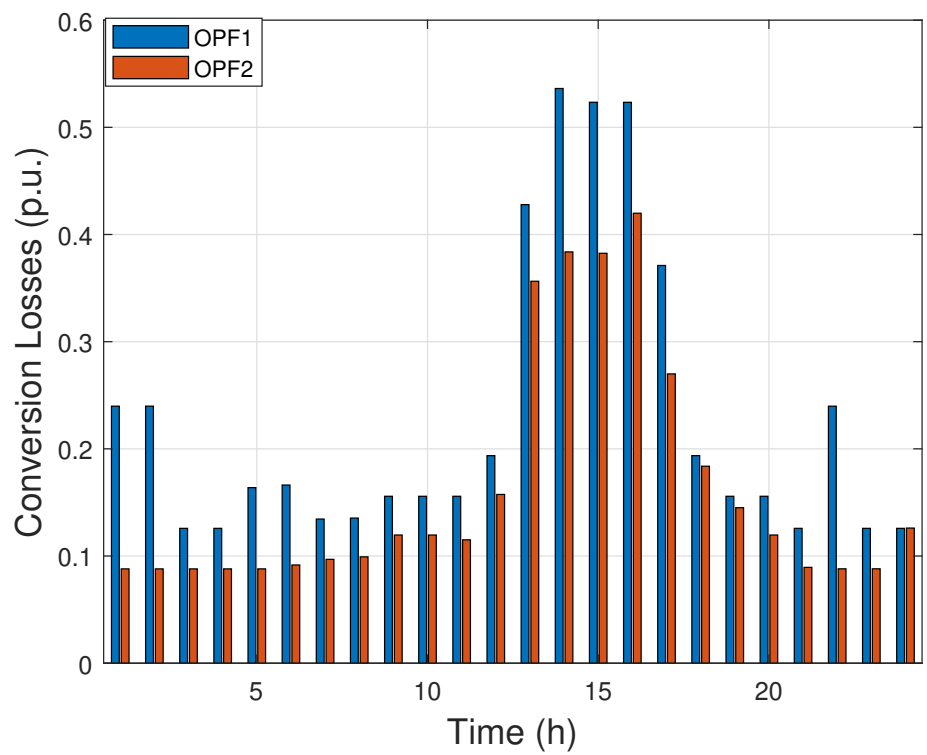


**Figure 5.14** Comparison of conversion losses of 14 bus system.

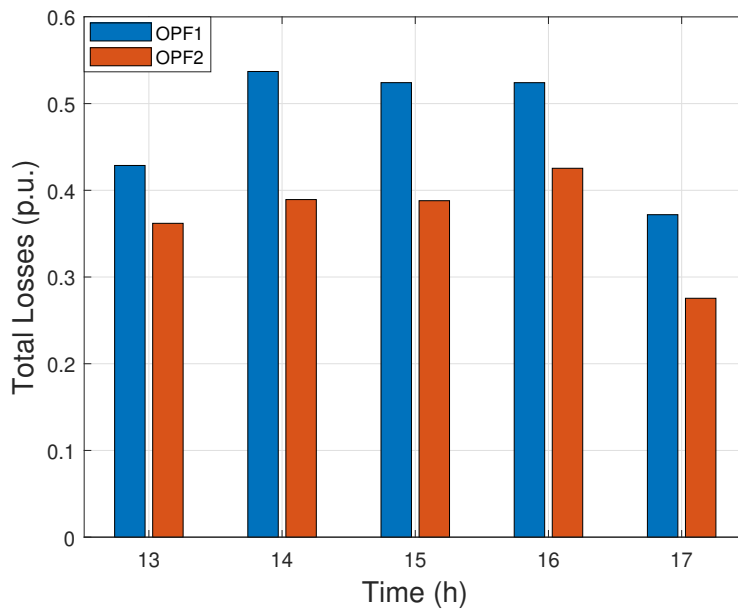
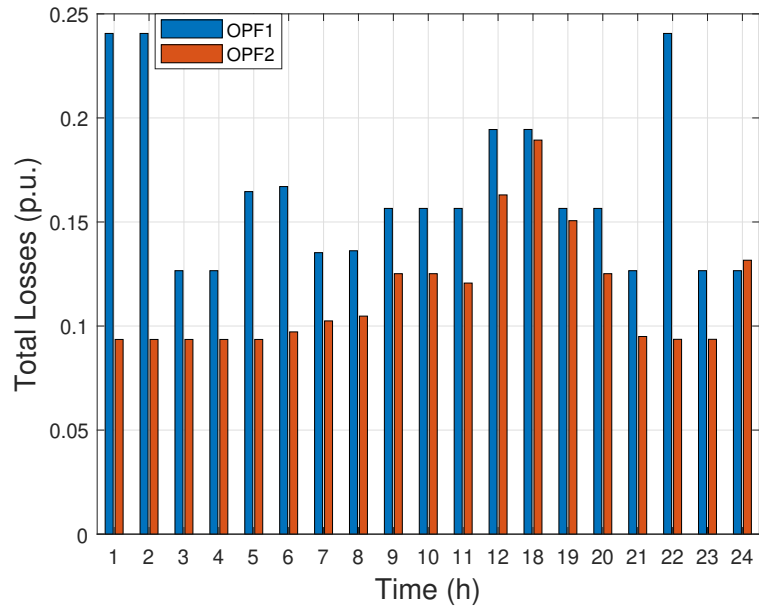


**Figure 5.15** Comparison of total losses of 14 bus system.



## **5.5 Optimal Power Dispatch in Islanded DC Clustered Nanogrids for Rural Electrification**

The microgrid system in this section consists of multiple users grouped into clusters and interconnected to achieve maximum resource sharing. The P2P (peer-to-peer) energy sharing allows a combined objective: optimal power dispatch with minimum system losses while optimally sharing power in the neighborhood. Each user is assumed to have PV and battery storage as DERs; however, other generation sources can also be used. Due to the intermittent nature of solar irradiance and the varying load pattern, each prosumer may have a surplus available power or a deficit.

### 5.5.1 DC Islanded Microgrid Model

The DC islanded microgrid model comprises  $N$  users connected to form a community microgrid model. The integrated microgrids have the advantage of scalability and resource-sharing. Each user can act as a prosumer or consumer depending on the availability or scarcity of power. Each user is assumed to be equipped with solar PV, battery, and DC load. The notions and details of the terms used for each variable are given in section 5.2.1. Fig. 5.1 shows the schematic diagram of our study’s household.

The nanogrid model illustrated in Fig. 5.1 is a fundamental block for the DGDS microgrid architecture, where multiple nanogrids are interconnected, as depicted in Fig. 5.2. The dotted lines among nanogrids indicate inter-connections, while the solid lines represent intra-connections. The interconnections offer an additional benefit of peer-to-peer power-sharing through individual resources. A detailed schematic of the distributed architecture, focusing on two nanogrids, is presented in Fig. 5.3.

The microgrid system is assumed to consist of twenty households, sub-divided into four clusters, each consisting of five houses. Fig. 5.16 shows the microgrid topology used in our study.

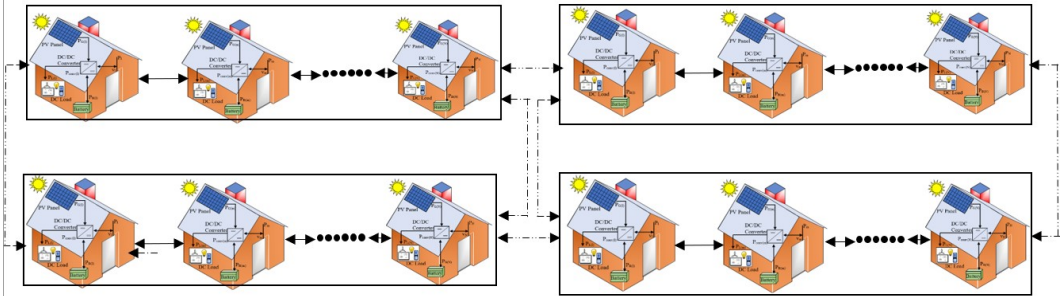


**Figure 5.16** Clusters of nanogrids in DGDS Architecture.

### 5.5.2 Proposed Algorithm

The proposed algorithm assumes some households have excess power generation while others have a deficit. This assumption helps determine the power dispatch at each household and

allows peer-to-peer power sharing among houses with excess power to those in deficit. Our algorithm is based on the centralized controller that gets access to data from all the nodes. The  $P_{Gx}$  is the varied control variable to satisfy the load demand and share power with neighbors to reduce distribution losses.

The algorithm compares the data from multiple nodes and splits them into two categories: i) excess of power and ii) deficit of power. The data from each category is compared based on the distance among them to find the neighbors or closely located nanogrids. The distance among houses is useful for selecting the neighbors with the least distance, so we have fewer distribution losses. The difference between power generation and load power for each nanogrid from the respective group is calculated, and the status of the battery and the state of charge for each nanogrid are determined. Based on the power availability, the power flows from one nanogrid to the other, e.g.,  $P_{i1}$ .

The power will be dispatched based on the least distance among nanogrids. The flowchart of our proposed optimization algorithm is shown in Fig. 5.17.

### 5.5.3 Test System

The test system is a community of 20 users connected in a group of interconnected clusters, as shown in Fig.5.16. Each user is equipped with a battery, PV, and DC load. The initial state of charge, load, and power generation are randomly distributed across all the users. The 20th household is assumed to have a community load with higher load demand and no PV or batteries connected.

Tables 5.5 and 5.6 show the results of the OPF for DC clustered microgrid system. The results indicate that the OPF-2 optimized both distribution and conversion losses while the OPF-1 only minimized the distribution losses. The number of converters operating for OPF-2 is less than OPF-1, but with higher efficiencies, thus resulting in fewer system losses.

The system is run for a day, i.e., 24 hours, and the system losses are calculated. The load and solar irradiance data are obtained from the National Renewable Energy Laboratory

**Table 5.5** OPF-1 for DC Clustered Microgrid System.

Bus No.	Pi (p.u.)	PBi (p.u.)	SOCi (%)	Nodal Voltage (p.u.)	Converter Efficiency (%)
1	0.122	0.469	83.91	1.05	79.09
2	0.000	0.400	63.33	1.05	Non-Op
3	0.000	0.600	65.00	1.05	Non-Op
4	0.000	0.200	71.67	1.04	Non-Op
5	0.000	0.200	61.67	1.04	Non-Op
6	0.167	0.422	83.51	1.05	79.61
7	0.000	0.000	60.00	1.04	Non-Op
8	0.000	0.300	62.50	1.03	Non-Op
9	0.000	0.600	85.00	1.02	Non-Op
10	0.000	0.200	71.67	1.01	Non-Op
11	0.000	0.700	65.83	1.04	Non-Op
12	0.000	0.550	84.58	1.05	Non-Op
13	0.107	0.535	74.46	1.05	78.91
14	0.000	0.200	81.67	1.05	Non-Op
15	0.000	0.000	60.00	1.04	Non-Op
16	0.000	0.600	75.00	1.03	Non-Op
17	0.000	0.400	83.33	1.02	Non-Op
18	0.000	0.600	85.00	1.01	Non-Op
19	0.526	0.039	60.32	1.00	83.94
20	-0.858			0.95	88.14

**Table 5.6** OPF-2 for DC Clustered Microgrid System.

Bus No.	Pi (p.u.)	PBi (p.u.)	SOCi (%)	Nodal Voltage (p.u.)	Converter Efficiency (%)
---------	--------------	---------------	-------------	-------------------------	-----------------------------

(*Solar Power Data for Integration Studies*- n.d.) and (*OpenDSS, EPRI Distribution System Simulator* n.d.). Figure.5.18 and Figure.5.19 show the power dispatch at the user nodes. It can be observed that in OPF-2, fewer users participate with higher efficiencies than in OPF-1. Figure.5.20 shows the total system losses of OPF-1 and OPF-2. It can be observed that OPF-2 has lower system losses than OPF-1, making the optimization solution efficient.

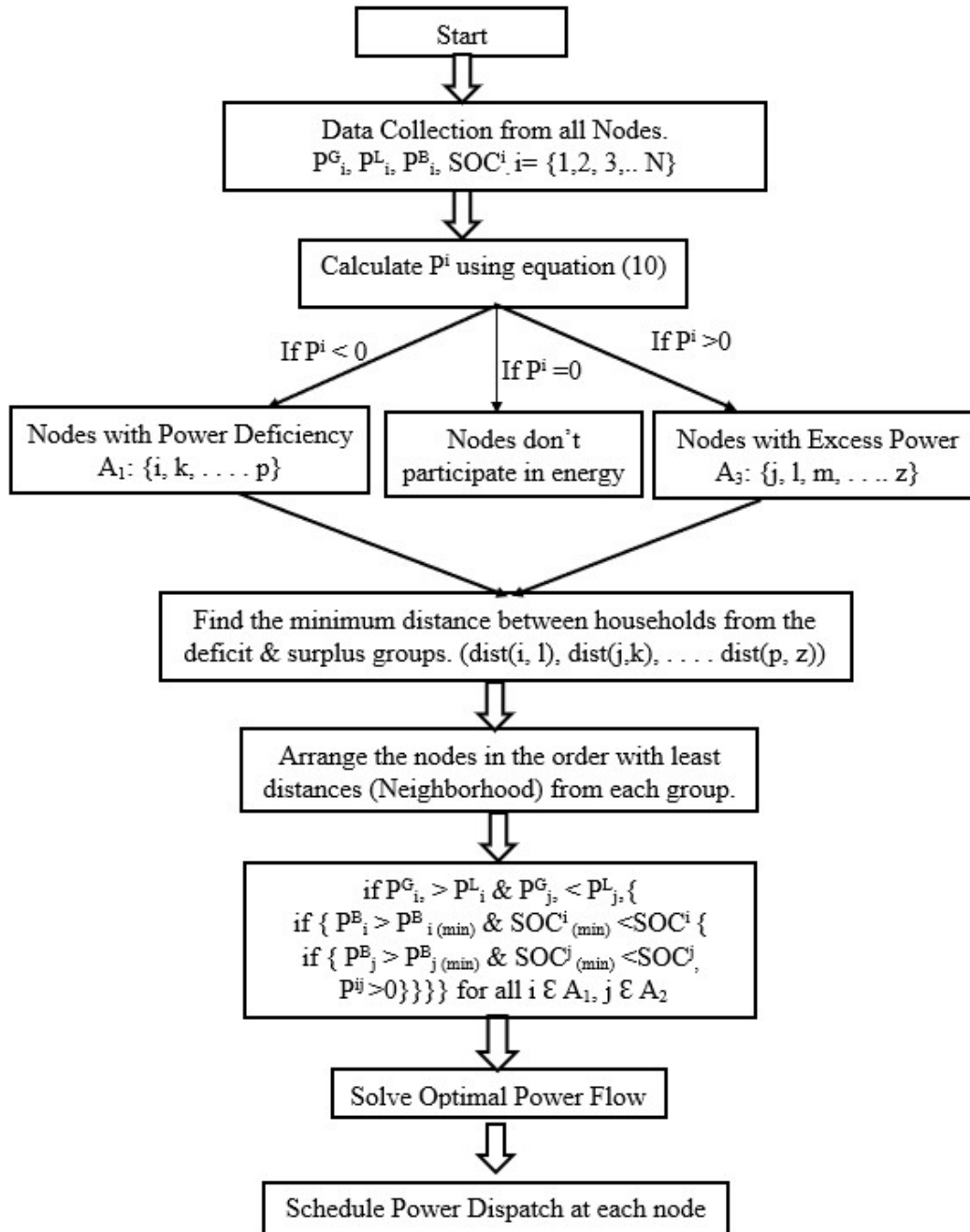


Figure 5.17 Proposed Algorithm For Power Dispatch Strategy

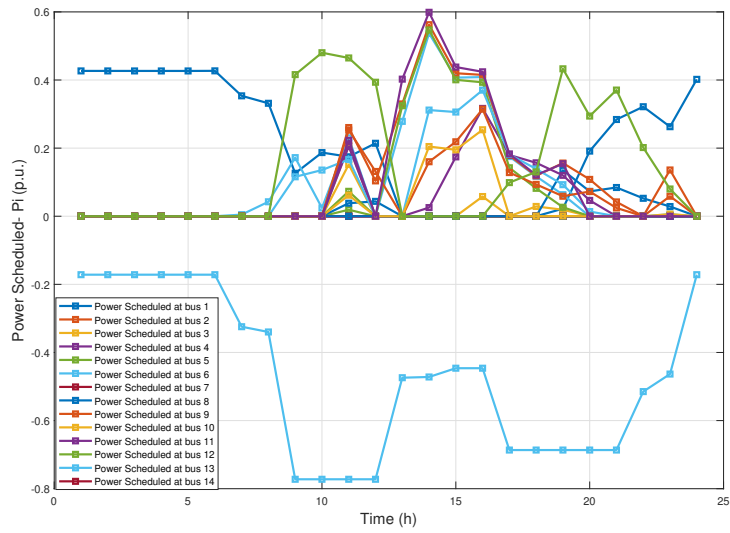


Figure 5.18 Power dispatch at users in OPF-2

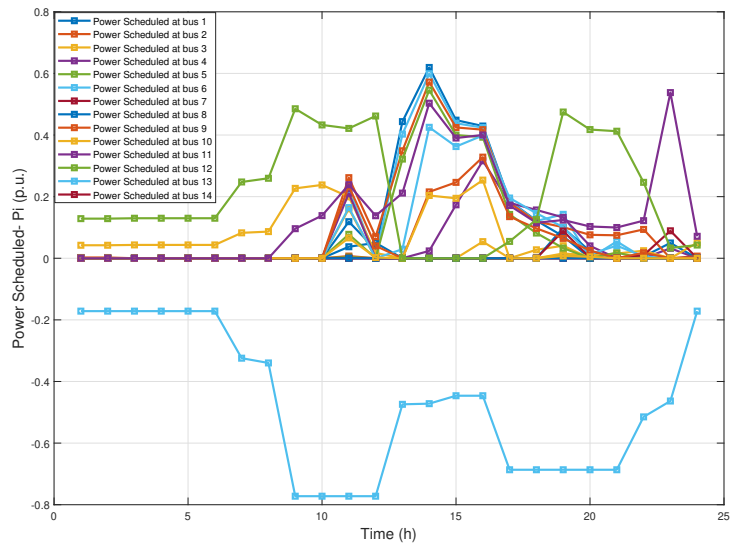
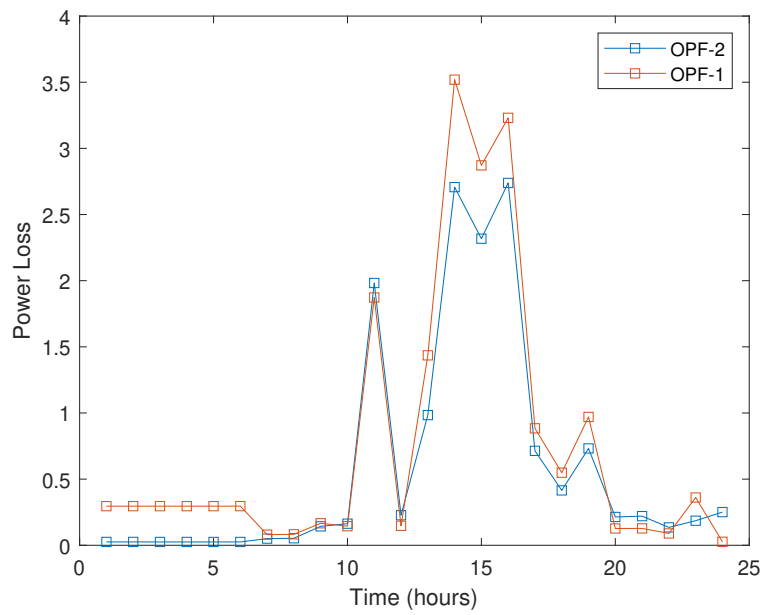


Figure 5.19 Power dispatch at users in OPF-1



**Figure 5.20** Total System losses in OPF-1 and OPF-2



## 5.6 Summary

This chapter proposes an optimal power dispatch and peer-to-peer power-sharing strategy for an islanded community of multiple prosumers. The objective of the optimization algorithm is to minimize system losses and enhance efficiency. A mathematical framework is developed using a modified branch flow model using distribution and conversion losses. The non-linear optimization problem is relaxed using convex relaxation through second-order conic programming, and the relaxed solutions are determined to be feasible and exact. The total system losses, including distribution and conversion losses, are modeled, calculated, and optimized. The proposed optimization algorithm allows usage diversity and resource sharing in a P2P energy-sharing manner. The results indicate that system efficiency is improved by 6%, and the total losses are reduced by 4% compared to when only distribution losses are considered. The results demonstrate that incorporating converter and distribution losses is essential for the system's optimal dispatch operation due to their high contribution to system losses. In our study, the converters operate at higher efficiency, utilizing batteries at a high state of charge to store energy or share it with other households.

## CHAPTER SIX

### CONCLUSIONS AND FUTURE WORK

Residents of remote rural regions without electricity access suffer from energy poverty and have reduced opportunities. Microgrid architectures with optimal planning, design, and operation strategies are essential to meet rural inhabitants' energy demands. DC microgrids based on photovoltaic panels and batteries are used for remote rural electrification. Centralized islanded systems have shortcomings, i.e., high distribution losses, less efficiency, and are comparatively more expensive than distributed microgrids. The distributed systems comprise independent household prosumers that may work independently or integrated. In this dissertation, the optimal power dispatch and peer-to-peer power-sharing among spatially distributed households are performed to minimize distribution losses and maximize power electronic conversion efficiency in a typical IDC MG for rural electrification. A branch flow model is proposed for modeling the power system with DC-DC converters. The optimal power flow is performed by relaxing the original non-convex constraints using second-order conic programming. It is implemented on the modified IEEE-14 bus system and a cluster of houses in the village. This generic framework can be used for optimal energy management in islanded microgrids using the regional solar irradiance information, climate situations, and energy requirements.

#### 6.1 Summary of Contributions

The primary contributions of this dissertation are categorized into three sections. To summarize, the key contribution of this dissertation is developing a mathematical framework based on the improved BFM, which offers detailed modeling of distribution and power electronics conversion losses for IDC MGs aimed at rural electrification.

### **6.1.1 Distribution Loss Analysis of Centralized and Distributed Microgrid Architectures**

The first objective of this dissertation is a detailed distribution loss analysis of both centralized and distributed microgrid architectures with dynamic load and generation profiles. The distribution loss modeling is extended to low-voltage, low-power islanded DC microgrids. A detailed network loss analysis of four different microgrid architectures is performed using modified Newton-Raphson power flow for DC systems. These architectures include 1) Centralized generation centralized storage (CGCS), 2) Centralized generation distributed storage (CGDS), 3) Distributed generation centralized storage (DGCS), and 4) Distributed generation distributed storage (DGDS), which are implemented with both radial and ring interconnection schemes using time-varying load demand and dynamic PV generation. A comparative distribution loss analysis with various conductor sizes and voltage levels shows that the distributed ring architecture is significantly advantageous based on low distribution losses, high efficiency, and low voltage drop. It offers an additional feature of scalability and low capital cost.

### **6.1.2 Mathematical Framework and Modeling of Distribution and Power Electronic Losses**

The second objective of this dissertation is a detailed distribution and conversion loss modeling and analysis for centralized and distributed microgrid architectures using the bus injection method and modified Newton-Raphson power flow method. A comparative power system and power electronic loss analysis for both architectures show that distributed architectures have higher efficiency and lower losses than centralized.

### **6.1.3 Optimal Power Dispatch and Peer-to-Peer Power Sharing Scheme for Rural Electrification**

The third objective of this dissertation is to develop a mathematical framework based on the improved BFM, which offers detailed modeling of distribution and power electronics conversion losses for IDC MGs aimed at rural electrification. It involves formulating a multi-objective optimization problem that seeks to maximize conversion efficiencies and minimize distribution losses within the system. Converter losses (constant, linear, and quadratic) are incorporated into the constraints to enhance the accuracy of the designed OPF problem. The optimal peer-to-peer energy sharing is done by efficiently utilizing the resources while minimizing system losses.

## **6.2 Future Research Directions**

The dissertation focuses on distribution and converter loss analysis in different microgrid systems. The dissertation provides a novel algorithm for optimal peer-to-peer power sharing and dispatch in DC islanded microgrid systems by incorporating distribution and conversion losses. A few possible future research directions are delineated here-

- To enable energy trading among multiple nanogrids, there must be a mechanism to monitor energy transactions among neighboring nanogrids. Although the energy trade mechanism will formulate a local energy market and help empower rural inhabitants, it will require a communication layer at neighborhood levels to ensure the monitoring of energy exchange.
- A key challenge for successfully implementing such a distributed system will be developing a theft monitoring mechanism based on remote monitoring and communication systems to ensure provisioned power flow.
- The DC-DC converters have been used in this dissertation because the focus of this


dissertation is on DC microgrid systems, but a similar study can be done on AC and hybrid microgrid systems with AC-AC, AC-DC, and DC-AC converters. The proposed framework can be implemented on other microgrid systems.


- Modeling multiple input multiple output DC-DC converter in the optimization problem is important to study the impact of multiple ports on the converter's performance.

### 6.3 Publications


#### Journals


R. Khan, L. Wang, S. Pannala, A.K. Srivastava, and N.N. Schulz, "DER-rich Electric Distribution Feeder Models: Limitations, Challenges, and Path-Forward," *under revision in IEEE Access 2024*.

 R. Khan, N.N. Schulz, M.Nasir, "An Optimal Neighborhood Energy Sharing Scheme Applied to Islanded DC Microgrids for Cooperative Rural Electrification." *IEEE Access (2023)*.

 B. Anderson, J. Rane, and R.Khan, "Distributed wind-hybrid microgrids with autonomous controls and forecasting," in *Applied Energy*, 333, (2023):120557.

#### Conferences

 R.Khan, L.A. Akande, and N.N.Schulz,"Optimal Neighborhood Level Power Sharing in DC Islanded Microgrids for Rural Electrification," *accepted in IEEE Power & Energy Society General Meeting (PESGM), 2024*, pp. 1-5.

 R.Khan, and N.N.Schulz, "Power-Electronic Loss Modeling and Analysis of DC Microgrids for Rural Electrification," *IEEE Global Humanitarian Technology Conference (GHTC), 2023*, pp. 1-6.

- ✉ R.Khan, and N.N.Schulz, "Optimal Peer-to-Peer Power Dispatch in Islanded DC Clustered Nanogrids for Rural Electrification," *IEEE Power & Energy Society General Meeting (PESGM)*, 2023, pp. 1-5.
- ✉ R. Khan and N.N. Schulz, "Network Loss Analysis of Low-Voltage Low-Power DC Microgrids for Rural Electrification," *IEEE/PES Transmission and Distribution Conference and Exposition (T&D)*, 2020, pp. 1-8.
- ✉ R. Khan, M. Nasir, and N.N. Schulz, "Distribution loss analysis of DC microgrids for rural electrification," *IEEE Global Humanitarian Technology Conference (GHTC)*, 2019, pp. 1-8.
- ✉ R.Khan, and N.N.Schulz, "Cost optimization of hybrid islanded microgrid for rural electrification," *IEEE Power & Energy Society General Meeting (PESGM)*, 2019, pp. 1-5.

## ✉ Technical Report

- ✉ R.Khan, C.Johnson, and F.Khan, "Standards guidance for electric two- and three-wheelers and charging infrastructure in PAKISTAN (technical report)," *National Renewable Energy Lab. (NREL), Golden, CO (United States)*, 2024.

## REFERENCES

- Ampacity*: (n.d.). Available at <https://en.wikipedia.org/wiki/Ampacity> (2024-02-21).
- Anand, Sandeep and BG Fernandes (2010). “Optimal voltage level for DC microgrids”. In: *IECON 2010-36th Annual Conference on IEEE Industrial Electronics Society*. IEEE, pp. 3034–3039.
- Balls, Jonathan N and Harry W Fischer (2019). “Electricity-centered clientelism and the contradictions of private solar microgrids in India”. In: *Annals of the American Association of Geographers* 109.2.
- Bardouille, Pepukaye et al. (2012). “From gap to opportunity: Business models for scaling up energy access”. In: *International Finance Corporation*.
- Desai, Akshayakumar Ramanlal (1994). *Rural sociology in India*. Popular Prakashan.
- Farivar, M. and S. H. Low (Aug. 2013). “Branch Flow Model: Relaxations and Convexification: Part I”. In: *IEEE Transactions on Power Systems* 28.3, pp. 2554–2564. ISSN: 0885-8950. DOI: [10.1109/TPWRS.2013.2255317](https://doi.org/10.1109/TPWRS.2013.2255317).
- Farooq, Rabiya et al. (2014). “Smart DC microgrids: Modeling and power flow analysis of a DC Microgrid for off-grid and weak-grid connected communities”. In: *2014 IEEE PES Asia-Pacific Power and Energy Engineering Conference (APPEEC)*. IEEE, pp. 1–6.
- Gan, Lingwen and Steven H Low (2014). “Optimal power flow in direct current networks”. In: *IEEE Transactions on Power Systems* 29, pp. 2892–2904.
- Gelani, Hasan Erteza, Faizan Dastgeer, et al. (2021). “AC vs. DC distribution efficiency: Are we on the right path?” In: *Energies* 14.13, p. 4039.

- Gelani, Hasan Erteza, Mashood Nasir, et al. (2017). “Efficiency comparison of alternating current (AC) and direct current (DC) distribution system at residential level with load characterization and daily load variation”. In: *Pakistan Academy of Sciences* 54.2.
- Glover, J Duncan, Mulukutla S Sarma, and Thomas Overbye (2012). *Power system analysis & design, SI version*. Cengage Learning.
- Grainger, John J and WUliam D Stevenson Jr (1994). *Power system analysis*. McGraw-Hill series in electrical and computer engineering.
- Hamza, Muhammad et al. (2017). “Design and analysis of solar PV based low-power low-voltage DC microgrid architectures for rural electrification”. In: *2017 IEEE Power & Energy Society General Meeting*. IEEE, pp. 1–5.
- Iqbal, Saqib, Kamyar Mehran, and Mashood Nasir (2021). “A Novel Approach of Peer to Peer Energy Sharing in DC Microgrid with Optimal Distribution Losses”. In: *2021 IEEE PES Innovative Smart Grid Technologies Europe (ISGT Europe)*, pp. 1–5. DOI: [10.1109/ISGTEurope52324.2021.9639947](https://doi.org/10.1109/ISGTEurope52324.2021.9639947).
- Jonnes, Jill (2004). *Empires of light: Edison, Tesla, Westinghouse, and the race to electrify the world*. Random House Trade Paperbacks.
- Khan, Jibran and Mudassar H Arsalan (2016). “Solar power technologies for sustainable electricity generation—A review”. In: *Renewable and Sustainable Energy Reviews* 55, pp. 414–425.
- Khan, Rabia and Noel N. Schulz (2020). “Network Loss Analysis of Low-Voltage Low-Power DC Microgrids for Rural Electrification”. In: *2020 IEEE/PES Transmission and Distribution Conference and Exposition (TD)*, pp. 1–5. DOI: [10.1109/TD39804.2020.9299657](https://doi.org/10.1109/TD39804.2020.9299657).



- Kolar, Johann W et al. (2012). “Extreme efficiency power electronics”. In: *2012 7th International Conference on Integrated Power Electronics Systems (CIPS)*. IEEE, pp. 1–22.
- Küfeoğlu, Sinan (2022). “SDG-7 Affordable and Clean Energy”. In: *Emerging Technologies: Value Creation for Sustainable Development*. Springer, pp. 305–330.
- Li, Jia et al. (2018). “Optimal power flow in stand-alone DC microgrids”. In: *IEEE Transactions on Power Systems* 33.5, pp. 5496–5506.
- Linard, Catherine et al. (2012). “Population distribution, settlement patterns and accessibility across Africa in 2010”. In: *PloS one* 7.2, e31743.
- Liu, Jianzhe et al. (2021). “Optimal power flow in DC networks with robust feasibility and stability guarantees”. In: *IEEE Transactions on Control of Network Systems* 9.2, pp. 904–916.
- Madduri, P Achintya et al. (2013). “Design and verification of smart and scalable DC microgrids for emerging regions”. In: *2013 IEEE Energy Conversion Congress and Exposition*. IEEE, pp. 73–79.
- Madduri, Parimalram Achintya et al. (2016). “Scalable DC microgrids for rural electrification in emerging regions”. In: *IEEE Journal of Emerging and Selected Topics in Power Electronics* 4.4, pp. 1195–1205.
- Maghami, Mohammad Reza et al. (2016). “Power loss due to soiling on solar panel: A review”. In: *Renewable and Sustainable Energy Reviews* 59.
- Martander, Olof (2002,). “DC grids for wind farms”. PhD thesis. Chalmers tekniska högsk.
- Mehta, VK and Rohit Mehta (2011). “Principles of power systems, S”. In: *CHAND, New Delhi, India*.

- Moksnes, Nandi et al. (2020). “Corrigendum: Electrification pathways for Kenya—linking spatial electrification analysis and medium to long term energy planning (2017 Environ. Res. Lett. 12 095008)”. In: *Environmental Research Letters* 15.12, p. 129501.
- Moner-Girona, M et al. (2017). “Mapping the least-cost option for rural electrification in Burkina Faso”. In: *European Commission Joint Research Centre*.
- Nasir, Mashood, Saqib Iqbal, Hassan A Khan, et al. (2020). “Sustainable Rural Electrification Through Solar PV DC Microgrids—An Architecture-Based Assessment”. In: *Processes* 8.11, p. 1417.
- Nasir, Mashood, Saqib Iqbal, and Hassan Abbas Khan (2017). “Optimal planning and design of low-voltage low-power solar DC microgrids”. In: *IEEE Transactions on Power Systems* 33.3, pp. 2919–2928.
- Nasir, Mashood, Zheming Jin, et al. (2018). “A decentralized control architecture applied to dc nanogrid clusters for rural electrification in developing regions”. In: *IEEE Transactions on Power Electronics* 34.2, pp. 1773–1785.
- Nasir, Mashood, Hassan Abbas Khan, Arif Hussain, et al. (2017). “Solar PV-based scalable DC microgrid for rural electrification in developing regions”. In: *IEEE Transactions on sustainable energy* 9.1.
- Nasir, Mashood, Hassan Abbas Khan, Kamran Ali Khan Niazi, et al. (2019). “Dual-loop control strategy applied to PV/battery-based islanded DC microgrids for swarm electrification of developing regions”. In: *The Journal of Engineering* 2019.18, pp. 5298–5302.
- Nasir, Mashood, Nauman Ahmad Zaffar, and Hassan Abbas Khan (2016). “Analysis on central and distributed architectures of solar powered DC microgrids”. In: *2016 Clemson University Power Systems Conference (PSC)*. IEEE.

- Nasir, Mshood (2018). “Scalable DC Microgrids for Rural Electrification”. PhD thesis. Syed Babar Ali School of Sciences and Engineering Lahore University of . . .
- Nations, United (2015). “Transforming our world: The 2030 agenda for sustainable development”. In: *New York: United Nations, Department of Economic and Social Affairs*.
- OpenDSS, EPRI Distribution System Simulator* (n.d.). Available at <https://sourceforge.net/projects/electricdss/#> (2024-02-21).
- Palit, Debajit (2013). “Solar energy programs for rural electrification: Experiences and lessons from South Asia”. In: *Energy for Sustainable Development* 17.3, pp. 270–279.
- PwC (2016). “Electricity Beyond the Grid. Accelerating Access to Sustainable Power for All”. In: PwC.
- Saadat, Hadi et al. (1999). *Power system analysis*. Vol. 2. McGraw-hill.
- Salomonsson, Daniel, Lennart Soder, and Ambra Sannino (2009). “Protection of low-voltage DC microgrids”. In: *IEEE Transactions on power delivery* 24.3, pp. 1045–1053.
- Solar Power Data for Integration Studies-* (n.d.). Available at <https://www.nrel.gov/grid/solar-power-data.html> (2024-02-21).
- Ubilla, Karen et al. (2014). “Smart microgrids as a solution for rural electrification: Ensuring long-term sustainability through cadastre and business models”. In: *IEEE Transactions on Sustainable Energy* 5.4, pp. 1310–1318.
- Wang, Jing, William G Dunford, and Konrad Mauch (1997). “Analysis of a ripple-free input-current boost converter with discontinuous conduction characteristics”. In: *IEEE transactions on power electronics* 12.4, pp. 684–694.

Williams, Nathaniel J et al. (2015). “Enabling private sector investment in microgrid-based rural electrification in developing countries: A review”. In: *Renewable and Sustainable Energy Reviews* 52, pp. 1268–1281.

Zhang, Li et al. (2011). “Power control of DC microgrid using DC bus signaling”. In: *2011 Twenty-Sixth Annual IEEE Applied Power Electronics Conference and Exposition (APEC)*. IEEE, pp. 1926–1932.

Zhao, Menghua, Zhe Chen, and Frede Blaabjerg (2006). “Modeling of DC/DC converter for DC load flow calculation”. In: *2006 12th International Power Electronics and Motion Control Conference*. IEEE, pp. 561–566.